Mathematical and Computational Techniques for Predicting the Squat of Ships

Tim Gourlay

Thesis submitted for the degree of
Doctor of Philosophy

THE UNIVERSITY OF ADELAIDE

Department of Applied Mathematics

February 2000

Contents

Abstract v

Signed Statement vi

Acknowledgement vii

General Introduction viii

Historical Summary ix

Overview xiv

PART I: CONSTANT DEPTH 2

1 Steady Squat in a Narrow Channel 2

1.1 Problem formulation 2

1.2 The hydraulic equations - fixed ship 4

1.3 Hull pressure, sinkage and trim 5

1.4 The linearized solution 8

1.5 Solution of the nonlinear problem - fixed ship 10

1.5.1 Choosing the correct solution 11

1.6 A consistent nonlinear theory for sinkage and trim 13

1.6.1 The hydraulic equations - ship free to squat 13

1.6.2 Special case: block-like ship 15

1.6.3 Simple case: fore-aft symmetric ship 16

1.6.4 General-shaped ship 16

1.7 Results for sinkage and trim 18
1.7.1 Fore-aft symmetric ship 18
1.7.2 Bulk carrier hull 20
1.8 Existence of steady flow 21
1.8.1 Fixed ship 23
1.8.2 Block-like ship free to squat 27
1.8.3 General ship free to squat 27
1.8.4 Results 28
1.9 The critical section 30
1.9.1 Fixed ship 30
1.9.2 Ship free to squat 34
1.10 Conclusions 35

2 Steady Transcritical Squat in Open Water 37

2.1 Shallow-water theory and experimental results 37
2.2 Modifying shallow-water theory 40
2.2.1 A general shallow-water derivation 41
2.2.2 Simplifying the equation 44
2.2.3 Dispersive or nonlinear theory? 45
2.2.4 The linear transcritical equation 49
2.3 Transcritical shallow-water theory (TSWT) 51
2.3.1 Solution by Fourier transform 51
2.3.2 Pressure, forces, and squat 53
2.3.3 Numerical method 56
2.3.4 Symmetric hulls 59
2.3.5 Finite-width channel 61
2.4 Finite-depth theory (FDT) 65
2.4.1 The original equations 65
2.4.2 Studying the $\Omega(k)$ integral 66
2.4.3 Numerical method 69
2.5 Scaling 70

2.6 Results 70
2.6.1 Comparing TSWT and FDT 70
2.6.2 Comparison with experimental results 73
2.6.3 Trim and stern sinkage 73
2.6.4 Maximum sinkage 75
2.7 Conclusions 76

PART II: NON-UNIFORM DEPTH 80

3 Unsteady Squat in a Narrow Channel 80
3.1 Problem formulation 80
3.2 The unsteady hydraulic equations 81
3.3 Analytic solution for a step depth change 83
3.3.1 Results for a simple hull 85
3.4 Numerical method for general depth profiles 90
3.4.1 Step depth change solution 92
3.4.2 Smoothly shelving sea floor 93
3.4.3 Ramp between two constant depths 95
3.5 Conclusions 96

4 Two-Dimensional Unsteady Squat 99
4.1 Unsteady slender-body shallow-water theory 99
4.1.1 The outer expansion 100
4.1.2 The inner expansion and matching 102
4.1.3 Vertical force, moment, sinkage and trim 103
4.2 An analytic solution for a step depth change 103
4.2.1 Constant depth solution 104
4.2.2 The method of images 105
4.2.3 Vertical force and trim moment 107
4.2.4 Finite-width channel 110
4.3 Numerical method 112

4.3.1 General depth profiles 112
4.3.2 Step depth change 113
4.4 Results for a step depth change 115
4.4.1 Numerical issues 115
4.4.2 Flow velocity 116
4.4.3 Vertical force and moment 117
4.4.4 Bow and stern sinkage 119
4.5 Conclusions 120

Appendix A: Nomenclature **121**

Appendix B: Some Mathematical Derivations **124**

B.1 The basis of hydraulic theory 124
B.2 Finite-width and open-water TSWT agree in the infinite-width limit . . . 127
B.3 FDT and TSWT agree in the shallow-water limit 132
B.4 Unsteady slender-body shallow-water theory agrees with unsteady hydraulic theory in the narrow-channel limit 137

Bibliography **139**

Abstract

This thesis deals with the squat of a moving ship; that is, the downward displacement and angle of trim caused by its forward motion. The thesis is divided into two parts, in which the ship is considered to be moving in water of constant depth and non-constant depth respectively. In both parts, results are given for ships in channels and in open water.

Since squat is essentially a Bernoulli effect, viscosity is neglected throughout most of the work, which results in a boundary value problem involving Laplace's equation. Only qualitative statements about the effect of viscosity are made.

For a ship moving in water of constant depth, we first consider a one-dimensional theory for narrow channels. This is described for both linearized flow, where the disturbance due to the ship is small, and nonlinear flow, where the disturbance due to the ship is large. For nonlinear flow we develop an iterative method for determining the nonlinear sinkage and trim. Conditions for the existence of steady flow are determined, which take into account the squat of the ship.

We then turn to the problem of ships moving in open water, where one-dimensional theory is no longer applicable. A well-known slender-body shallow-water theory is modified to remove the singularity which occurs when the ship's speed is equal to the shallow-water wave speed. This is done by including the effect of dispersion, in a manner similar to the derivation of the Korteweg-deVries equation. A finite-depth theory is also used to model the flow near the critical speed.

For a ship moving in water of non-uniform depth, a linearized one-dimensional theory is derived which is applicable to unsteady flow. This is applied to simple bottom topographies, using analytic as well as numerical methods. A corresponding slender-body shallow-water theory for variable depth is also developed, which is valid for ships in channels or open water. Numerical results are given for a step depth change, and an analytic solution to the problem is discussed.

Signed Statement

This work contains no material which has been accepted for the award of any other degree or diploma in any university or other tertiary institution and, to the best of my knowledge and belief, contains no material previously published or written by another person, except where due reference has been made in the text.

I consent to this copy of my thesis being available in the University Library for loan and photocopying.

SIGNED: Tim Gourlay DATE: 23/2/2000

Acknowledgement

My supervisor, Prof. Ernie Tuck, has provided a wealth of information on the topic and a constant stream of new ideas. Most of the present work has been done in collaboration with him, resulting in several co-authored journal articles. I would like to thank him for his enthusiasm and for never being too busy to answer my questions.

During the course of my research, I have participated several times in tank testing at the Australian Maritime College in Launceston. This, as well as liaising with staff and students at the college, has allowed experimental confirmation of the theoretical results. Thanks particularly to Martin Renilson and Jonathon Duffy.

The Head of the Applied Mathematics Department at Adelaide University, Dr. Peter Gill, has always been willing to help with administrative matters. I am especially indebted to Dianne Parish, for her advice and assistance with everything from conference registrations to thesis printing. My fellow students have been invaluable in helping to sort out computing problems and making the work bearable.

Finally, thanks to my close friends and family for their encouragement and support.

General Introduction

When a ship is travelling forward in calm water, it sits in a different vertical position to when it is at rest. This phenomenon is known as "squat". It is characterized by an overall vertical displacement of the ship, called the sinkage, as well as a certain angle of trim.

Squat can be thought of as a simple Bernoulli effect, caused by the increased flow speed beneath the ship's hull, which decreases the fluid pressure on the hull. The vertical displacement of the ship is therefore usually downward.

This means that when a ship is travelling through shallow water, squat may in fact cause it to strike the bottom, despite the fact that it may have had sufficient clearance when at rest. In fact, sinkage usually increases with speed, so that the faster a ship is moving, the more it is at risk of grounding. The problem is exacerbated by the fact that the trim of the ship will make either the bow or the stern particularly vulnerable to grounding.

If a ship's squat can be accurately predicted under given conditions, sufficient allowance can be made for the ship to pass through shallow water in safety. Conversely, since the cargo capacity of a ship is often limited by conservative squat predictions for its passage through shallow water, accurately predicting the squat allows the ship to carry as much cargo as is safe. At the same time, the ship's captain can know the maximum speed at which the ship can travel for each depth of water.

Our aim is therefore to be able to predict accurately the squat of any ship at any given speed and water depth. This will be done by building on existing techniques and developing some new ones.

Historical Summary

The phenomenon of ships settling downwards in the water when they are under way has been known to mariners for centuries. What has not been well known, however, is how the magnitude of this sinkage varies with water depth and vessel speed. It is only in quite recent times that these have been included in prediction of a ship's sinkage. Indeed, in former times, a fixed allowance, say one foot, would often be allowed for this sinkage whatever the water depth or vessel speed.

Early analytic methods

Early attempts to predict ship squat mathematically were made by assuming water of infinite depth, using methods previously developed for studying ship waves. Havelock (1939) determined analytically the sinkage of an elliptical hull form in infinite depth of water. This theory was of limited usefulness, however, as the problem of most practical importance is that of a ship travelling in shallow water. This is the situation in which the ship is most likely to hit the sea floor and do serious damage, so its squat needs to be accurately predicted under these circumstances. As it was known that the presence of the sea floor has a profound effect on the hydrodynamics, subsequent squat prediction methods attempted to take the water depth into account.

A subsequent important early work on squat considered a very different physical problem: that of a ship travelling in a shallow, narrow channel. Under these assumptions, Constantine (1961) asserted that flow around the ship could be studied in much the same way as open-channel flow, using one-dimensional "hydraulic" theory. He considered the ship to be stationary and the water to be moving past it, which meant that the flow was usually steady in this frame of reference. Constantine found that three different types of flow were possible in this situation.

At low speeds the flow was predicted to accelerate past the ship, producing a pressure decrease beneath the hull and a downward sinkage of the ship. However, once the ship reached a certain speed, which is dependent on the ship and channel dimensions, no such steady flow could be found. In this "critical" speed range, Constantine predicted that a one-dimensional bore would be formed, travelling ahead of and faster than the ship. At higher speeds the ship would catch up to this bore, resulting in a new type of steady flow. This "supercritical" flow would be characterized by a decelerated flow past the ship, causing the ship to rise in the water.

In 1966, Tuck developed a slender-ship theory that was valid for shallow water. In fact, it was valid *only* for shallow water, as one of the assumptions was that the water depth must be small compared to the ship's length. This revolutionary approach yielded expressions for the ship's sinkage and trim that were roughly quadratic in the ship's speed. For practical speed ranges, the theory generally gave good results for sinkage and trim, and was used extensively over the next decades. However, a problem with the theory was its behaviour as the ship speed approached the natural speed of waves in shallow water. In this case the theory became singular and predicted infinite sinkage and trim.

Whereas the original theory was developed for water of infinite lateral extent, it was later modified (Tuck 1967) for channels of arbitrary width. Provided that the ship's beam remained small compared to the channel width, the final solution was found to approach the linearized version of Constantine's solution in the narrow channel limit. Thus this theory was uniformly valid for any width of channel, and provided a link between Constantine's one-dimensional theory and Tuck's infinite-width theory.

There still remained the problem of the singularity when the ship approached the shallow-water wave speed, for which Tuck and Taylor (1970) proposed a remedy. They found the velocity potential for a ship moving in a *finite* depth of water by rejecting the shallow-water assumption completely. However, the resulting formulas were extremely complicated and were only studied for some simple test cases.

Meanwhile, in the same article and a subsequent article by Tuck (1974), the one-dimensional theory for a ship in a narrow channel was also being extended. The limits of steady flow were more accurately defined for either block-like ships free to squat or general-shaped ships fixed vertically.

Empirical methods

The sinkage formula given by Tuck (1966) was too complicated for routine use by mariners, as it required computation of a double integral. In an attempt to find a simpler expression that would be easier to implement in practice, Tuck & Taylor (1970) studied the properties of this double integral. They found that over a wide range of hull shapes it was roughly proportional to the ship's displacement divided by the square of its length, and used this to produce a much simpler expression for ship sinkage.

Experiments performed by Hooft (1974) showed excellent agreement with the sinkage formula of Tuck & Taylor. However, a compilation of experimental results from several testing laboratories was made by Huuska (1976) which showed that the formula tended to underestimate the sinkage. This was later confirmed by Millward (1992). Since the general speed dependence was accurate, Huuska proposed that a corrective multiplicative constant be introduced into the formula.

This empirical squat prediction method started a new phase in squat research. Subsequent researchers attempted to fit a universal curve to the experimental results for

different ships, which had as its parameters the ship speed, water depth and ship dimensions.

Some of these formulas, such as those of Huuska (1976) and Millward (1992) used the speed dependence calculated by Tuck (1966) but with a simplified dependence on hull shape. Others matched experimental results to some power of the ship speed: Eryuzlu & Hausser (1978), Eryuzlu et al (1994), and Barrass (1979) put forward empirical expressions for squat with very different dependences on speed and draught-to-depth ratio.

These empirical methods have been shown to perform well for ships and channels in the range that they were designed for. Despite having little or no physical basis, they give accurate squat predictions in the case of ship types, channel types and speed ranges for which experimental data are available. However, they cannot be expected to perform well for all hull forms, channel types and speed ranges.

The critical region

For ships travelling in wide channels, the experiments of Graff et al (1964) showed that sinkage and trim were not unbounded as the ship approached the shallow-water wave speed. Instead the sinkage reached a maximum before becoming quite small thereafter.

The finite-depth theory of Tuck & Taylor (1970), which was developed for open water, predicted the correct overall form of the sinkage as a function of speed. A shallow-water approach by Lea & Feldman (1972) concentrated on a ship travelling at exactly the shallow-water wave speed, and included the leading nonlinear term to solve for sinkage and trim. Mei (1976) developed a slender-ship theory for open water similar to that of Tuck (1966) but including the leading nonlinear and dispersive terms. However, his paper concentrated on wave resistance and did not calculate sinkage and trim.

Although the flow around a ship travelling in water of constant depth is steady at any speed if the ship is in *open water*, a very interesting type of flow was found to occur experimentally for a ship travelling in a *channel* at close to the shallow-water wave speed. Thews & Landweber (1935) observed in model experiments that in this case the flow was unsteady, with waves propagating ahead of the model. Huang et al (1982) found that these waves had the same form as solitary waves, or "solitons", which are single crests capable of travelling along a channel unchanged in form. However, these solitons were produced almost periodically, breaking away from the bow of the ship and travelling ahead of and faster than the model. This was a more complicated scenario than the simple bore solutions predicted by Constantine (1961) although the generating mechanism was the same. In fact, at higher speeds in the critical region, where solitary wave production was impossible, Constantine's bores were witnessed in the experiments.

The production of solitary waves by a ship in a channel provoked much interest, and is still the topic of intensive research today. Huang et al (1982) found that the first soliton produced was invariably the largest, and the first one to break at higher speeds. Ertekin et al (1985) observed that small solitary waves could be formed at ship speeds well below

the previously accepted critical region. They observed experimentally that the drag on the ship fluctuated almost periodically as solitons were produced. It was suggested that the amplitude of successive waves would gradually tend toward zero if the ship speed is less than the shallow-water wave speed; however, this issue still remains unresolved.

An attempt to model ship solitons mathematically was made by Wu & Wu (1982) using Boussinesq equations generalized to allow 2-D wave propagation. Ertekin et al (1985) compared this method to that of Naghdi (1978) and used both methods to solve numerically for the free surface profile ahead of the model as a function of time. The two methods, which are the same to leading order in the soliton amplitude, both predicted solitons of gradually decreasing amplitude for ship speeds less than the wave speed.

Since the Korteweg-DeVries equation was known to be able to model solitary waves accurately, most mathematical treatments of the problem used KdV-type methods. Wu (1986) derived a KdV-type equation with a forcing term from the generalized Boussinesq equations, and used this to calculate the evolution of solitons. He also used energy and momentum conservation to relate soliton and trailing trough amplitudes, as well as the components of wave drag.

Mei & Choi (1987) used matched asymptotics to study the solitary waves produced by a ship in a channel, and explicitly calculated sinkage and trim. The general form of their results compared reasonably well with the experimental results of Graff et al (1964).

Since the mid-1980's there has been a large quantity of research published on the subject of solitary waves; this has been only a brief review, as solitary waves will not be studied in detail in this thesis.

[*subsequent note*: An examiner has pointed out that some of this nonlinear research is more relevant to the topic than the author had appreciated. In particular, a significant body of research by Xue-Nong Chen (e.g. Chen & Sharma 1995) improves upon the linear transcritical results of Chapter 2 of the present thesis.]

Squat in water of non-uniform depth

Interest in this topic came about through the grounding of several ships in shoaling water. In 1992, for example, the QE2 grounded in Vineyard Sound, Massachusetts, causing serious damage (see USCG 1993, NTSB 1993). The accident occurred in shoaling water as a result of the ship's squat. In an investigation into the incident (NTSB 1993), researchers predicted the squat of the ship using constant depth formulae, as there were no methods available for non-uniform depth. Then, as now, the best estimate of squat in non-uniform depth was obtained by using the average depth under the ship in the constant-depth formulae. However, it was not known whether this method would over- or under-predict the squat for a ship moving towards shallower water, for example.

Even in recent years, little research has been done in this area. Renilson & Hatch (1998) and Duffield (1997) have carried out experimental investigations into the transient squat

of a ship travelling through water of non-uniform depth. However, few serious attempts have been made to treat the problem mathematically.

Overview

In this thesis I shall develop some new mathematical methods for predicting the squat of a ship. This is done with a view to practical evaluation of the squat of a moving ship, so that with better squat estimates, ships can pass through shallow water in safety.

Part I of the thesis deals with a ship travelling in water of constant depth. This simplifies the analysis, because the flow can usually be considered steady in this case.

Chapter 1 introduces a simple one-dimensional theory for flow past a ship in a narrow channel. We first discuss the commonly-used procedure of solving for the flow with the ship held fixed in its rest position, rather than in its squatted position. A consistent nonlinear method for computing sinkage and trim is then developed, which takes into account the flow changes that occur when a ship squats.

According to this theory, there are conditions under which no steady flow exists, namely a finite range of speeds that includes the critical speed of shallow-water waves. Explicit forms of these conditions are found for a ship of arbitrary shape that is held fixed vertically, and also for a ship that is allowed to squat.

Chapter 2 describes two improved methods for determining the squat of a ship moving in open water. These methods are valid at all ship speeds, even those close to the shallow-water wave speed. Firstly, a generalized shallow-water theory is discussed that makes allowance for the variation of wave speed with wavelength. Then, a previously-developed finite-depth theory is improved upon and studied in detail. Computational techniques are developed for evaluating the resulting formulae, and the two theories are compared to experimental results for sinkage and trim. The predicted maximum sinkage is in close agreement with experiment.

Part II of the thesis attempts to solve the more difficult unsteady flow problem of a ship moving in water of non-uniform depth. This is first done in Chapter 3 using a one-dimensional theory similar to Chapter 1, but now modified to allow for unsteadiness. It is found that the sinkage and trim can be found analytically for a ship travelling in a channel with a sudden depth change to deeper or shallower water.

In Chapter 4, a slender-ship theory is described which is able to treat a general non-uniform water depth. It is found that the problem can be solved analytically for the case of a ship approaching a sudden depth change in open water or a channel. For the case of a ship in a channel, a stable finite-difference method is found for solving the governing

equation. Numerical results are given for step depth changes.

Detailed mathematical proofs are left to the Appendix; these discuss the conditions under which the hydraulic theory is valid, as well as showing that the theories developed here match each other in the appropriate limits.

Part I

Constant Depth

Chapter 1

Steady Squat in a Narrow Channel

In this chapter we consider a ship travelling in a narrow, shallow channel. In practice this might represent a ship travelling down a river, dredged harbour entrance, or canal such as the Suez Canal.

1.1 Problem formulation

Figure 1.1 shows a cross-section through the ship and channel in this situation. Although the channel might have any shape below the waterline, we will depict it as a rectangle for simplicity. The ship and channel parameters shown in Figure 1.1 will be defined shortly.

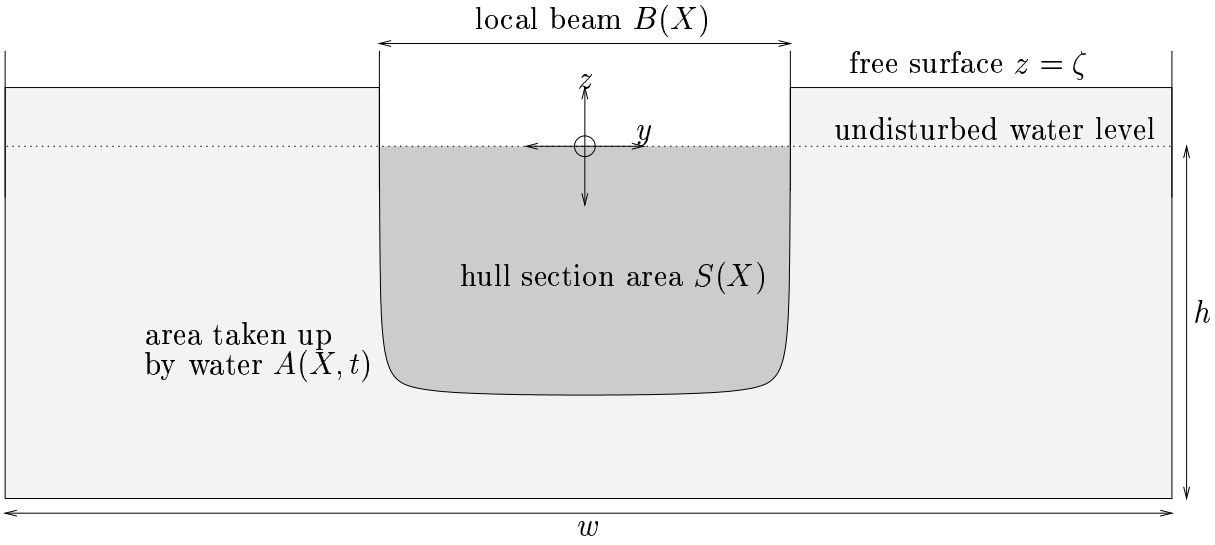

Figure 1.1: Cross-section of a ship in a channel

We will be considering channels of constant cross-section, with the ship moving in a straight line along the axis of the channel, but not necessarily in the centre. Since we are considering channels of arbitrary cross-section, we will define h as the *mean* channel depth

across the channel. w represents the width of the channel *at the waterline*. Therefore the undisturbed underwater cross-sectional area of the channel is $S_0 = wh$.

The channel's waterline width w and mean depth h are both assumed small compared to the ship's length. Under these and other restrictions, the main fluid velocity component is in the direction of the ship's motion. Also, this fluid velocity is approximately constant across any cross-section of the channel. This allows us to use a one-dimensional "hydraulic theory" to describe the flow. A justification of hydraulic theory and the assumptions under which it is valid are described mathematically in Appendix B.1.

Since the flow relative to the ship may be considered steady, we will use a frame of reference in which the ship is considered stationary. This is known as a "body-fixed" frame of reference. If the ship's speed in a conventional "earth-fixed" frame of reference is U, in our body-fixed frame there is a free stream flowing past the stationary ship, with the free stream having undisturbed speed U.

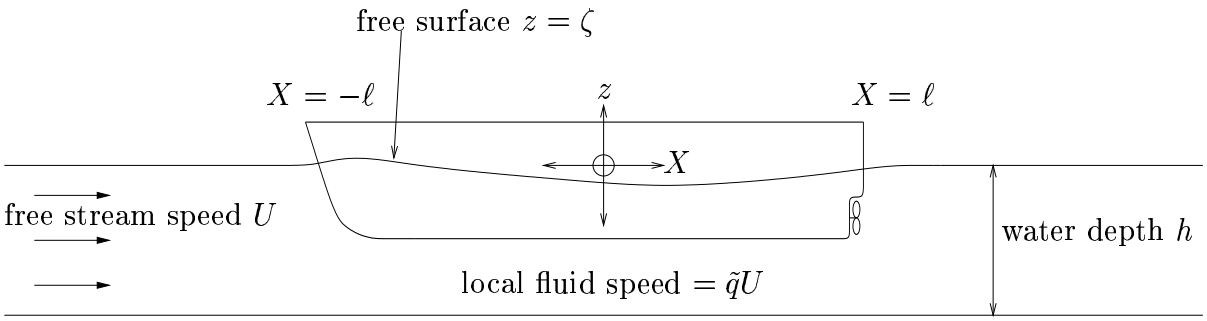

Figure 1.2: Body-fixed frame of reference

Figure 1.2 shows a side-on view of the ship in the channel. The body-fixed frame of reference is defined with its origin centred at the middle of the ship, and the $X-$coordinate pointing directly down the channel. Far ahead of the ship there is a free stream of speed U, but the ship disturbs this stream so that its local speed is changed by a factor $\tilde{q}$.

The bow and stern of the ship are at $X = -\ell$ and $X = \ell$ respectively. The total shiplength is $L = 2\ell$. The centre of the ship in the longitudinal direction, or "midships", is at $X = 0$.

The vertical coordinate is z, which is centred at the height of the undisturbed free surface. The actual free surface is at $z = \zeta$, with $\zeta \to 0$ far upstream of the ship. Note that although Figure 1.1 is drawn with $\zeta > 0$, in practice the free surface normally drops due to the presence of the ship, meaning that ζ is usually negative.

Returning to Figure 1.1 we can now define the ship's local beam B and local cross-sectional area S as functions of the $X-$coordinate. Our third spatial coordinate, the transverse coordinate y, is centred at the centreline of the ship. However, this coordinate is not needed explicitly in hydraulic theory. Since, according to hydraulic theory, the free surface height is a function of X only (see Appendix B.1), it is flat across any cross-section $X =$ constant.

1.2 The hydraulic equations - fixed ship

In previous works on hydraulic theory (e.g. Dand & Ferguson 1973, Tuck 1974) a ship of general shape was considered to be held fixed vertically in its rest position while solving for the flow field. We shall call this the "fixed-ship" approach. This is the situation depicted in Figures 1.1 and 1.2 that we shall consider now.

In hydraulic theory we need two equations to describe the flow: the continuity equation and the Bernoulli equation.

The equation of continuity for steady one-dimensional hydraulic flow is obtained by matching the flux across any cross-section X = constant to the flux far upstream. This gives

$$\tilde{q}UA(X) = US_0 \ . \tag{1.1}$$

The area $A(X)$ is the local cross-sectional area taken up by the water as it passes the ship. This area is equal to the undisturbed water area S_0, minus the submerged section area of the ship S, and adding the difference due to the rise or fall of the free surface. From Figure 1.1, we can see that this area has the form

$$A(X) = S_0 - S + (w - B)\zeta \ . \tag{1.2}$$

For simplicity we have assumed that the ship and channel walls are vertical at the waterline. However we have made no assumptions about the underwater shape of the ship and channel.

By combining equations (1.1) and (1.2) the continuity equation simplifies to

$$\tilde{q}\left[1 - \frac{S}{S_0} + \left(1 - \frac{B}{w}\right)\tilde{\zeta}\right] = 1 \tag{1.3}$$

in non-dimensional form. Here S/S_0 is termed the "blockage coefficient" and B/w is the ship-beam/channel-width ratio. We have also introduced the scaled free surface height $\tilde{\zeta} = \zeta/h$.

The Bernoulli equation as used here states that the quantity

$$\frac{P}{\rho} + gz + \frac{1}{2}|\mathbf{q}|^2 \tag{1.4}$$

is constant throughout any simply-connected fluid domain if the flow is incompressible and irrotational. Here P is the actual fluid pressure, measured in excess of atmospheric pressure. ρ is the fluid density, g is the acceleration due to gravity and $\mathbf{q}$ is the fluid velocity vector. Applying the Bernoulli equation on the free surface and equating it to the value far upstream tells us that

$$g\zeta + \frac{1}{2}(\tilde{q}U)^2 = \frac{1}{2}U^2 \ . \tag{1.5}$$

By using the depth-based Froude number $F_h = U/\sqrt{gh}$ we can write this in the non-dimensional form

$$\tilde{q}^2 + \frac{2\tilde{\zeta}}{F_h^2} = 1 \ . \tag{1.6}$$

The continuity equation (1.3) and Bernoulli equation (1.6) constitute two simultaneous equations which can be solved for the unknowns $\tilde{\zeta}$ and $\tilde{q}$ at each value of X.

1.3 Hull pressure, sinkage and trim

Once the free surface height and fluid speed have been found, the fluid pressure on the ship's hull can be determined. We start by equating the general Bernoulli expression (1.4) to its value far upstream on the free surface. This gives

$$\frac{P}{\rho} + gz + \frac{1}{2}(\tilde{q}U)^2 = \frac{1}{2}U^2 \ . \tag{1.7}$$

We can then subtract this relation from equation (1.5) to give the following general expression for the fluid pressure:

$$P = \rho g(\zeta - z) \ . \tag{1.8}$$

Since the pressure is equal to ρg multiplied by the distance beneath the free surface, the pressure is *hydrostatic*, or the same as if the fluid were at rest (but with the free surface in its disturbed position). We can therefore use Archimedes' principle to say that the volume displaced by the ship when it is moving must be the same as the volume displaced when it is at rest.

In order to show this mathematically, let us first consider the upward force Z on a moving ship that is unable to squat. This force consists of the gravitational force on the ship (which is negative) plus the upward component of the force exerted by fluid pressure over the submerged hull surface. The gravitational force is the same as would be on an equal volume of water, by Archimedes principle, that is $\rho g \Delta$. Here Δ is the displacement of the ship, which is its volume below the waterline when it is at rest. Therefore we have

$$Z = -\rho g \Delta + \int\int -P \ d\mathbf{S}.\hat{\mathbf{z}} \tag{1.9}$$

where the surface integral is evaluated over the submerged hull surface. Here $\mathbf{S}$ is a hull surface area element with direction normal to and *out of* the hull surface. $\hat{\mathbf{z}}$ is a unit vector in the positive z-direction.

Since $P(X, z)$ is zero on the free surface $\zeta(X)$, we can extend the surface integral in (1.9) to include a slice through the hull at the level of the free surface. Since P is independent of y, on this slice P is equal to its value where the free surface meets the hull, i.e. zero. Therefore we can add the surface integral over this slice to equation (1.9), as its value

is identically zero. We now have a closed surface integral to which we can apply the divergence theorem, so that (1.9) becomes

$$Z = -\rho g \Delta + \int\int\int -\nabla P . \hat{\mathbf{z}} \, dV$$

with the volume element dV equal to $dX\, dy\, dz$. The volume integral is evaluated over that part of the hull lying beneath the free surface. Substituting expression (1.8) into the volume integral, this becomes

$$\begin{aligned} Z &= -\rho g \Delta + \int\int\int \rho g \, dV \\ &= \rho g \left\{ \text{volume displaced while moving} - \Delta \right\} . \end{aligned} \tag{1.10}$$

Since the ship is held vertically fixed and the free surface is usually displaced downwards, the displaced volume will be less than the rest displacement, producing a net downward force on the ship.

In order to simplify this force we will again assume that the ship walls are vertical at and near the waterline. In this case the change in submerged cross-section area of the ship at any point X, due to a rise or fall in the free surface, is $B(X)\zeta(X)$. Integrating this over the length of the ship gives the difference in displaced volume due to changes in the free surface height, so that equation (1.10) becomes

$$Z = \rho g \int_{-\ell}^{\ell} B(X)\zeta(X) \, dX \, . \tag{1.11}$$

This force, which is usually negative (downward) causes the ship to sink lower in the water until it reaches equilibrium. Also, because of the variation in pressure along the ship's hull, the ship will rotate about the y-axis until it adopts a certain angle of trim.

The fixed-ship method of predicting squat assumes that the flow will only change negligibly when the ship is allowed to squat. This means that the free surface height and flow speed can be calculated with the ship fixed vertically in its rest position, and then sinkage and trim calculated as follows.

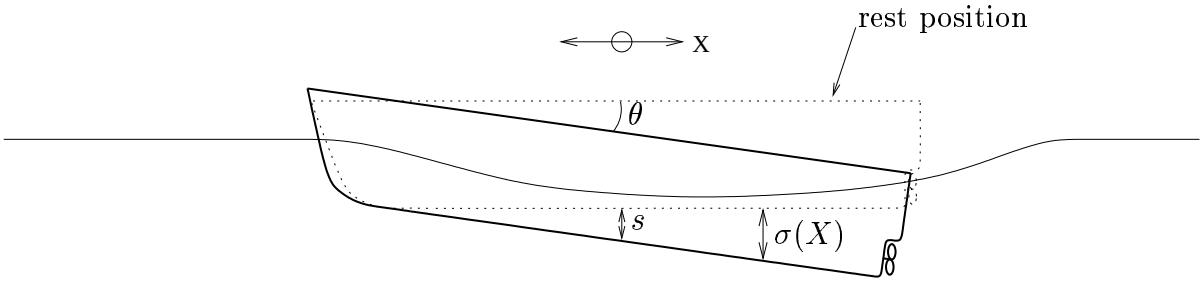

Figure 1.3: Midship sinkage, trim angle and local sinkage

If the middle of the ship ($X = 0$) sinks down by an amount s, and the ship adopts a bow-up angle of trim θ, then the actual sinkage of any point along the ship's length is $\sigma(X) = s + X \tan\theta$.

While at this point no assumption is being made about the magnitude of the midship sinkage, we know that the angle of trim is generally very small in practice. Typically, for bulk carriers or container ships that are not travelling at close to the "critical speed" (to be discussed later) the trim angle is normally less than 0.5 degrees.

This allows us to safely neglect the effect of rotation on the cross-sectional area of the ship's hull at a given value of X. As such, the increase in submerged hull cross-sectional area at any point X, due to the sinkage of the ship, is given simply by $B(X)\sigma(X)$.

Integrating this over the length of the ship gives

$$\int_{-\ell}^{\ell} B(X)\,\sigma(X)\,dX$$

for the increase in displaced volume due to the sinkage of the ship. Therefore the total increase in displaced volume due to the change in free surface height and the sinkage of the ship is

$$\int_{-\ell}^{\ell} B(X)\,\zeta(X)\,dX + \int_{-\ell}^{\ell} B(X)\,\sigma(X)\,dX\ ,$$

so that the net upward force on the ship is now

$$Z = \rho g \int_{-\ell}^{\ell} B(X)\ \{\zeta(X) + \sigma(X)\}\ dX\ . \tag{1.12}$$

In the same way, the change in bow-up moment due to the change in free surface height and sinkage of the ship is

$$\begin{aligned} M &= -\int_{-\ell}^{\ell} X\,dZ \\ &= -\rho g \int_{-\ell}^{\ell} X\,B(X)\ \{\zeta(X) + \sigma(X)\}\ dX\ . \end{aligned} \tag{1.13}$$

For the ship to be in equilibrium, Z and M must both be zero. Therefore $\sigma(X)$ must satisfy the simultaneous equations

$$\begin{aligned} \int_{-\ell}^{\ell} B(X)\ \{\zeta(X) + \sigma(X)\}\ dX &= 0 \\ \int_{-\ell}^{\ell} X\,B(X)\ \{\zeta(X) + \sigma(X)\}\ dX &= 0\,. \end{aligned} \tag{1.14}$$

Using $\sigma(X) = s + X\tan\theta$, we can solve equations (1.14) for s and θ to give

$$s = \frac{I_{\rm W}\int_{-\ell}^{\ell} B(X)\,\zeta(X)\,dX - M_{\rm W}\int_{-\ell}^{\ell} X\,B(X)\,\zeta(X)\,dX}{M_{\rm W}^2 - A_{\rm W}I_{\rm W}}$$

$$\tan\theta = \frac{A_{\rm W}\int_{-\ell}^{\ell} X\,B(X)\,\zeta(X)\,dX - M_{\rm W}\int_{-\ell}^{\ell} B(X)\,\zeta(X)\,dX}{M_{\rm W}^2 - A_{\rm W}I_{\rm W}}\ . \tag{1.15}$$

Here the ship parameters $A_{\rm W}, M_{\rm W}, I_{\rm W}$ are defined by

$$\begin{aligned} A_{\rm W} &= \int_{-\ell}^{\ell} B(X)\, dX \\ M_{\rm W} &= \int_{-\ell}^{\ell} X\, B(X)\, dX \\ I_{\rm W} &= \int_{-\ell}^{\ell} X^2\, B(X)\, dX\ . \end{aligned} \tag{1.16}$$

It is important to remember that according to the fixed-ship method, $\zeta(X)$ is calculated with the ship in its rest position rather than in its squatted position.

1.4 The linearized solution

For hydraulic theory to be valid, we require the width and depth of the channel to be small compared to the length of the ship. However, a further simplification can be made if the blockage coefficient S/S_0 and beam/channel-width ratio B/w are both small. This is more likely to be true in practice for a *slender* ship whose beam and draught are both small compared to its length. In this case there is only a small disturbance to the free stream, so that the scaled fluid speed $\tilde{q}$ is close to 1 and the scaled free surface height $\tilde{\zeta}$ (above the undisturbed level) is close to zero. This can be seen from equations (1.3) and (1.6) as $S/S_0 \to 0$, $B/w \to 0$.

Instead of using the scaled fluid speed $\tilde{q}$ in this case, we introduce the velocity *perturbation* (in the X-direction) to the free stream, which is defined as u. Therefore the actual fluid speed past the ship in our body-fixed frame of reference is $U + u$, so that

$$\tilde{q}U = U + u\ .$$

The velocity perturbation u and scaled free surface height $\tilde{\zeta}$ are now both small quantities. In terms of u and $\tilde{\zeta}$ the continuity equation (1.3) is written

$$\left[1 + \frac{u}{U}\right]\left[1 - \frac{S}{S_0} + \left(1 - \frac{B}{w}\right)\tilde{\zeta}\right] = 1\ .$$

Upon neglecting second-order terms in the small quantities u/U, S/S_0, B/w and $\tilde{\zeta}$, this becomes

$$\frac{u}{U} - \frac{S}{S_0} + \tilde{\zeta} = 0\ . \tag{1.17}$$

Note that this linearized continuity equation and the resulting analysis do not require the ship and channel walls to be vertical at the waterline; however, they must not be excessively sloping.

The Bernoulli equation (1.6) when written as

$$\left(1 + \frac{u}{U}\right)^2 + \frac{2\tilde{\zeta}}{F_h^2} = 1$$

becomes, on linearizing,

$$\frac{u}{U} + \frac{\tilde{\zeta}}{F_h^2} = 0 \, . \tag{1.18}$$

Equations (1.17) and (1.18) can be solved simultaneously to yield the velocity perturbation

$$u = \frac{US}{S_0(1 - F_h^2)} \tag{1.19}$$

and scaled free surface height

$$\tilde{\zeta} = \frac{-F_h^2 S}{S_0(1 - F_h^2)} \, . \tag{1.20}$$

In §1.3 we showed how to calculate the ship's sinkage and trim once the flow field is known. This method was derived assuming that the flow will only change negligibly when the ship is allowed to squat. In order to test the validity of that assumption for linearized flow, let us assume that the beam/channel-width ratio is ϵ, a small quantity. If the draught of the ship is comparable to the average water depth in the channel, then S/S_0 is also $O(\epsilon)$. From equations (1.19) and (1.20) we see that both u/U and $\tilde{\zeta}$ are small, of order ϵ. Similarly, from equations (1.14) we see that the local sinkage σ is of the same order as ζ.

Considering the change in free surface height $\delta\tilde{\zeta}$ that results from the sinkage of the ship, we can say using equation (1.20) that

$$\delta\tilde{\zeta} = \frac{-F_h^2 \, \delta S}{S_0(1 - F_h^2)} \, ,$$

where δS is the difference in section area between the ship in its rest position and in its squatted position. This takes the value $B(X)\sigma(X)$.

The fractional change in free surface height when the ship is allowed to squat is

$$\frac{\delta\tilde{\zeta}}{\tilde{\zeta}} = \frac{\delta S}{S} = \frac{B\sigma}{S} = O\left(\frac{B\zeta}{BT}\right)$$

where T is the ship's draught. Therefore

$$\frac{\delta\tilde{\zeta}}{\tilde{\zeta}} = O\left(\frac{\zeta}{h}\right) O\left(\frac{h}{T}\right) = O(\epsilon)$$

since h/T is order 1. This tells us that allowing the ship to squat has only a second-order effect on the free surface height. Since the sinkage is of the same order as the free surface height, the sinkage obtained using the fixed-ship method will be correct to leading order in ϵ. Therefore, for linearized flow, it is valid to determine the flow with the ship fixed in its rest position, in order to find the ship's sinkage and trim.

It is instructive to consider the special case of a fore-aft symmetric ship in order to see how the sinkage depends on each parameter. In this case equations (1.15) are greatly

simplified, since $B(X)$ and $\zeta(X)$ are both even functions of X. This implies that $M_{\rm W} = 0$ and $\theta = 0$. The sinkage satisfies

$$s = -\frac{\int_{-\ell}^{\ell} B(X)\zeta(X)\,dX}{A_{\rm W}} \ .$$

Substituting (1.20) for ζ then gives

$$s = \frac{1}{1-F_h^2}\,\frac{U^2}{gS_0A_{\rm W}}\,\int_{-\ell}^{\ell} B(X)S(X)\,dX \ . \tag{1.21}$$

As well as being a simple estimate of the sinkage of a slender ship in a channel, this equation gives us a good insight into how the sinkage depends on speed, channel dimensions and ship dimensions. For example:

* In most practical situations F_h is quite small, so that $1/(1-F_h^2)$ is close to 1. This means that the sinkage is roughly proportional to the square of the ship's speed. However, at higher speeds, when F_h approaches 1, there is a singularity. When F_h is greater than one the sinkage is negative, meaning that the ship rises in the water instead of sinking.
* s is inversely proportional to S_0. For example, halving either the width or average depth of the channel will double the sinkage.
* For a given *shape* of ship, the sinkage is proportional to the maximum section area $S_{\rm max}$. Stretching the ship longitudinally will have no effect on the sinkage. Doubling the size of the ship in all dimensions, while keeping U and S_0 constant, will quadruple $S_{\rm max}$ and therefore quadruple the sinkage.

The singularity as $F_h \to 1$ is a resonance effect as the ship speed U approaches $\sqrt{gh}$, the natural speed of one-dimensional long waves in shallow water. Since the linearized theory predicts that any wave can travel unchanged in form at this speed, there is in effect no restoring force on the free surface. Therefore the ship sinks down indefinitely as $F_h \to 1$ from below, or rises indefinitely as $F_h \to 1$ from above. Since this situation does not happen in practice, the linearized solution is not valid when F_h is close to 1; in this region other effects have to be taken into account.

1.5 Solution of the nonlinear problem - fixed ship

If the ship's beam is comparable to the channel width, we cannot use the linearized approach, as the free surface height and velocity perturbation cannot be assumed small. In this case we must solve the simultaneous equations (1.3) and (1.6) exactly.

Eliminating $\tilde{q}$ between these equations gives the following cubic equation for the scaled free surface height $\tilde{\zeta}$:

$$\begin{aligned} &\frac{2}{F_h^2}\left(1-\frac{B}{w}\right)^2\tilde{\zeta}^3 + \left[\frac{4}{F_h^2}\left(1-\frac{S}{S_0}\right)\left(1-\frac{B}{w}\right) - \left(1-\frac{B}{w}\right)^2\right]\tilde{\zeta}^2 \\ +\ &\left[\frac{2}{F_h^2}\left(1-\frac{S}{S_0}\right)^2 - 2\left(1-\frac{S}{S_0}\right)\left(1-\frac{B}{w}\right)\right]\tilde{\zeta} - \left(1-\frac{S}{S_0}\right)^2 + 1 = 0 \ . \end{aligned} \tag{1.22}$$

Once $\tilde{\zeta}$ is found for all X, the sinkage and trim can be determined using equations (1.15).

1.5.1 Choosing the correct solution

The cubic equation (1.22) can have between one and three real roots, so we must be careful to choose the correct root.

The real root which is always present represents a backflow ($\tilde{q} < 0$) with $A(X) < 0$. This is unphysical and inadmissible. In order to find the correct solution, we can plot the continuity relation (1.3) and Bernoulli equation (1.6) for various values of F_h. This is depicted in Figure 1.4, with typical values $B/w = 0.15$ and $S/S_0 = 0.1$ having been chosen. Only the physically admissible branch $\tilde{q} > 0$ is shown. Since the continuity and Bernoulli relations must both be satisfied, the solution is given by the intersection of these curves for a given F_h.

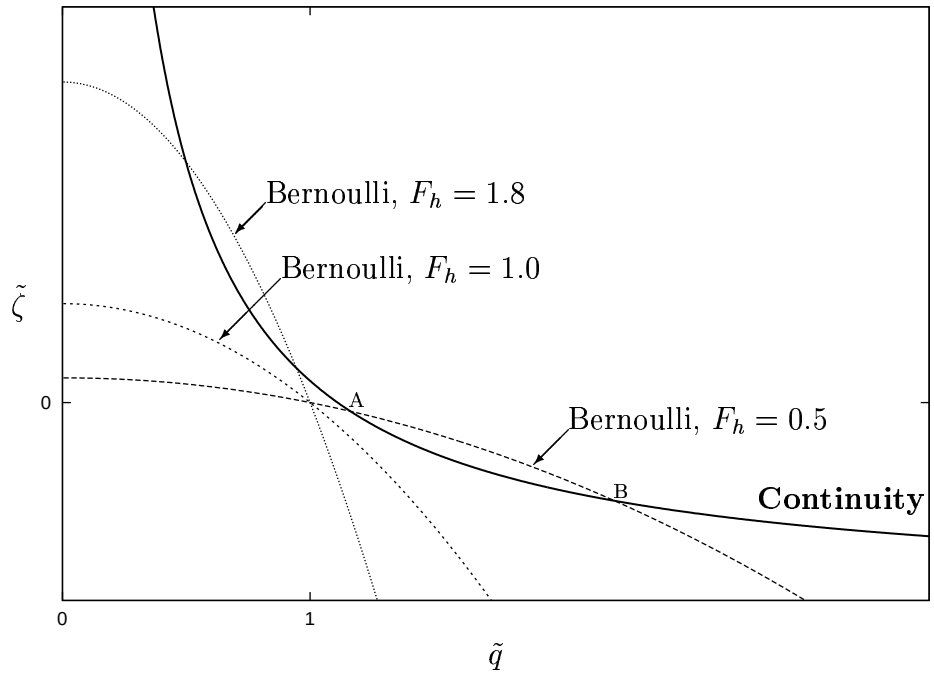

Figure 1.4: Typical continuity and Bernoulli relations between scaled free surface height $\tilde{\zeta}$ and scaled fluid speed $\tilde{q}$.

The continuity relation represents a hyperbola in the $\left(\tilde{q}, \tilde{\zeta}\right)$ plane, which is not explicitly dependent on F_h. The Bernoulli equation defines a concave-down parabola whose steepness increases with F_h. As recognized by Constantine (1961), there are three distinct flow scenarios, depending on the value of F_h.

We see that at low F_h (e.g. F_h=0.5 in Figure 1.4) there are two intersection points A,B in the region $\tilde{q} > 0$, both of which have $\tilde{q} > 1$. One of these (point B) represents a greatly accelerated flow past the ship ($\tilde{q} \gg 1$), with a greatly depressed free surface ($\tilde{\zeta} \ll 0$). The other intersection point (A) represents a slightly accelerated flow with a slightly

depressed free surface. In order to study the static stability of each of these solutions we write equation (1.7) as

$$\tilde{\zeta} + \frac{P_s}{\rho g h} = F_h^2 \left(1 - \tilde{q}^2\right) \tag{1.23}$$

where P_s is the actual fluid surface pressure. The Bernoulli curve corresponds to the equilibrium case when $P_s = 0$.

Looking first at intersection point A, we consider a small change in the free surface height, with continuity still satisfied, and see how this affects P_s. From Figure 1.4, when the free surface is raised from the intersection point (i.e. $\tilde{\zeta}$ is increased), the continuity curve lies above the Bernoulli curve. Therefore, following the continuity curve will give

$$\tilde{\zeta} > F_h^2 \left(1 - \tilde{q}^2\right)$$

and hence, from equation (1.23), $P_s < 0$. This drop in pressure will allow the atmospheric pressure to drive the free surface back to its equilibrium height. Similarly, a fall in free surface height will give $P_s > 0$ and a restoring force again. Therefore this intersection point is stable in a static sense.

Following the same reasoning with the other intersection point (B) shows that a small rise in the free surface from this equilibrium position will give a positive surface pressure. This will cause the free surface to continue rising rather than return to this equilibrium position. Similarly a small fall in the free surface height will cause it to keep falling. Therefore this situation of greatly accelerated flow past the ship, although it satisfies the continuity and Bernoulli equations, is unstable.

The two intersection points correspond to the "hydraulic jump" observed in channels (Stoker 1957). This is a sudden transition from a high speed, low free surface height flow to a low speed, large free surface height flow. Although both of these flow regimes satisfy the Bernoulli and continuity conditions, the latter only occurs downstream, with energy being lost across the transition. This is a special case of the problem solved here, in which no ship is present so that B/w and S/S_0 are zero.

The stable flow regime of slightly accelerated flow with a slightly depressed free surface, which occurs at low Froude numbers, is known as "subcritical" flow. This is the regime in which ships most often travel.

For intermediate values of F_h (e.g. F_h=1.0 in Figure 1.4) there are no intersection points with $\tilde{q} > 0$. This is the "critical" region in which no steady hydraulic flow exists, a situation which will be discussed in §1.8.

When F_h is large (e.g. F_h=1.8 in Figure 1.4) there are again two intersection points in the region $\tilde{q} > 0$. In this case, however, both roots have $\tilde{q} < 1$ and $\tilde{\zeta} > 0$. As for subcritical flow, we can show using surface pressure arguments that only the root with the higher free surface and lower speed is stable in a static sense. However, this solution involves a discontinuity at the bow and stern of the ship, which is inaccurate.

This 'supercritical" flow past a ship is therefore difficult to model using hydraulic theory. In any case, it is of less practical interest than subcritical flow for ships in narrow channels,

as a very high speed is normally required for steady supercritical flow to exist. We shall concentrate on subcritical flow for most of the remainder of this chapter.

1.6 A consistent nonlinear theory for sinkage and trim

In §1.4 we showed that the fixed-ship method is valid for linearized flow, as the flow field changes negligibly when the ship is allowed to squat. In this case the difference in flow velocities between a ship fixed in its equilibrium position and the same ship allowed to squat is of the same order as other terms already neglected.

However, if the ship's beam and draught are comparable to the width and depth respectively of the channel, the disturbance due to the ship is no longer small and we must use nonlinear theory. In this case the sinkage is also large, so that allowing the ship to squat will significantly change the flow. The fixed-ship method, which assumes that the flow will only change negligibly when the ship is allowed to squat, will be inaccurate.

Any nonlinear treatment of the problem should therefore solve the flow field as a function of the ship's sinkage and trim, and it is this method that we shall now develop. An outline of this method has appeared in Gourlay (1999).

Although the problem is solved here using one-dimensional hydraulic theory, the method for calculating sinkage and trim is applicable to any nonlinear theory for ship dynamics.

1.6.1 The hydraulic equations - ship free to squat

If the ship is in its squatted position as shown in Figure 1.3, this has the effect of changing the hull's underwater section area. If the ship sinks downwards the hull section area is effectively increased. When a hull cross-section of beam $B(X)$ sinks downwards by an amount $\sigma(X)$, the hull section area effectively increases by an amount $\sigma(X)B(X)$. Therefore equation (1.2) for the area taken up by the water passing the ship is replaced by

$$A(X) = S_0 - (S + \sigma B) + (w - B)\zeta \ . \tag{1.24}$$

Using equation (1.1), the continuity equation then becomes (c.f. equation (1.3))

$$\tilde{q}\left[1 - \frac{S}{S_0} - \tilde{\sigma}\frac{B}{w} + \left(1 - \frac{B}{w}\right)\tilde{\zeta}\right] = 1 \ , \tag{1.25}$$

where we have introduced the scaled local sinkage $\tilde{\sigma} = \sigma/h$. The Bernoulli equation (1.6) remains unchanged when the ship is allowed to squat.

If $\tilde{\sigma}(X)$ is known, the continuity equation (1.25) and Bernoulli equation (1.6) constitute two simultaneous equations which can be solved for the unknowns $\tilde{\zeta}$ and $\tilde{q}$ at each value

of X. Specifically, eliminating $\tilde{q}$ gives the following cubic equation for the scaled free surface height $\tilde{\zeta}$:

$$\frac{2}{F_h^2}\left(1-\frac{B}{w}\right)^2\tilde{\zeta}^3+\left[\frac{4}{F_h^2}\left(1-\frac{S}{S_0}-\tilde{\sigma}\frac{B}{w}\right)\left(1-\frac{B}{w}\right)-\left(1-\frac{B}{w}\right)^2\right]\tilde{\zeta}^2 \tag{1.26}$$
$$+\left[\frac{2}{F_h^2}\left(1-\frac{S}{S_0}-\tilde{\sigma}\frac{B}{w}\right)^2-2\left(1-\frac{S}{S_0}-\tilde{\sigma}\frac{B}{w}\right)\left(1-\frac{B}{w}\right)\right]\tilde{\zeta}-\left(1-\frac{S}{S_0}-\tilde{\sigma}\frac{B}{w}\right)^2+1=0\,.$$

The nature of these solutions and the criteria for choosing the correct solution are the same as in §1.5.1.

So if $\tilde{\sigma}(X)$ is known, we can determine the correct profile of $\tilde{\zeta}(X)$ using Newton's iterative method to solve (1.26) for each value of X. However, $\tilde{\sigma}(X)$ is not known in advance; the two equations which determine its two unknowns s,θ are the vertical force and trim moment equilibrium equations (1.14). Dividing these equations through by h, we write them in terms of the non-dimensional quantities $\tilde{\zeta},\tilde{\sigma}$ as

$$\int_{-\ell}^{\ell} B(X)\,\left\{\tilde{\zeta}(X)+\tilde{\sigma}(X)\right\}\,dX=0 \tag{1.27}$$

and

$$\int_{-\ell}^{\ell} X\,B(X)\,\left\{\tilde{\zeta}(X)+\tilde{\sigma}(X)\right\}\,dX=0\,. \tag{1.28}$$

Using $\sigma = s + X\tan\theta$, equations (1.26),(1.27) and (1.28) now constitute three simultaneous equations for the unknowns s,θ and $\tilde{\zeta}(X)$. In general these cannot be solved explicitly, so an iterative method is required.

As was done in §1.4, we can infer a few things at this point about how the sinkage and trim scale with the different parameters. For example, equation (1.26) is in the dimensionless form

$$f_1\left(\tilde{\zeta},\tilde{\sigma},\frac{S}{S_0},\frac{B}{w},F_h\right)=0 \tag{1.29}$$

for some function f_1. If we scale the expressions (1.15) with respect to suitable length scales in the X and y directions (e.g. ship length L and maximum beam $B_{\max}$ respectively), we find that these length scales cancel for s and result in a $(1/L)$ factor for $\tan\theta$. Scaling by the depth h in the z direction results in a factor of h for both s and $\tan\theta$. Therefore, from (1.15), we can state that

$$s = h\,f_2\left(\tilde{\zeta}\right)$$

$$\tan\theta = \frac{h}{L}\,f_3\left(\tilde{\zeta}\right)$$

where the dimensionless functions f_2, f_3 depend only on the *shape* of ship and are unaffected by stretching in the X and y directions. Combining each of these with the relation (1.29) allows us to infer that

$$\frac{s}{h} = f_4\left(\frac{S_{\max}}{S_0},\frac{B_{\max}}{w},F_h\right)$$

$$\tan\theta = \frac{h}{L}\, f_5\left(\frac{S_{\max}}{S_0}, \frac{B_{\max}}{w}, F_h\right)$$

for some dimensionless functions f_4, f_5.

Obviously this dimensional analysis does not give us nearly as much information as the simple solution furnished by linearized theory. However, we can infer the following: if, for a given shape of ship, the parameters are changed in such a way as to keep $S_{\max}/S_0, B_{\max}/w$ and F_h the same, then s/h and $L\tan\theta/h$ will stay the same. For example, stretching the ship in the longitudinal direction will have no effect on the midship sinkage s, but $\tan\theta$ will change in inverse proportion to the ship length. As another example, changing the ship's beam and the channel width by the same factor will have no effect on the sinkage or trim.

We now consider three different cases of varying complexity for a ship that is free to squat.

1.6.2 Special case: block-like ship

The problem of nonlinear hydraulic flow around a block-shaped ship that is free to squat was solved by Constantine (1961). In this case $B(X)$ and $S(X)$ are constant along the entire length of the ship, corresponding to a ship of constant cross-section with a blunt bow and stern. Although the assumptions of hydraulic theory are violated near these discontinuities, the hydraulic theory is only invalid over a small region. Overall quantities such as sinkage as trim are presumed to be negligibly affected.

If $B(X)$ and $S(X)$ are constant, this means that the free surface elevation $\zeta(X)$ is also constant along the entire length of the ship (with a step discontinuity at the bow and stern). Since the fluid pressure is hydrostatic (see §1.3), Archimedes' principle states that the ship must sink the same amount as the free surface. In other words, the waterline always remains at the same level on the ship. Therefore

$$\sigma = -\zeta \tag{1.30}$$

which greatly simplifies the solution. Equation (1.24) for $A(X)$ now becomes

$$A(X) = S_0 - S + w\zeta\ .$$

We notice that in this case the ship's beam has no effect on the hydrodynamics.

In fact, this problem is equivalent to that of a ship with the same cross-sectional area but zero beam. In that case it does not matter whether the ship is fixed or free to squat. Alternatively, it could represent the flow over an underwater hump. In all cases a free surface elevation of ζ changes $A(X)$ by an amount $w\zeta$.

Using the above expression for $A(X)$, the cubic equation for $\tilde{\zeta}$ becomes

$$\begin{aligned} &\frac{2}{F_h^2}\tilde{\zeta}^3 + \left[\frac{4}{F_h^2}\left(1-\frac{S}{S_0}\right) - 1\right]\tilde{\zeta}^2 \\ +\ &\left[\frac{2}{F_h^2}\left(1-\frac{S}{S_0}\right)^2 - 2\left(1-\frac{S}{S_0}\right)\right]\tilde{\zeta} - \left(1-\frac{S}{S_0}\right)^2 + 1 = 0\ . \end{aligned} \tag{1.31}$$

This is solved using the constant values of S and B. The sinkage σ, which is also constant along the entire length of the ship, is then found using (1.30).

1.6.3 Simple case: fore-aft symmetric ship

For a fore-aft symmetric ship, the hydraulic theory predicts zero trim angle ($\theta = 0$) whenever a steady solution exists. $\tilde{\sigma}$ is therefore constant in X, and we only require the force balance equation (1.27) in addition to the cubic (1.26) for $\tilde{\zeta}(X)$. Whereas for the block ship just considered the sinkage was equal to the constant free surface depression, for a fore-aft symmetric ship the sinkage is a weighted average of the free surface depression.

Since we cannot solve (1.26) and (1.27) explicitly for $\tilde{\sigma}$, we consider the scaled net vertical force function

$$f(\tilde{\sigma}) = \int_{-\ell}^{\ell} B(X) \left\{ \tilde{\zeta}(X) + \tilde{\sigma}(X) \right\} dX \ , \tag{1.32}$$

which we require to be zero. Guessing an initial value for $\tilde{\sigma}$ gives the corresponding profile of $\tilde{\zeta}(X)$ by solving (1.26) at every position X. This is then used in (1.32) to find $f(\tilde{\sigma})$. If we do this with two different guesses $\tilde{\sigma} = \tilde{\sigma}_0, \tilde{\sigma}_1$ we can use the secant method (see e.g. Kreyszig 1993) to find a better estimate $\tilde{\sigma} = \tilde{\sigma}_2$, namely

$$\tilde{\sigma}_2 = \frac{\tilde{\sigma}_1 f(\tilde{\sigma}_0) - \tilde{\sigma}_0 f(\tilde{\sigma}_1)}{f(\tilde{\sigma}_0) - f(\tilde{\sigma}_1)} \ . \tag{1.33}$$

Discarding whichever of the previous estimates $\tilde{\sigma}_0$ and $\tilde{\sigma}_1$ has the largest value of $|f(\sigma)|$, we can then continue the process until the converged solution for $\tilde{\sigma}$ and corresponding profile of $\tilde{\zeta}(X)$ are found.

In practice, the numerical method involves discretizing X, so that equation (1.26) is solved at a finite number of gridpoints. The integral (1.32) is then evaluated using Simpson's method.

1.6.4 General-shaped ship

For a general-shaped ship, the sinkage function $\sigma(X)$ has two unknowns, s and θ. These, along with $\tilde{\zeta}(X)$, must satisfy the force balance equation (1.27), moment balance equation (1.28) and cubic (1.26) for $\tilde{\zeta}(X)$. As such we have three equations and three unknowns. However, for any pair of values for (s, θ) we can solve (1.26) explicitly for $\tilde{\zeta}(X)$. Therefore, in effect, we need only consider the two simultaneous equations (1.27) and (1.28), with $\tilde{\zeta}(X)$ being a known function of (s, θ).

In order to solve the two simultaneous equations, we employ a simple Newton method that uses secant-type approximations to the derivatives. The general method is described in Broyden (1965).

The force and moment balance equations (1.27) and (1.28) can be written in terms of the two functions

$$f(s,\theta) = \int_{-\ell}^{\ell} B(X) \left\{ \tilde{\zeta}(X) + \frac{s}{h} + \frac{X}{h}\tan\theta \right\} dX \tag{1.34}$$

and

$$m(s,\theta) = \int_{-\ell}^{\ell} X\, B(X) \left\{ \tilde{\zeta}(X) + \frac{s}{h} + \frac{X}{h}\tan\theta \right\} dX \ , \tag{1.35}$$

both of which we require to be zero for the ship to be in equilibrium. In equations (1.34) and (1.35), $\tilde{\zeta}(X)$ is found in terms of (s,θ) by using Newton's iterative method to solve (1.26). The correct solution for $\tilde{\zeta}(X)$ is chosen in the same manner as described in §1.5.1.

Suppose the correct solution that we are seeking for (s,θ) is $(\bar{s},\bar{\theta})$, and we make an estimate (s_0,θ_0). A Taylor Series approximation states that

$$f(s_0,\theta_0) + \frac{\partial f}{\partial s}(\bar{s}-s_0) + \frac{\partial f}{\partial \theta}(\bar{\theta}-\theta_0) \approx f(\bar{s},\bar{\theta}) = 0$$

$$m(s_0,\theta_0) + \frac{\partial m}{\partial s}(\bar{s}-s_0) + \frac{\partial m}{\partial \theta}(\bar{\theta}-\theta_0) \approx m(\bar{s},\bar{\theta}) = 0 \ , \tag{1.36}$$

where all derivatives are supposed to be evaluated at (s_0,θ_0).

If we can approximate the derivatives in equations (1.36), we can solve simultaneously for $(\bar{s},\bar{\theta})$ to give

$$\bar{s} \approx s_0 + \frac{f(s_0,\theta_0)\frac{\partial m}{\partial \theta} - m(s_0,\theta_0)\frac{\partial f}{\partial \theta}}{\frac{\partial f}{\partial \theta}\frac{\partial m}{\partial s} - \frac{\partial m}{\partial \theta}\frac{\partial f}{\partial s}}$$

$$\bar{\theta} \approx \theta_0 + \frac{f(s_0,\theta_0)\frac{\partial m}{\partial s} - m(s_0,\theta_0)\frac{\partial f}{\partial s}}{\frac{\partial f}{\partial s}\frac{\partial m}{\partial \theta} - \frac{\partial m}{\partial s}\frac{\partial f}{\partial \theta}} \ . \tag{1.37}$$

In order to approximate the derivatives in equations (1.37) we need two more points $(s_1,\theta_1),(s_2,\theta_2)$ and their associated functional values for $f(s,\theta)$ and $m(s,\theta)$. Using a similar Taylor expansion to (1.36) we can write

$$f(s_1,\theta_1) \approx f(s_0,\theta_0) + \frac{\partial f}{\partial s}(s_1-s_0) + \frac{\partial f}{\partial \theta}(\theta_1-\theta_0)$$

$$f(s_2,\theta_2) \approx f(s_0,\theta_0) + \frac{\partial f}{\partial s}(s_2-s_0) + \frac{\partial f}{\partial \theta}(\theta_2-\theta_0) \tag{1.38}$$

and similarly for the function $m(s,\theta)$. Again, the derivatives are presumed evaluated at (s_0,θ_0).

We can now solve equations (1.38) simultaneously for the partial derivatives, since all the other quantities are known. This gives

$$\frac{\partial f}{\partial s} \approx \frac{(\theta_2 - \theta_0)\,[f(s_1,\theta_1) - f(s_0,\theta_0)] - (\theta_1 - \theta_0)\,[f(s_2,\theta_2) - f(s_0,\theta_0)]}{(\theta_2 - \theta_0)(s_1 - s_0) - (\theta_1 - \theta_0)(s_2 - s_0)}$$

$$\frac{\partial f}{\partial \theta} \approx \frac{(s_2 - s_0)\,[f(\theta_1,s_1) - f(\theta_0,s_0)] - (s_1 - s_0)\,[f(\theta_2,s_2) - f(\theta_0,s_0)]}{(s_2 - s_0)(\theta_1 - \theta_0) - (s_1 - s_0)(\theta_2 - \theta_0)} \tag{1.39}$$

with similar expressions for $m(s,\theta)$. These derivatives can then be substituted into the approximation (1.37) for $(\bar{s},\bar{\theta})$.

Once the new estimate from equations (1.37) is found, the process can then be repeated using this new point (s,θ) and two of the old points. To decide which of the old points to reject, we use here the error criterion $|f(s_j,\theta_j)| + |m(s_j,\theta_j)|$, and reject the pair of values (s,θ) with the largest error under this criterion. A satisfactory solution is obtained when the error falls below a small pre-determined value.

1.7 Results for sinkage and trim

Here we show results for sinkage and trim as predicted by the nonlinear free-ship method. For comparison we show how these results differ from those obtained using the nonlinear fixed-ship method.

We consider two different hull shapes: a fore-aft symmetric parabolic hull and a non-symmetric bulk carrier hull.

1.7.1 Fore-aft symmetric ship

As an example of a fore-aft symmetric ship, we consider a Wigley hull (Shearer & Cross 1965). This mathematically-defined hull has constant draught, with a parabolic water-plane and parabolic cross-sections. Its local beam and section area curves satisfy

$$B(X) = B_{\max}\left(1 - \frac{X^2}{\ell^2}\right)$$

$$S(X) = \frac{2}{3}TB(X)\,, \tag{1.40}$$

where $B_{\max}$ is the maximum beam and T is the constant draught.

For the purpose of these results we have chosen the ship to be of length $2\ell = 200$ metres, maximum beam $B_{\max} = 40$ metres and draught $T = 9$ metres. It is travelling in a channel of width $w = 100$ metres and average depth $h = 12$ metres. Therefore in this situation we have $B_{\max}/w = 0.4$. The maximum blockage coefficient is

$$S_{\max}/S_0 = \frac{2}{3}\,\frac{TB_{\max}}{wh} = 0.2\,.$$

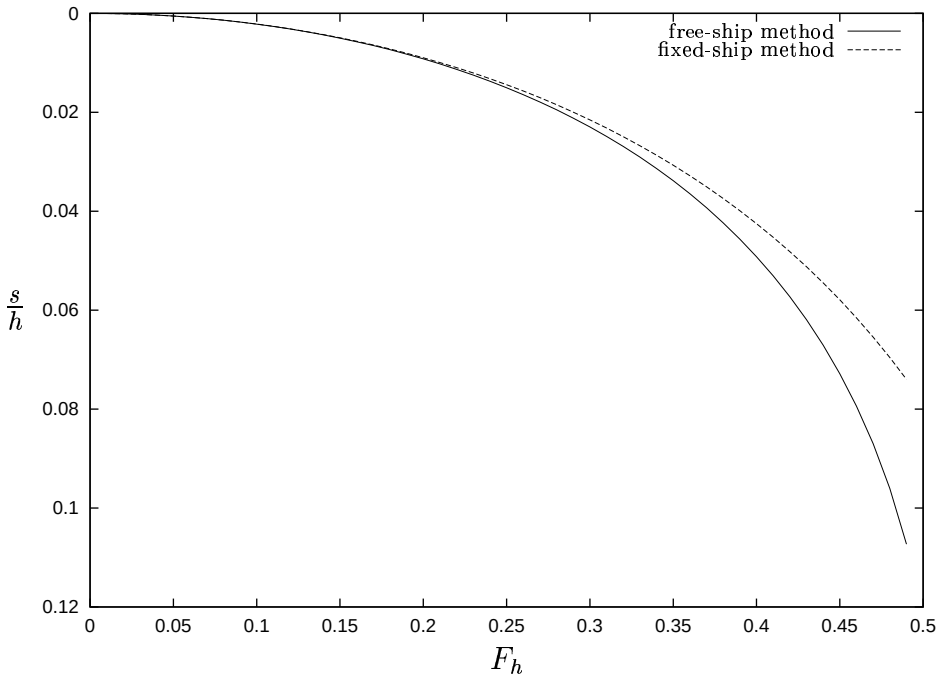

Figure 1.5: Scaled sinkage relative to water depth, as a function of Froude number, for a Wigley hull with $B_{\max}/w = 0.4$, $S/S_0 = 0.2$.

Figure 1.5 gives the scaled sinkage s/h of the Wigley hull as a function of Froude number. This is found using both the free-ship and fixed-ship methods. The range of F_h chosen is from zero up to 0.49, which is near the upper limit of steady subcritical flow for this ship and channel.

We can see that the fixed-ship method provides a good approximation when F_h is small. This is to be expected because ζ and σ are also small and the flow is not significantly affected by allowing the ship to squat.

However, for larger subcritical F_h, there is a marked increase in the sinkage from that predicted using the fixed-ship method. This is because the sinkage is now large enough to significantly affect the flow. Specifically, the ship's sinkage increases the effective hull section area, causing a greater free surface depression than for the fixed ship and giving a larger predicted sinkage. For large subcritical sinkages, this effect becomes increasingly apparent.

For example, we see that when $F_h = 0.38$ (corresponding to a ship speed of 4.1 m/s or 8.0 knots) we have a scaled sinkage s/h of 0.0423, compared to 0.0374 for the fixed-ship method. This corresponds to an actual sinkage of 0.51 metres, compared to 0.45 metres as predicted by the fixed-ship method.

When $F_h = 0.49$ (corresponding to a ship speed of 5.3 m/s or 10.3 knots) the sinkage is 1.28 metres, compared to only 0.89 metres as predicted by the fixed-ship method.

1.7.2 Bulk carrier hull

We now consider a MarAd L-Series hull (Roseman 1987) of the same length, draught and maximum beam as the Wigley hull described in §1.7.1, travelling along the same channel. This ship is much more block-like, so the maximum blockage coefficient is $S_{\max}/S_0 = 0.297$. Because of the larger blockage coefficient, the sinkage is larger than for the Wigley hull at a given Froude number. Also, as we shall see in §1.8, this larger blockage coefficient decreases the upper limit of steady subcritical flow. In this case, steady subcritical flow is only possible up to $F_h \approx 0.38$.

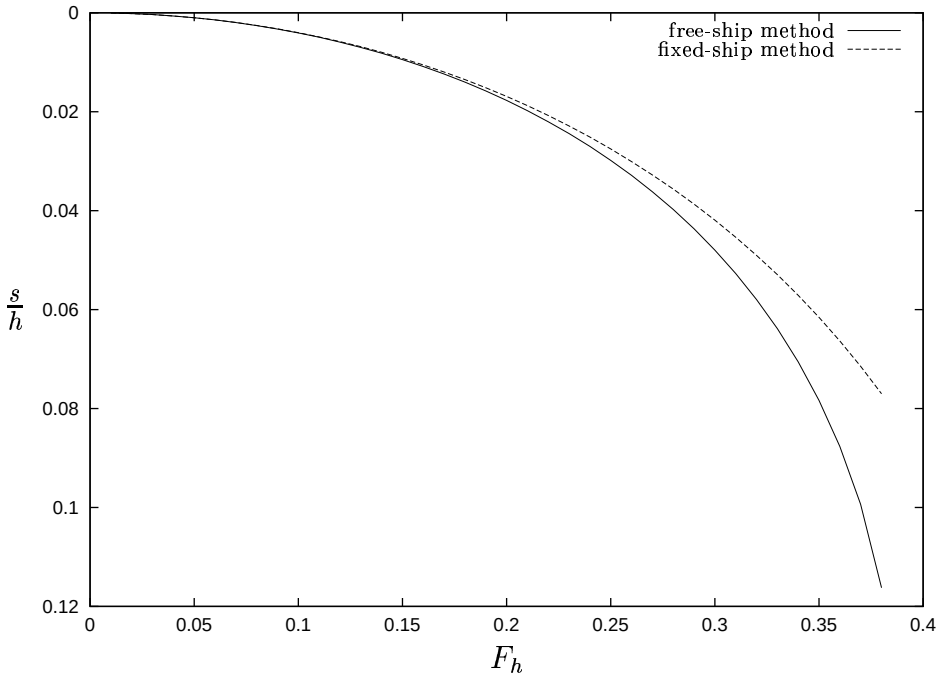

Figure 1.6: Scaled midships sinkage for a MarAd hull, with $B_{\max}/w = 0.4$, $S_{\max}/S_0 = 0.297$, $2\ell/h = 200/12$.

Figure 1.6 shows the scaled midship sinkage of the MarAd hull, using both the free-ship and fixed-ship methods. We can see again that the fixed-ship method greatly underestimates the sinkage for larger Froude numbers.

The trim angle of the MarAd hull as a function of Froude number is plotted in Figure 1.7. Because $S(X)$ is greater toward the bow than the stern for this ship (the centre of buoyancy lies forward of midships) the trim is bow-down, or negative by our definition.

As for the midship sinkage, the trim has a roughly quadratic dependence on speed. Also, we see that the magnitude of the free-ship trim increases markedly from the fixed-ship prediction when we allow the ship to squat.

From the graphs we see that when $F_h = 0.38$ (corresponding to a ship speed of 4.1 m/s or 8.0 knots) we have a scaled midship sinkage s/h of 0.116 and bow-down trim angle of 0.376 degrees. Because of this bow-down trim, the bow of the ship will have a greater sinkage (s_{bow}) than the stern (s_{stern}).

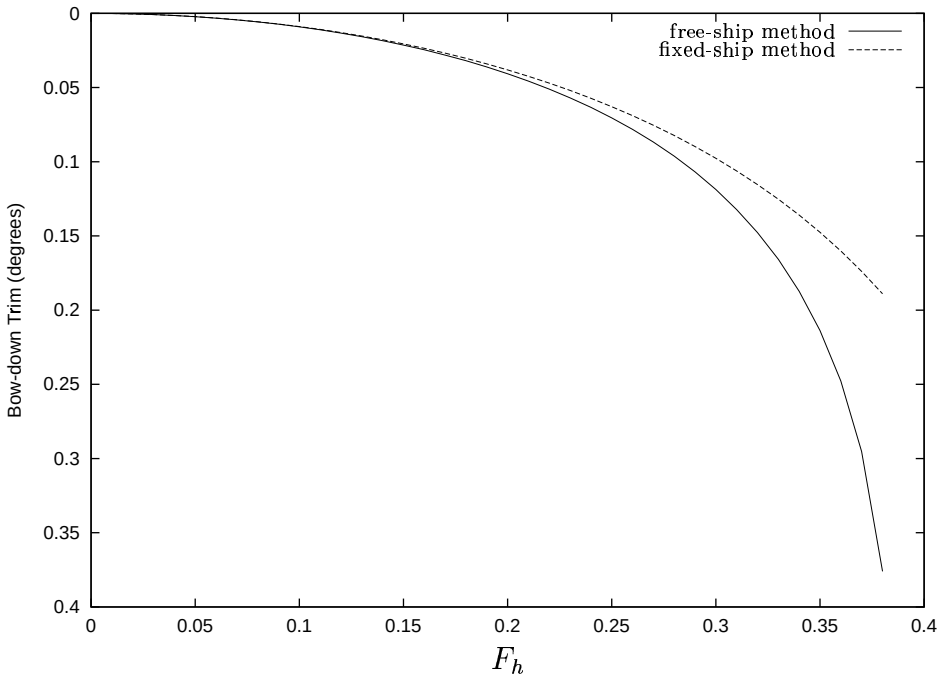

Figure 1.7: Bow-down trim (in degrees) for a MarAd hull, with $B_{\max}/w = 0.4$, $S_{\max}/S_0 = 0.297$, $2\ell/h = 200/12$.

We can use the relationship

$$\begin{aligned} s_{\text{bow}} &= s - \ell \sin\theta \\ s_{\text{stern}} &= s + \ell \sin\theta \,, \end{aligned} \tag{1.41}$$

noting that θ is measured positive in the bow-up sense, to find the bow and stern sinkage explicitly.

When $F_h = 0.38$, the free-ship method gives a stern sinkage $s_{\text{stern}} = 0.736$ metres and bow sinkage $s_{\text{bow}} = 2.05$ metres. In comparison, the fixed-ship method only predicts $s_{\text{stern}} = 0.594$ metres and $s_{\text{bow}} = 1.25$ metres. Here we see clearly how much the fixed-ship method can underestimate the sinkage.

1.8 Existence of steady flow

We saw in §1.4 that linearized hydraulic theory predicts a singularity in the flow when $F_h = 1$. Then, in §1.5.1, we found that the more accurate nonlinear theory predicts that no steady solution will exist in a "critical" region of finite extent around $F_h = 1$.

In this critical region, there is no admissible steady hydraulic flow for which the continuity and Bernoulli conditions can be satisfied simultaneously. Physically, continuity past the ship cannot be satisfied without an increase in the energy of the system. This leads to a piling up of water at the bow of the ship and, according to hydraulic theory, a shelf of water radiating away ahead of the ship and a trough behind (Constantine 1961). This

"bore" solution only occurs near the upper end of the critical region; at lower Froude numbers, the actual process involves nearly-periodic production of solitary waves that move ahead of the ship (see e.g. Huang et al 1982).

Here we show how the boundaries of steady flow, according to nonlinear hydraulic theory, can be calculated. We will denote these boundaries as the "limiting Froude numbers" $F_{\rm lim}^-$ and $F_{\rm lim}^+$, such that no steady hydraulic flow exists when F_h is in the range $F_{\rm lim}^- < F_h < F_{\rm lim}^+$. Like the sinkage and trim, the values of $F_{\rm lim}^-$ and $F_{\rm lim}^+$ change when we allow the ship to squat.

Let us consider the general case of a ship that is free to squat. In this case the flow is governed by the continuity equation (1.25) and Bernoulli equation (1.6). Writing $\tilde{\zeta}$ as the subject of each of these equations yields the alternative forms

$$\tilde{\zeta} = \frac{1}{1-\frac{B}{w}}\left(\frac{1}{\tilde{q}} - 1 + \frac{S}{S_0} + \tilde{\sigma}\frac{B}{w}\right) \tag{1.42}$$

and

$$\tilde{\zeta} = \frac{F_h^2}{2}\left(1-\tilde{q}^2\right) \ . \tag{1.43}$$

These are the relations plotted in Figure 1.4, with the parameters $S/S_0 = 0.1$, $B/w = 0.15$ and $\tilde{\sigma} = 0$ having been chosen.

We saw in §1.5.1 that for either low or high Froude numbers, the continuity and Bernoulli curves had two intersection points for which $\tilde{q} > 0$. At intermediate Froude numbers there were no intersection points with $\tilde{q} > 0$, and this is when no steady solution exists. Therefore, the boundaries of the critical region will occur at those Froude numbers for which the continuity and Bernoulli curves are *tangent* to each other.

To find when this occurs, we equate the gradients $d\tilde{\zeta}/d\tilde{q}$ of the two curves (1.42) and (1.43), giving

$$-\frac{1}{\tilde{q}^2\left(1-\frac{B}{w}\right)} = -F_h^2\tilde{q} \ .$$

However, $\tilde{q}$ is known in terms of F_h, by solving equations (1.42) and (1.43) simultaneously to give

$$\frac{1}{1-\frac{B}{w}}\left(\frac{1}{\tilde{q}} - 1 + \frac{S}{S_0} + \tilde{\sigma}\frac{B}{w}\right) = \frac{F_h^2}{2}\left(1-\tilde{q}^2\right) \ .$$

Eliminating $\tilde{q}$ between these two equations gives the equation satisfied by the limiting Froude numbers:

$$3\left[F_h^2\left(1-\frac{B}{w}\right)\right]^{1/3} - F_h^2\left(1-\frac{B}{w}\right) = 2\left(1-\frac{S}{S_0}-\tilde{\sigma}\frac{B}{w}\right) \ . \tag{1.44}$$

The transcendental equation (1.44) can be solved for F_h using a simple Newton iterative method.

As an example, solving equation (1.44) with the parameters used in Figure 1.4 ($S/S_0 = 0.1$, $B/w = 0.15$ and $\tilde{\sigma} = 0$) gives the two solutions $F_{\rm lim}^- = 0.6755$ and $F_{\rm lim}^+ = 1.5125$.

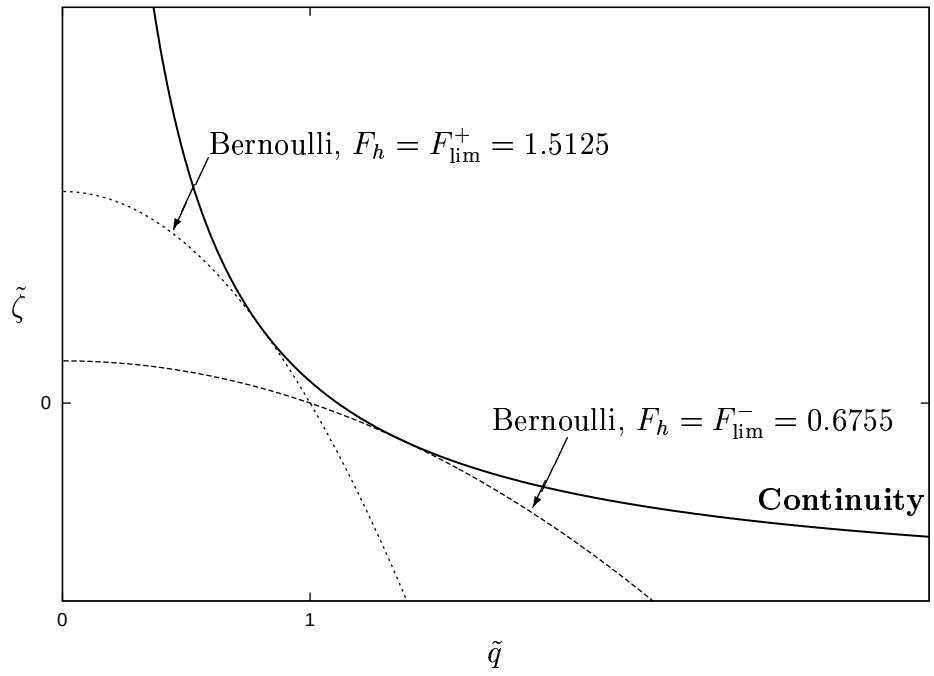

Figure 1.8: Continuity and Bernoulli relations at the limiting Froude numbers $F^-_{\rm lim}$ and $F^+_{\rm lim}$, with $S/S_0 = 0.1$, $B/w = 0.15$ and $\tilde{\sigma} = 0$.

In Figure 1.8 we have plotted the Bernoulli curves for each of these Froude numbers, along with the continuity equation. We can see how the continuity and Bernoulli curves become tangent to each other at these limiting Froude numbers.

We now consider separately the cases of a fixed ship, block ship free to squat and general ship free to squat.

1.8.1 Fixed ship

For a fixed ship, we need only consider the special case of equation (1.44) in which $\tilde{\sigma} = 0$. In this case the limiting Froude numbers are the solutions of

$$3\left[F_h^2\left(1-\frac{B}{w}\right)\right]^{1/3} - F_h^2\left(1-\frac{B}{w}\right) = 2\left(1-\frac{S}{S_0}\right) \tag{1.45}$$

which was obtained by Tuck (1974).

Until now we have not discussed exactly how equation (1.44) is to be implemented. The hydraulic theory is a local theory in that the flow at any station X depends only on the values of S and B at that station. This is not quite true for a free ship, because $\tilde{\sigma}$ depends on the values of S and B over the entire shiplength. However, for a fixed ship, the flow speed, free surface height and corresponding limiting Froude numbers depend only on the local values of S and B.

This means that every station X, having different values of S and B, can be considered to have its own limiting Froude numbers. These *local* limiting Froude numbers $F^-(X)$ and $F^+(X)$ are the solutions of equation (1.45) for particular values of $S(X)$ and $B(X)$. However, for a steady flow to exist, it must exist along the entire length of the ship. Therefore, the actual limiting Froude numbers for a particular ship are given by

$$F^-_{\text{lim}} = \min_X F^-(X)$$

$$F^+_{\text{lim}} = \max_X F^+(X) \ . \tag{1.46}$$

These extremes may occur anywhere along the ship's length, although they usually occur at the ship cross-section of largest area.

At this point it is worthwhile making a few observations about the local limiting Froude numbers. Firstly, F^- and F^+ both move further away from unity as the blockage coefficient S/S_0 increases. This is well known. However, it is not just the blockage coefficient that determines whether a steady solution exists.

For a fixed ship, any change $\delta\zeta$ in the free surface height produces a change $(w-B)\delta\zeta$ in $A(X)$, the local cross-sectional area taken up by the water. Therefore, if the ship's beam is comparable to the width of the channel, the free surface can drop markedly with little effect on $A(X)$. This allows subcritical flow to exist at higher Froude numbers, since dropping the free surface allows the fluid speed to increase (by Bernoulli's equation), so that continuity can still be satisfied.

We can see explicitly the effect of beam/channel-width ratio by writing (1.45) in the form

$$F^- = \frac{1}{\sqrt{1-\frac{B}{w}}}\, G^-\left(\frac{S}{S_0}\right)$$

$$F^+ = \frac{1}{\sqrt{1-\frac{B}{w}}}\, G^+\left(\frac{S}{S_0}\right) \tag{1.47}$$

for some functions G^-, G^+.

This shows that increasing the B/w ratio while maintaining a fixed blockage coefficient S/S_0 will increase both F^- and F^+ by the factor $1/\sqrt{1-\frac{B}{w}}$. Of particular interest, F^- decreases with S/S_0 but increases with B/w.

In Figures 1.9 and 1.10 we have solved (1.45) numerically for a range of blockage coefficients and beam/channel-width ratios. Here we see clearly how F^- and F^+ increase with the beam/channel-width ratio. In fact, for hull sections with small blockage coefficients but large beam/channel-width ratios (e.g. a section of small draught but large beam), F^- may be greater than one.

For a block-like ship, it is actually possible to have $F^- > 1$ along the entire ship, so that $F^-_{\text{lim}} > 1$. Hence, a fixed block-like ship of small draught and large beam can sustain steady flow, according to hydraulic theory, at Froude numbers up to and above $F_h = 1$.

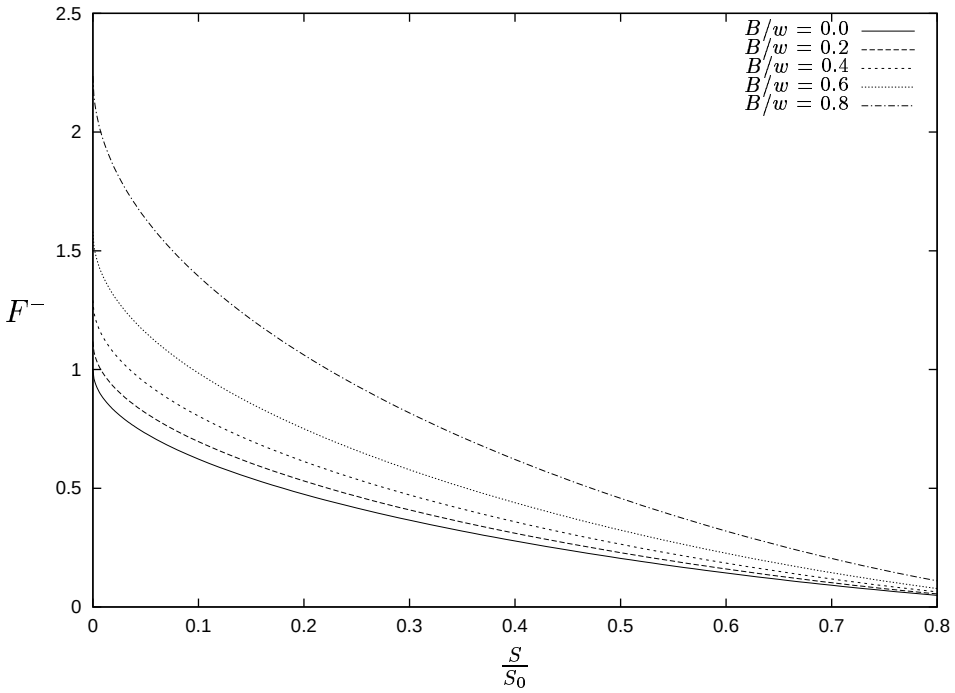

Figure 1.9: Local limiting Froude number for steady subcritical flow around a fixed ship, as a function of blockage coefficient. Five different beam/channel-width ratios are considered.

However, this is impossible in practice; the hydraulic theory is not valid in this case, as the assumptions for one-dimensional flow are violated at a blunt bow or stern.

Because of the contrasting dependence of F^- on S and B, the "critical section" of the ship, where $F^-_{\text{lim}} = F^-$, need not necessarily be the hull section of largest area. It could occur anywhere along the ship, even at the ends.

For example, a section with small blockage coefficient but large beam/channel-width ratio can have $F^- > 1$, as mentioned previously. If the ship has a sharp bow or stern, it must have $F^- = 1$ at the ends (because $F^- \to 1$ as $S, B \to 0$). Therefore in this case the ship sustains steady flow at Froude numbers up to $F_h = 1$, when the ends dictate the beginning of unsteady flow.

One more property of equation (1.45) is that the point on the ship where F^- is minimized will in general not be the same point where F^+ is maximized. That is, the critical section that determines F^-_{lim} will not always be the same critical section that determines F^+_{lim}.

Comparison with experimental results

Tests were undertaken by the author at the Australian Maritime College, in part to study the transition between unsteady critical and steady supercritical flow. A 1.6 metre-long high-speed displacement hull was used, which was fixed to the carriage in its design waterline position and not allowed to sink or trim. The model and channel were such

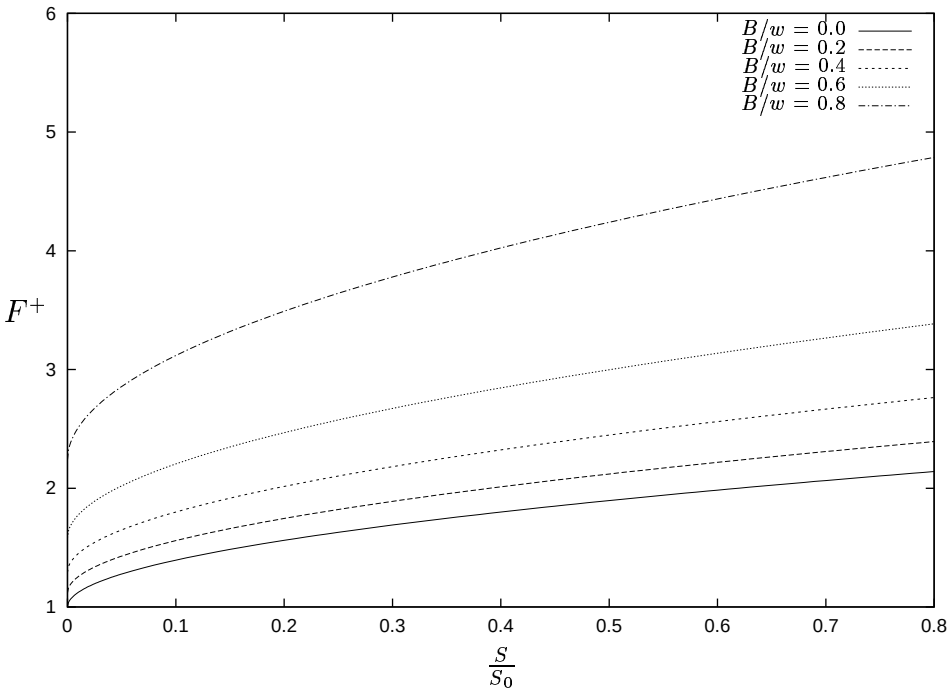

Figure 1.10: Local limiting Froude number for steady supercritical flow around a fixed ship, as a function of blockage coefficient. Five different beam/channel-width ratios are considered.

that $B_{\max}/w = 0.1143$.

Runs were made for gradually incremented speeds, with wave probes positioned along the tank and video footage showing the changing nature of the waves ahead of the ship. For Froude numbers near the upper end of the critical range, a one-dimensional bore was radiated ahead of the ship. At higher Froude numbers, a sudden transition to steady supercritical flow was witnessed, as the bore ceased to be produced. The Froude number at which this occurred was measured and compared to that predicted by equation (1.45).

Two different water depths were used. For the shallower water ($h/T = 1.14$), the maximum blockage coefficient was $S_{\max}/S_0 = 0.0802$. For this ship and channel the critical section is the largest section; substituting the maximum values of S/S_0 and B/w into equation (1.45) gives a Froude number limit of $F^+_{\text{lim}} = 1.44$ as predicted by the hydraulic theory. The transition occurred experimentally at $F_h = 1.48$.

In the deeper water ($h/T = 2.05$), the maximum blockage coefficient was $S_{\max}/S_0 = 0.0446$. This gives $F^+_{\text{lim}} = 1.34$ according to the hydraulic theory, compared to the experimental transition at $F_h = 1.31$. We see that for both these depths the hydraulic theory predicts the transition to steady supercritical flow with reasonable accuracy.

1.8.2 Block-like ship free to squat

As we saw in §1.6.2, the hydraulic equations for a block-like ship that is free to squat can be obtained by setting $B = 0$ in the general free-ship hydraulic equations. If we set $B = 0$ in equation (1.44), we find that the limiting Froude numbers satisfy

$$3F_h^{2/3} - F_h^2 = 2\left(1 - \frac{S}{S_0}\right) \tag{1.48}$$

for a block-like ship that is free to squat. This simple equation was obtained by Tuck & Taylor (1970). We do not need to use $F^-(X)$ and $F^+(X)$ here, since S/S_0 is constant along the ship's entire length. The solutions of (1.48) for F_h are the overall limiting Froude numbers F_{lim}^- and F_{lim}^+.

Because the ship's beam has no effect on the hydrodynamics in this case, the limiting Froude numbers depend only on the blockage coefficient. As we can see from the $B/w = 0$ case in Figures 1.9 and 1.10 (which corresponds to a block-like ship free to squat), F_{lim}^- and F_{lim}^+ tend to the linearized critical value of 1 as $S/S_0 \to 0$.

1.8.3 General ship free to squat

When we were computing the sinkage of the Wigley and MarAd hulls described in §1.7.1 and §1.7.2, we increased the Froude number slowly so that we were able to get quite close to the Froude number limit of steady subcritical flow. Due to the iterative process, solutions for $\tilde{\zeta}(X)$ cannot always be found when F_h is close to this limit. However, increasing the Froude number slowly and using the previous value for $\tilde{\sigma}$ as a first estimate will give a fair estimate of the limiting Froude number for a ship that is free to squat. For example, F_{lim}^- is slightly greater than 0.49 for the Wigley hull considered, and slightly greater than 0.38 for the MarAd hull.

A more direct method of finding F_{lim}^- for a general ship that is free to squat is to solve equation (1.44). However, in this case the problem is more complicated, since $\tilde{\sigma}$ in turn depends on the Froude number being considered. If we consider $\tilde{\sigma}(X)$ to be a known function of F_h (as solved using the methods of §1.6), then we in effect have two simultaneous equations for the limiting Froude number and the value of the sinkage at this Froude number.

For simplicity we shall consider here a fore-aft symmetric ship, where the maximum values of S and B occur at the midsection. We shall also only consider hull forms for which the midsection is the critical section. Therefore the values of S and B used in (1.44) are those of the midsection. The more general case, where the critical section might occur anywhere along the ship's length, will be considered subsequently.

Because the problem is non-local, we do not use $F^-(X)$; only the overall limiting Froude number F_{lim}^- has meaning in this case.

Solving equation (1.44) for F_h gives the limiting Froude number F_{lim}^- in terms of $\tilde{\sigma}$. However, $\tilde{\sigma}$ must also satisfy the force balance equation (1.27), where $\tilde{\zeta}(X)$ is determined through the cubic (1.26).

These three simultaneous equations allow F_{lim}^- to be determined by the secant method. Guessing a value for $\tilde{\sigma}$, equation (1.44) gives the corresponding value of F_h which makes the midsection on the edge of critical flow. Since we have assumed that the midsection is the critical section, if steady flow exists here it must exist everywhere.

We now know that a solution for $\tilde{\zeta}$ can be found for all X using equation (1.26). This then allows us to calculate $f(\tilde{\sigma})$ as in (1.32), and if we do this for two initial guesses $\tilde{\sigma}_0$ and $\tilde{\sigma}_1$, we will find a better estimate $\tilde{\sigma}_2$ using equation (1.33). Continuing this process until acceptable convergence is reached, we obtain the limiting value of $\tilde{\sigma}$ and corresponding F_{lim}^-.

A note on the limit of steady supercritical flow

In §1.5.1 it was stated that steady supercritical hydraulic flow is difficult to model, since it is not clear which root of the cubic free surface height equation we should choose. Because of this, we have avoided giving results for steady supercritical sinkage and trim.

This problem becomes relevant when determining the Froude number limit F_{lim}^+ of steady supercritical flow for a ship that is free to squat. In this case the sinkage of the ship must be found as part of the process, and this in turn depends on the free surface height along the entire length of the ship. Because of this we shall not give results for F_{lim}^+ for a ship that is free to squat.

In the cases of a fixed ship or a block ship free to squat, we are only concerned with the conditions under which the Bernoulli and continuity relations become tangent to each other. Therefore we do not have to choose between the two intersection points of steady supercritical flow, as they are both coincident when $F_h = F_{\text{lim}}^+$. Because of this, equations (1.45) and (1.48) are valid for the limiting Froude number of steady supercritical flow; this is irrespective of which intersection point we choose for the free surface height.

1.8.4 Results

Figure 1.11 shows the limiting Froude numbers F_{lim}^- for a Wigley hull that is either fixed or free to squat. These were calculated using $B_{\max}/w = 0.4$ and varying values of S/S_0. Since for the Wigley hull $S/S_0 = 2T/3h$ (using equation (1.40)), we have used the draught-to-depth ratio T/h to show the results.

The varying draught/depth ratios could represent ships with different draughts in the same channel, or the same ship in channels of different depth. The range of T/h was chosen high enough ($T/h > 0.5$) to ensure that the midsection is the critical section. Results were not given for $T/h > 0.82$, because the ship was then found to strike the channel bottom before the critical Froude number could be reached.

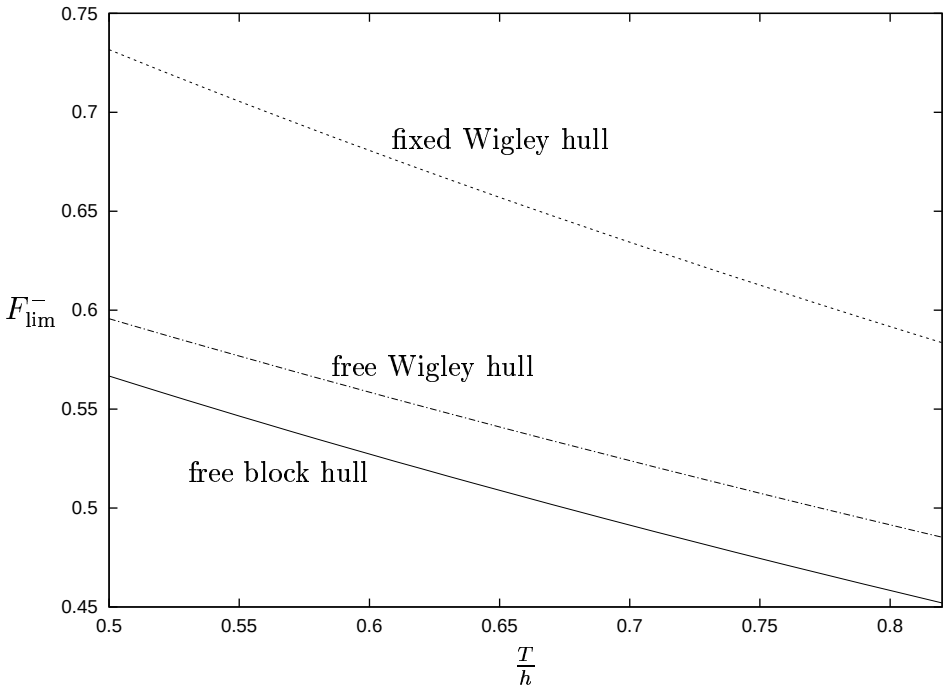

Figure 1.11: Limiting Froude number for steady subcritical flow as a function of draught/depth ratio, for a Wigley hull with $B_{\max}/w = 0.4$. Results are independent of ship length.

From this graph we can find the limiting Froude number for the ship and channel considered in Section 1.7.1. In this case $T/h = 0.75$, so we can read off that $F_{\text{lim}}^{-} = 0.507$.

Comparing results for the free and fixed Wigley hull, we see that F_{lim}^{-} is significantly decreased when the ship is allowed to squat. For example, when $T/h = 0.6$, the fixed Wigley hull considered here can sustain steady subcritical flow up to $F_h = 0.68$, whereas the same ship allowed to squat can only sustain steady flow up to $F_h = 0.56$. The reason for this is that allowing the ship to squat effectively increases the blockage, making subcritical flow become unsteady at a lower Froude number.

The limiting Froude numbers of the block-like hull which is allowed to squat have also been included for comparison. This hull has a constant cross-section which is the same as the midsection of the Wigley hull. If this hull were held fixed, its limiting Froude number would be the same as for the fixed Wigley hull. This is because it is only the characteristics of the critical section that determine F_{lim}^{-} for a fixed ship.

The free block-like hull has larger section area towards the bow and stern than the Wigley hull. This means that its sinkage is larger, causing the midsection flow to become unsteady at a lower Froude number than for the Wigley hull. This clearly shows that it is not just the characteristics of the critical section that determine the limiting Froude number for a ship that is free to squat.

1.9 The critical section

Here we outline a procedure for determining whether the largest section is in fact the critical section. If the critical section is not the largest section, we show how to locate it and find the corresponding limiting Froude number.

1.9.1 Fixed ship

Determining whether the largest section is the critical section

For a fixed ship, the critical section can be found by solving equation (1.45) numerically for $F^-(X)$ and $F^+(X)$, and then using equation (1.46) to find $F^-_{\rm lim}$ and $F^+_{\rm lim}$. A more direct approach is described here. Again, as the approach is equivalent for $F^-_{\rm lim}$ and $F^+_{\rm lim}$, we shall consider here $F^-_{\rm lim}$, the upper limit of steady subcritical flow. For simplicity we shall consider sharp-ended vessels which have their maximum beam and section area at the same station X, although this need not be at midships.

We can use the relationship between a ship's local section area and its local beam to find the relationship between its blockage coefficient and beam/channel-width ratio, given particular channel dimensions. This is plotted in Figure 1.12 for the MarAd hull and channel described in §1.7.2. The upper branch is the forward part of the ship and the lower branch is the aft part of the ship; these meet at the blockage coefficient and beam/channel-width ratio of the largest section. The bow and stern points both coincide at the origin.

By solving equation (1.45) at the largest section $X = X_{\rm m}$, where $B = B_{\rm max}$ and $S = S_{\rm max}$, we can find $F^-(X_{\rm m})$, denoted $F^-_{\rm m}$. Writing equation (1.45) in the form

$$\frac{S}{S_0} = 1 - \frac{3}{2}\left[F_h^2\left(1 - \frac{B}{w}\right)\right]^{1/3} + \frac{F_h^2}{2}\left(1 - \frac{B}{w}\right) \tag{1.49}$$

and substituting $F_h = F^-_{\rm m}$, we can consider this as a relationship between S/S_0 and B/w for which the limiting Froude number is $F^-_{\rm m}$. This curve is also plotted in Figure 1.12.

Any combination of S/S_0 and B/w lying on this curve has a limiting Froude number of $F^-_{\rm m}$, the same as the largest section. All points below this curve have higher values of F^-, while all points above the curve have lower values of F^-. Therefore, in order for the largest section to have the lowest value of F^- and be the critical section, the ship's S/S_0 – B/w curve must lie entirely below the $F^-_{\rm m}$ curve. This is seen to be true in Figure 1.12, such that the largest section is indeed the critical section in this case.

This method is much quicker than finding $F^-(X)$ for all X, since equation (1.45) only has to be solved at $X = X_{\rm m}$.

Although plotting these curves shows comprehensively whether or not the midsection is the critical section, a necessary and usually sufficient condition can be simply found as follows.

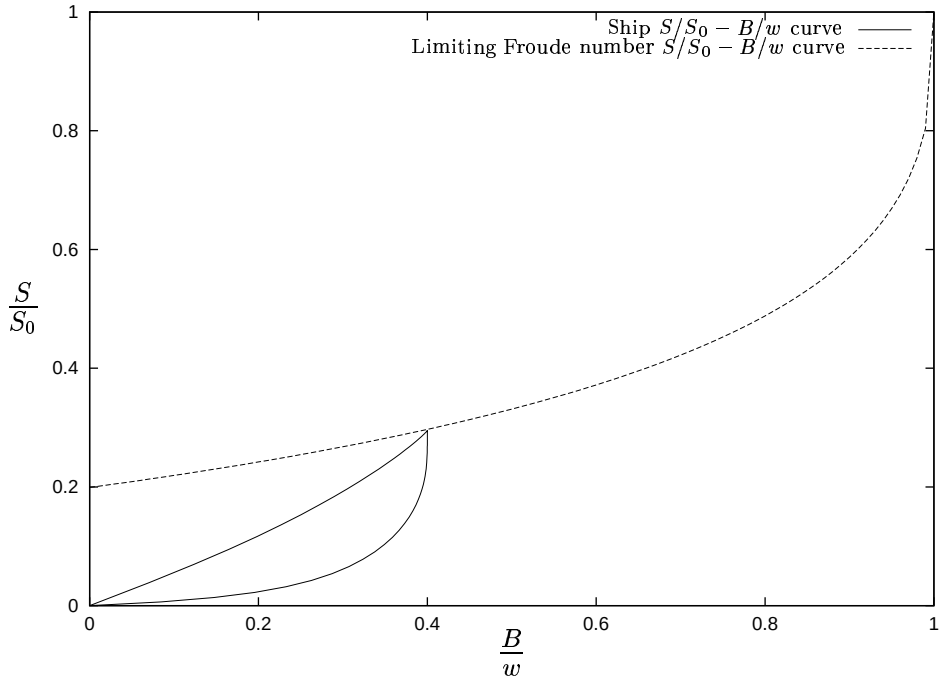

Figure 1.12: Blockage coefficient vs. beam/channel-width ratio curve for MarAd hull, with corresponding limiting Froude number curve from largest section.

Comparing the gradients of the ship's $S/S_0 - B/w$ curve and the F_{m}^{-} curve at the largest section, we see that in order for the largest section to be critical, both branches of the ship's $S/S_0 - B/w$ curve must have gradients greater than that of the F_{m}^{-} curve.

Using the relationship $S/S_0 = f(B/w)$, with f' the derivative of S/S_0 with respect to B/w, this condition can be written

$$f' > \frac{(F_{\mathrm{m}}^{-})^2}{2}\left\{\left[(F_{\mathrm{m}}^{-})^2\left(1-\frac{B}{w}\right)\right]^{-\frac{2}{3}} - 1\right\} \qquad \text{at } B/w = B_{\max}/w\ , \tag{1.50}$$

which must be true for both branches of the ship's $S/S_0 - B/w$ curve. As well as being a necessary condition for the largest section to be critical, it will also be sufficient for practical ships, the only possible exception being ships with extremely bulbous underwater profiles.

Finding the critical section when it is not the largest section

In the case that the largest section is not the critical section, we suggest an alternative method for finding the limiting Froude number, and the hull section to which it corresponds.

Every point on the ship's $S/S_0 - B/w$ curve has its own limiting Froude number F^{-}, and a corresponding curve on which this value of F^{-} is constant according to equation (1.49). The minimum value of F^{-} has a curve that will just touch the ship's $S/S_0 - B/w$ curve.

This is shown in Figure 1.13, where for this example we are using the Wigley hull and channel described in §1.7.1, except that the channel width is now halved and the depth doubled. For the Wigley hull the $S/S_0 - B/w$ curve is a straight line, since the sectional area at any station X is proportional to the local beam.

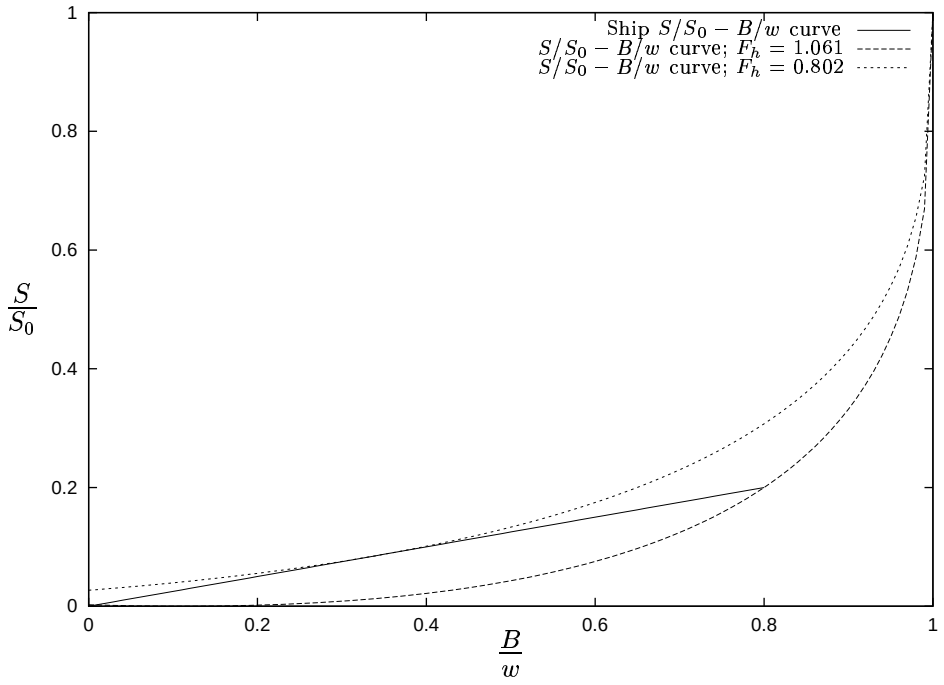

Figure 1.13: Blockage coefficient vs. beam/channel-width ratio curve for Wigley hull, with corresponding limiting Froude number curve from largest section and critical section. Here $B_{\max}/w = 0.8$ and $S_{\max}/S_0 = 0.2$.

The critical section and Froude number can be determined by finding which limiting Froude number curve meets the ship's $S/S_0 - B/w$ curve at a tangent. This condition becomes

$$f' = \frac{(F^-)^2}{2}\left\{\left[(F^-)^2\left(1-\frac{B}{w}\right)\right]^{-\frac{2}{3}} - 1\right\} . \tag{1.51}$$

For a non-fore-aft-symmetric ship, each branch of the ship's $S/S_0 - B/w$ curve must be considered separately, in order to find the lowest value of F^-.

Equation (1.51) combined with equation (1.49) (with $F_h = F^-$) gives two simultaneous equations for finding the critical section and the limiting Froude number. Writing equations (1.51) and (1.49) in the respective forms

$$-2\left(1-\frac{B}{w}\right)f' = v - v^{\frac{1}{3}}$$

and

$$f = 1 - \frac{3}{2}v^{\frac{1}{3}} + \frac{v}{2} ,$$

where $v = (F^-)^2(1 - B/w)$, allows us to eliminate v or $v^{\frac{1}{3}}$, giving in each case

$$v^{\frac{1}{3}} = 1 - f - \left(1-\frac{B}{w}\right)f' \tag{1.52}$$

and

$$v = 1 - f - 3\left(1 - \frac{B}{w}\right) f' \,. \tag{1.53}$$

From equations (1.52) and (1.53) we obtain the following expression for the value of B/w at the critical section:

$$1 - f - 3\left(1 - \frac{B}{w}\right) f' = \left[1 - f - \left(1 - \frac{B}{w}\right) f'\right]^3 \,. \tag{1.54}$$

Once this is found, the limiting Froude number $F^-_{\rm lim}$ can be found using equation (1.53) to be

$$F^-_{\rm lim} = \sqrt{\frac{1-f}{1-\frac{B}{w}} - 3f'} \,. \tag{1.55}$$

In the case of hull shapes having $S/S_0 = k(B/w)$ for some constant k, the problem is greatly simplified. Equation (1.54) for the critical section now gives

$$\frac{B}{w} = \frac{k(3-k)}{2} \,, \tag{1.56}$$

while the corresponding limiting Froude number, using equation (1.55), is

$$F^-_{\rm lim} = \frac{1-k}{\sqrt{1-\frac{k}{2}}} \,. \tag{1.57}$$

We are assuming here that a tangent solution exists, which requires that the B/w value found in (1.56) is less than $B_{\rm max}/w$. In particular, since B/w must always be less than 1, k must lie in the range (0,1) or (2,3). However, only the range (0,1) corresponds to real values of $F^-_{\rm lim}$. As such, k must always lie in the range (0,1) for a tangent solution to occur. In addition, $B_{\rm max}/w$ must be greater than the value of B/w given by equation (1.56). If this is not true, the largest section must be the critical section.

For parallel-sided ships of constant draught T, we have $S = BT$ and hence $k = T/h$. For Wigley hulls, $S = 2BT/3$ so that $k = 2T/3h$. Since the conditions under which a tangent solution exists are that k is small and $B_{\rm max}/w$ is large, this will most likely be true for vessels of large beam but small draught, or those travelling in narrow but deep channels.

For the Wigley hull and channel configuration depicted in Figure 1.13, $S_{\rm max}/S_0 = 0.2$ and $B_{\rm max}/w = 0.8$, meaning that $k = 0.25$. In this case the critical section occurs at $B/w = 0.344$, from equation (1.56). The value of the limiting Froude number can be found from equation (1.57) to be $F^-_{\rm lim} = 0.802$. This limiting Froude number curve is depicted in Figure 1.13; it can be seen to become tangent to the ship's S/S_0 – B/w curve at the critical section $B/w = 0.344$. In this case the critical section is closer to the ends of the ship than it is to the largest section (where $B/w = 0.8$).

1.9.2 Ship free to squat

Determining whether the largest section is the critical section

A method for finding the limiting Froude number for the largest section of a ship that is free to squat has been described in §1.8.3. This requires solution over the whole shiplength of the scaled free surface height $\tilde{\zeta}(X)$. If the largest section is indeed the critical section, this will always be possible. However, if at any station X a solution cannot be found for $\tilde{\zeta}(X)$, we know that the critical section is not the largest section.

Finding the critical section when it is not the largest section

For simplicity, only symmetric hulls will be considered here. The problem can be solved as for the fixed ship (§1.9.1), but using the iterative method to find $\tilde{\sigma}$ as in §1.6.4. The critical section must be found separately for each value of $\tilde{\sigma}$.

Guessing an initial value for $\tilde{\sigma}$, each point on the ship's S/S_0 - B/w curve now has a new curve of constant F^- passing through it, according to equation (1.44). Equating gradients, the point at which this curve meets the ship's S/S_0 – B/w curve at a tangent now satisfies

$$f' = \frac{(F^-)^2}{2}\left\{\left[(F^-)^2\left(1-\frac{B}{w}\right)\right]^{-\frac{2}{3}} - 1\right\} - \tilde{\sigma}\,, \tag{1.58}$$

which, on eliminating F^- through equation (1.44), becomes

$$\begin{aligned} & 1 - f - \tilde{\sigma}\frac{B}{w} - 3\left(1-\frac{B}{w}\right)(\tilde{\sigma}+f') \\ = \quad & \left[1 - f - \tilde{\sigma}\frac{B}{w} - \left(1-\frac{B}{w}\right)(\tilde{\sigma}+f')\right]^3 \,. \end{aligned} \tag{1.59}$$

Once this critical section is found, the limiting Froude number is the solution of

$$F^-_{\rm lim} = \sqrt{\frac{1 - f - \tilde{\sigma}\frac{B}{w}}{1-\frac{B}{w}} - 3\,(\tilde{\sigma}+f')}\,. \tag{1.60}$$

With the limiting Froude number calculated for a given value of $\tilde{\sigma}$ in this way, the iterative procedure for finding the correct value of $\tilde{\sigma}$ and $F^-_{\rm lim}$ is the same as in §1.8.3.

In the case that $S/S_0 = k(B/w)$, equation (1.59) for the critical section simplifies to

$$\frac{B}{w} = \frac{(k+\tilde{\sigma})(3-k-\tilde{\sigma})}{2}\,. \tag{1.61}$$

Since $\tilde{\sigma} > 0$ for subcritical flow, this expression is more restrictive than the similar expression (1.56) for the fixed ship. In other words, a larger value of $B_{\rm max}/w$ will be needed for a tangent solution to exist if the ship is allowed to squat.

The corresponding limiting Froude number for a given value of $\tilde{\sigma}$ satisfies

$$F_{\text{lim}}^{-} = \frac{1 - k - \tilde{\sigma}}{\sqrt{1 - \frac{k+\tilde{\sigma}}{2}}} \,. \tag{1.62}$$

The iterative procedure was carried out for the same Wigley hull and channel configuration described in §1.9.1, but with the ship free to squat. The limiting value of $\tilde{\sigma}$ in this case is 0.411, with the corresponding limiting Froude number of $F_{\text{lim}}^{-} = 0.414$ occurring at the critical section $B/w = 0.773$.

We notice that this is a very different scenario to when the ship is held fixed. The limiting Froude number of $F_{\text{lim}}^{-} = 0.414$ is much lower than the value of $F_{\text{lim}}^{-} = 0.802$ for a fixed ship. In addition, the critical section occurs much closer to midships for the free ship, at $B/w = 0.773$, compared to $B/w = 0.344$ for the fixed ship.

1.10 Conclusions

We have outlined a consistent nonlinear method for computing the flow around a ship that is free to squat, travelling in a uniform channel. This method recognizes the fact that allowing the ship to sink and trim will give a different flow from that obtained by fixing the ship vertically in its rest position.

Although the fixed-ship method is valid for linearized flow, it is inconsistent to use it for cases in which the blockage coefficient and beam/channel-width ratio are not small quantities.

In the subcritical speed range, the midship sinkage increases the blockage coefficient of the ship in the channel. This further accelerates the flow past the ship, resulting in a greater midship sinkage than is predicted using the fixed-ship theory. The trim, whether it be bow-up or bow-down, is also underestimated by the fixed-ship theory.

The discrepancy increases as the depth-based Froude number approaches the upper limit of steady subcritical flow, as this is when the sinkage and trim are large. In this case it is no longer acceptable to use a theory in which the ship is considered vertically fixed.

The limiting Froude numbers for steady flow are also affected by allowing the ship to squat. We studied the limiting Froude numbers first for a fixed ship, showing that they depend only on the characteristics of one particular section. This "critical section" need not be the largest section, especially when the beam/channel-width ratio is large. In that case it may occur anywhere along the ship's length, and will be in a different position for supercritical flow than for subcritical flow. We compared the predicted limiting Froude number for steady supercritical flow to that observed experimentally, showing that the theory's predictions were reasonably accurate.

For a ship that is free to squat, the entire ship has to be taken into account when determining the limiting Froude numbers, as the overall sinkage must be determined as

part of the problem. Allowing the ship to squat significantly decreases the maximum Froude number for steady subcritical flow, so that unsteady critical flow begins at a lower Froude number.

Chapter 2

Steady Transcritical Squat in Open Water

In this chapter we compute the sinkage and trim of a ship travelling in open water of constant depth, with emphasis on the behaviour near the critical speed.

We shall use the same body-fixed coordinate system as in Chapter 1. In this case, however, the water is of infinite lateral extent, with no side walls. We represent the velocity field using the disturbance velocity potential ϕ, such that the total flow velocity is given by

$$\mathbf{q} = U\mathbf{i} + \nabla\phi \; .$$

We shall be extending two previously proposed methods: the shallow-water theory of Mei (1976) and the finite-depth theory of Tuck & Taylor (1970). These, in turn, are an improvement on the slender-body shallow-water theory of Tuck (1966).

2.1 Shallow-water theory and experimental results

Let us first consider a simple shallow-water theory (SWT), in which it is assumed that the water depth is small compared to the ship's length. Michell (1898) considered a slender vertical-sided obstruction extending from bottom to top of a shallow stream of depth h and infinite width. He showed that the small disturbance velocity potential ϕ is independent of z, and satisfies the linearized equation of shallow water theory

$$(1 - F_h^2)\phi_{XX} + \phi_{yy} = 0 \; . \tag{2.1}$$

This is the same equation that describes linearized aerodynamic flow past a thin airfoil (see e.g. Newman 1977 p.375), with F_h replacing the Mach number.

For a slender ship of a general cross-section shape, Tuck (1966) solved the problem using two regions: an "outer" region away from the ship and an "inner" region close to the

ship. He showed that the outer disturbance potential ϕ was still independent of z and satisfied the same equation (2.1). Tuck used the hull boundary condition to describe the inner flow, before matching this to the outer flow; the matching required that the outer potential $\phi(X, y)$ must satisfy the boundary condition

$$\phi_y(X, 0_\pm) = \pm \frac{US'(X)}{2h} \ . \tag{2.2}$$

Here, as in Chapter 1, $S(X)$ is the ship's submerged cross-section area (with an undisplaced free surface) at station X. Note that due to the slenderness of the ship, the matching states that the boundary condition is applied on $y = 0$. In the aerodynamic analogy, the boundary condition (2.2) indicates that the ship behaves in the (X, y) horizontal plane as if it were a symmetric thin airfoil of thickness $S(X)/h$. This thickness is equal to the average of the ship's cross-section thickness over the water depth.

There are also boundary conditions at infinity, essentially that the disturbance velocity $\nabla\phi$ vanishes in subcritical flow ($F_h < 1$), or else behaves like an outgoing wave in supercritical flow ($F_h > 1$).

The solution of (2.1) is well known from aerodynamics for either fully subcritical flow (where it is elliptic) or fully supercritical flow (where it is hyperbolic). In either case, the solution has a singularity as $F_h \to 1$. In particular, the subcritical (positive upward) vertical force is given by Tuck (1966) as

$$Z = \frac{\rho U^2}{2\pi h \sqrt{1 - F_h^2}} \int\int B'(X)\, S'(\xi)\, \log|X - \xi|\, dX\, d\xi \tag{2.3}$$

with $B(X)$ the local beam at station X. Here and subsequently the integrations are over the wetted length of the ship, i.e. $-\ell < X < \ell$.

This force Z is usually negative, i.e. downward, and for a fore-aft symmetric ship, the resulting midship sinkage is given hydrostatically by

$$s = \left(\frac{\Delta}{L^2}\right) C_S \, \frac{F_h^2}{\sqrt{1 - F_h^2}} \ . \tag{2.4}$$

Here L is the ship's length and Δ its displaced volume; the hull coefficient C_S is given by

$$C_S = -\frac{L^2}{2\pi A_W \Delta} \int\int B'(X)\, S'(\xi)\, \log|X - \xi|\, dX\, d\xi \ . \tag{2.5}$$

Again, $A_W = \int_{-\ell}^{\ell} B(X) dX$ is the ship's waterplane area. The non-dimensional coefficient $C_S \approx 1.4$ has been shown by Tuck & Taylor (1970) to be almost a universal constant, depending only weakly on the ship's hull shape.

From equation (2.4) we see that the sinkage appears to tend to infinity as $F_h \to 1$, according to this linear dispersionless theory. However in practice the sinkage is finite, reaching a maximum value at just below $F_h = 1$ before becoming quite small thereafter.

Accurate full-scale experimental data for transcritical sinkage are scarce. However, according to linear inviscid theory, the maximum sinkage is directly proportional to the shiplength for a given shape of ship and depth-to-draught ratio (see §2.5). This means that model experiments for maximum sinkage (e.g. Graff et al 1964) can be scaled proportionally to length to yield full-scale results, provided the depth-to-draught ratio remains the same.

For ships travelling in confined waterways, the width of the channel becomes increasingly important around $F_h = 1$, when the flow is unsteady and solitons are emitted forward of the ship (see e.g. Wu & Wu 1982). Hence experiments performed in narrow channels cannot be used to accurately predict maximum sinkage for ships in open water. The experiments of Graff et al were done in a wide tank, approximately 36 times the model beam, which should reasonably approximate open water. However, even with this extreme tank width, reliable results were not given for $h/T < 4.0$, presumably because of unsteadiness due to finite-width effects.

The magnitude of the maximum sinkage is considerable. For example, the Taylor Series A3 model studied by Graff et al (1964) had a maximum sinkage of 0.89% of the shiplength for the depth-to-draught ratio $h/T = 4.0$. This corresponds to a midship sinkage of 1.88 metres for a 200 metre ship. Experiments on maximum squat were also performed by Du & Millward (1991) using NPL round bilge series hulls. They obtained a maximum midship sinkage of 1.4% of the shiplength for model 150B with $h/T = 2.3$. This corresponds to 2.8 metres midship sinkage for a 200 metre ship. Taking into account the fact that there is usually a significant bow-up trim angle at the speed where the maximum sinkage occurs, the downward displacement of the stern can be even greater, of the order of 4 metres or more for a 200-metre long ship.

It is important to note that only ships that are capable of travelling at transcritical Froude numbers will ever reach this maximum sinkage. Therefore, maximum sinkage predictions will be less relevant for slower ships such as bulk carriers.

Most of the fast, non-planing monohulls or catamarans that regularly travel at transcritical speeds are comparatively slender. We can take advantage of this by using "slender-body theory" to describe the flow, which assumes that the ship's draught and maximum beam are both small compared to its length. Both of the theories that we shall be considering are slender-body theories.

The failing of the basic shallow-water theory (2.1) when F_h is close to 1 is principally due to neglect of dispersive effects, which only become important in this Froude number range. In this chapter we attempt to include these effects, in order to determine the sinkage at transcritical Froude numbers. Special emphasis will be placed on predicting the maximum sinkage, and results will be compared to the experimental results of Graff et al (1964). These are still among the most thorough and precise results available on transcritical sinkage and trim.

2.2 Modifying shallow-water theory

In the shallow-water equation (2.1), the flow is assumed to be steady in the body-fixed frame of reference. This is a special case of a more general equation governing unsteady linearized flow in constant depth (see Stoker 1957 p. 419). In earth-fixed coordinates (x, y), it has the form

$$\phi_{tt} = gh\,(\phi_{xx} + \phi_{yy}) \ .$$

We can see that this equation is *dispersionless* in that it allows wave solutions for which the wave speed is independent of wavelength. For example, one-dimensional wave solutions travelling in the positive $x-$direction have the form

$$\phi = \phi\left(x - \sqrt{gh}\,t\right) \ ,$$

so that these waves travel with constant speed $\sqrt{gh}$ and remain unchanged in form.

According to this dispersionless theory, there will be a resonance effect as the ship speed approaches the wave speed $\sqrt{gh}$. Since, according to this theory, any one-dimensional wave can travel unchanged in form at a speed $\sqrt{gh}$, there is in effect no restoring force on the free surface when the ship is travelling at this speed. The free surface, and therefore the ship, could sink or rise indefinitely, resulting in an undefined sinkage.

In order to see the effect of dispersion, let us consider a one-dimensional wave travelling in water of finite (not necessarily shallow) depth h. We shall here consider a pure harmonic wave, which has a sinusoidal free surface profile. If this wave is to satisfy the Laplace equation and free surface boundary conditions, its speed must satisfy (see Stoker 1957 p. 46)

$$c^2 = \frac{g}{k}\tanh(kh) \ . \tag{2.6}$$

Here k is the wave number, which is equal to 2π divided by the wavelength. We can see that the speed of such a wave does depend on its wavelength.

An arbitrary one-dimensional travelling wave can be considered to be a linear superposition of harmonic waves of varying wavelengths. Therefore any such wave will be *dispersive*, as its components of differing wavelengths will travel at different speeds.

The shallow-water wave speed is found by taking the $h \to 0$ limit of equation (2.6), whereupon $\tanh(kh) \to kh$ and $c^2 \to gh$. Only in this limit is the wave speed independent of k. For example, a more accurate shallow-water approximation uses the Taylor expansion

$$\tanh(kh) \approx kh - \frac{(kh)^3}{3}$$

to give

$$c^2 \approx gh\left(1 - \frac{(kh)^2}{3}\right) \ .$$

This gives us the leading dispersion correction term to the wave speed in shallow-water theory. Although the correction is of higher order in the small quantity h, it becomes vitally important when the ship speed approaches $\sqrt{gh}$.

The transcritical shallow-water theory that we shall use includes this dispersion correction to the wave speed. The derivation given here follows that of Mei (1976).

2.2.1 A general shallow-water derivation

We start by considering the equations governing steady potential flow in water of constant depth. In body-fixed coordinates, we have the Laplace equation

$$\phi_{XX} + \phi_{yy} + \phi_{zz} = 0 \,, \tag{2.7}$$

subject to the wall condition on the sea floor

$$\phi_z = 0 \qquad \text{on } z = -h \,. \tag{2.8}$$

On the free surface we have the kinematic boundary condition

$$\phi_z = (U + \phi_X)\zeta_X + \phi_y \zeta_y \qquad \text{on } z = \zeta \tag{2.9}$$

as well as the Bernoulli condition

$$g\zeta + \frac{1}{2}\left(\phi_X^2 + \phi_y^2 + \phi_z^2\right) + U\phi_X = 0 \qquad \text{on } z = \zeta \,. \tag{2.10}$$

Since we are considering the "outer" flow far from the ship, we do not need the hull boundary condition at this stage.

The shallow-water approximation for the outer flow makes use of the fact that the vertical length scale h is much smaller than the length scale L in the X and y directions. As we shall see, this implies that the flow is two-dimensional to leading order.

In order to exploit this small$-h$ assumption we scale the space dimensions by their typical length scales. The scaled variables $\mathsf{X}, \mathsf{y}, \mathsf{z}$ are given by

$$\mathsf{X} = X/L$$

$$\mathsf{y} = y/L$$

$$\mathsf{z} = z/h \,.$$

For convenience we shall also use the scaled free surface height $\tilde{\zeta} = \zeta/h$.

In terms of the new variables, and introducing the small parameter $\mu = h/L$, equations (2.7)–(2.10) now become

$$\mu^2 \left(\phi_{\mathsf{XX}} + \phi_{\mathsf{yy}}\right) + \phi_{\mathsf{zz}} = 0 \tag{2.11}$$

$$\phi_{\mathsf{z}} = 0 \qquad \text{on } \mathsf{z} = -1 \tag{2.12}$$

$$\frac{\phi_{\mathsf{z}}}{\mu^2} = (UL + \phi_{\mathsf{X}})\tilde{\zeta}_{\mathsf{X}} + \phi_{\mathsf{y}}\tilde{\zeta}_{\mathsf{y}} \qquad \text{on } \mathsf{z} = \tilde{\zeta} \tag{2.13}$$

$$gh\tilde{\zeta} + \frac{1}{2L^2}\left(\phi_{\mathsf{X}}^2 + \phi_{\mathsf{y}}^2\right) + \frac{\phi_{\mathsf{z}}^2}{2h^2} + \frac{U}{L}\phi_{\mathsf{X}} = 0 \qquad \text{on } \mathsf{z} = \tilde{\zeta} \,. \tag{2.14}$$

In terms of F_h, the scaled Bernoulli equation (2.14) may be written

$$\tilde{\zeta} = -\frac{F_h^2}{2U^2L^2}\left(\phi_{\mathsf{x}}^2 + \phi_{\mathsf{y}}^2 + \frac{\phi_{\mathsf{z}}^2}{\mu^2}\right) - \frac{F_h^2}{UL}\phi_{\mathsf{x}} = 0 \qquad \text{on } \mathsf{z} = \tilde{\zeta}\ . \tag{2.15}$$

It is assumed that although h is a small quantity, the ship speed U is such that $F_h = U/\sqrt{gh}$ is of order 1, i.e. asymptotically independent of μ.

The general solution of the scaled Laplace equation (2.11) subject to the boundary condition (2.12) can be written using the small-μ expansion introduced by Rayleigh:

$$\phi = \phi_0 - \frac{\mu^2}{2!}(\mathsf{z}+1)^2\nabla^2\phi_0 + \frac{\mu^4}{4!}(\mathsf{z}+1)^4\nabla^4\phi_0 + ... \tag{2.16}$$

Here $\phi_0 = \phi_0(\mathsf{X}, \mathsf{y})$ only. The differential operator ∇^2 is equal to $\partial^2/\partial\mathsf{X}^2 + \partial^2/\partial\mathsf{y}^2$, with $\nabla^4 = \nabla^2\nabla^2$.

We shall now substitute this expansion into the kinematic condition (2.13) and Bernoulli equation (2.15) and neglect high order terms in the small quantity μ. In addition, we will use the slender-body approximation that the magnitude of the velocity potential ϕ is also small when compared to standard potential dimensions UL. However, it is important to note that at this stage the small quantities μ and ϕ are allowed to tend towards zero *independently*.

The derivatives in equations (2.13) and (2.15) can be found using the Rayleigh expansion (2.16) as follows:

$$\phi_{\mathsf{z}}|_{\mathsf{z}=\tilde{\zeta}} = -\mu^2(1+\tilde{\zeta})\nabla^2\phi_0 + \frac{\mu^4}{3!}(1+\tilde{\zeta})^3\nabla^4\phi_0 + ...$$

$$\phi_{\mathsf{x}}|_{\mathsf{z}=\tilde{\zeta}} = \phi_{0\mathsf{x}} - \frac{\mu^2}{2}(1+\tilde{\zeta})^2\nabla^2\phi_{0\mathsf{x}} + \frac{\mu^4}{4!}(1+\tilde{\zeta})^4\nabla^4\phi_{0\mathsf{x}} + ...$$

$$\phi_{\mathsf{y}}|_{\mathsf{z}=\tilde{\zeta}} = \phi_{0\mathsf{y}} - \frac{\mu^2}{2}(1+\tilde{\zeta})^2\nabla^2\phi_{0\mathsf{y}} + \frac{\mu^4}{4!}(1+\tilde{\zeta})^4\nabla^4\phi_{0\mathsf{y}} + ...$$

Substituting these derivatives into the Bernoulli equation (2.15) we obtain

$$\tilde{\zeta} = -\frac{F_h^2}{2U^2L^2}\left(\phi_{0\mathsf{x}}^2 + \phi_{0\mathsf{y}}^2\right) - \frac{F_h^2}{UL}\left(\phi_{0\mathsf{x}} - \frac{\mu^2}{2}\nabla^2\phi_{0\mathsf{x}}\right) + O(\mu^4\phi, \mu^2\phi^2) = 0\ . \tag{2.17}$$

The kinematic condition (2.13) becomes

$$\begin{aligned} -(1+\tilde{\zeta})\nabla^2\phi_0 \ &+\ \frac{\mu^2}{3!}(1+\tilde{\zeta})^3\nabla^4\phi_0 + ... \\ &=\ \left(UL + \phi_{0\mathsf{x}} - \frac{\mu^2}{2}(1+\tilde{\zeta})^2\nabla^2\phi_{0\mathsf{x}} + \frac{\mu^4}{4!}(1+\tilde{\zeta})^4\nabla^4\phi_{0\mathsf{x}} + ...\right)\tilde{\zeta}_{\mathsf{x}} \\ &+\ \left(\phi_{0\mathsf{y}} - \frac{\mu^2}{2}(1+\tilde{\zeta})^2\nabla^2\phi_{0\mathsf{y}} + \frac{\mu^4}{4!}(1+\tilde{\zeta})^4\nabla^4\phi_{0\mathsf{y}} + ...\right)\tilde{\zeta}_{\mathsf{y}} \end{aligned}$$

which, on substituting expression (2.17) to eliminate $\tilde{\zeta}$, gives

$$\begin{aligned} -\left(1-\frac{F_h^2}{UL}\phi_{0\mathsf{x}}\right)\nabla^2\phi_0 \;&+\; \frac{\mu^2}{3!}\nabla^4\phi_0 \\ &= UL\left[-\frac{F_h^2}{2U^2L^2}\left(\phi_{0\mathsf{x}}^2+\phi_{0\mathsf{y}}^2\right)_{\mathsf{x}}-\frac{F_h^2}{UL}\left(\phi_{0\mathsf{xx}}-\frac{\mu^2}{2}\nabla^2\phi_{0\mathsf{xx}}\right)\right] \\ &+\; \phi_{0\mathsf{x}}\frac{-F_h^2}{UL}\phi_{0\mathsf{xx}}+\phi_{0\mathsf{y}}\frac{-F_h^2}{UL}\phi_{0\mathsf{xy}}+O(\mu^4\phi,\mu^2\phi^2,\phi^3)\;. \end{aligned}$$

Here we have included both the leading $O(\mu^2\phi)$ dispersive terms and the leading $O(\phi^2)$ nonlinear terms.

Upon rearranging, we obtain

$$\begin{aligned} &\nabla^2\phi_0-F_h^2\,\phi_{0\mathsf{xx}}+\frac{\mu^2F_h^2}{2}\nabla^2\phi_{0\mathsf{xx}}-\frac{\mu^2}{6}\nabla^4\phi_0 \\ &-\frac{F_h^2}{UL}\left[\left(\phi_{0\mathsf{x}}^2+\phi_{0\mathsf{y}}^2\right)_{\mathsf{x}}+\phi_{0\mathsf{x}}\nabla^2\phi_0\right]+O(\mu^4\phi,\mu^2\phi^2,\phi^3)=0\;. \end{aligned} \tag{2.18}$$

We can now use this expression for ϕ_0 to find the depth-averaged potential $\bar{\phi}$, defined by

$$(1+\tilde{\zeta})\bar{\phi}=\int_{-1}^{\tilde{\zeta}}\phi\;d\mathsf{z}\;.$$

Using the Rayleigh expansion (2.16) gives

$$(1+\tilde{\zeta})\bar{\phi}=\phi_0(1+\tilde{\zeta})-\frac{\mu^2}{2}\nabla^2\phi_0\frac{(1+\tilde{\zeta})^3}{3}+\ldots$$

and hence

$$\bar{\phi}=\phi_0-\frac{\mu^2}{6}\nabla^2\phi_0+O(\mu^4\phi,\mu^2\phi^2)\;.$$

In order to insert this into equation (2.18), we solve for ϕ_0, giving

$$\phi_0=\bar{\phi}+\frac{\mu^2}{6}\nabla^2\bar{\phi}+O(\mu^4\phi,\mu^2\phi^2)\;,$$

whereupon equation (2.18) becomes, in terms of the depth-averaged potential $\bar{\phi}$:

$$\begin{aligned} &\nabla^2\bar{\phi}-F_h^2\,\bar{\phi}_{\mathsf{xx}}+\frac{\mu^2F_h^2}{3}\nabla^2\bar{\phi}_{\mathsf{xx}} \\ &-\frac{F_h^2}{UL}\left[\left(\bar{\phi}_{\mathsf{x}}^2+\bar{\phi}_{\mathsf{y}}^2\right)_{\mathsf{x}}+\bar{\phi}_{\mathsf{x}}\nabla^2\bar{\phi}\right]+O(\mu^4\phi,\mu^2\phi^2,\phi^3)=0\;. \end{aligned} \tag{2.19}$$

Rearranging gives the approximation

$$\begin{aligned} &(1-F_h^2)\bar{\phi}_{\mathsf{xx}}+\bar{\phi}_{\mathsf{yy}}+\frac{\mu^2F_h^2}{3}\left(\bar{\phi}_{\mathsf{xxxx}}+\bar{\phi}_{\mathsf{yyyy}}\right) \\ &-\frac{F_h^2}{UL}\left(3\bar{\phi}_{\mathsf{x}}\bar{\phi}_{\mathsf{xx}}+\bar{\phi}_{\mathsf{x}}\bar{\phi}_{\mathsf{yy}}+2\bar{\phi}_{\mathsf{y}}\bar{\phi}_{\mathsf{xy}}\right)\approx 0\;. \end{aligned} \tag{2.20}$$

This equation, which has an error of $O(\mu^4\phi,\mu^2\phi^2,\phi^3)$, is quite general. As yet we have made no assumption about F_h except that it is asymptotically independent of μ. Also, no assumption has been made about the comparative sizes of μ and ϕ/UL.

2.2.2 Simplifying the equation

Let us now consider some simplifications of equation (2.20). Firstly, for any $F_h = O(1)$ but not necessarily close to 1, the first two terms of (2.20) are dominant. The remaining terms are $O(\mu^2\phi, \phi^2)$. Therefore if $\mu^2 \gg \phi/UL$ we can neglect the nonlinear terms, and the equation becomes

$$(1 - F_h^2)\bar{\phi}_{\mathsf{xx}} + \bar{\phi}_{\mathsf{yy}} + \frac{\mu^2 F_h^2}{3}\left(\bar{\phi}_{\mathsf{xxxx}} + \bar{\phi}_{\mathsf{yyyy}}\right) \approx 0 \, .$$

We note that this is the same as the shallow-water equation (2.1) but includes the leading-order dispersive terms. This equation could be used as an improved shallow-water equation at arbitrary F_h.

If $\mu^2 \ll \phi/UL$ we can neglect the dispersive terms in (2.20), leading to the equation

$$(1 - F_h^2)\bar{\phi}_{\mathsf{xx}} + \bar{\phi}_{\mathsf{yy}} - \frac{F_h^2}{UL}\left(3\bar{\phi}_{\mathsf{x}}\bar{\phi}_{\mathsf{xx}} + \bar{\phi}_{\mathsf{x}}\bar{\phi}_{\mathsf{yy}} + 2\bar{\phi}_{\mathsf{y}}\bar{\phi}_{\mathsf{xy}}\right) \approx 0 \, .$$

This could be used to model the leading-order effect of nonlinearity at arbitrary F_h.

Both of these differential equations are hard to solve. The linear equation can be solved by Fourier transform, but it is more difficult than the simple linear equation that we shall consider later. In addition, we already know that the simple shallow-water theory (2.1) gives good results for sinkage when F_h is not close to 1, and all of the correction terms in equation (2.20) become negligible in that case.

Therefore, we really only need to consider the correction terms that are important when F_h is close to 1. In order to study this, let us introduce the small quantity β, defined by

$$\beta = 1 - F_h^2 \, .$$

In terms of β, equation (2.20) can be written

$$\begin{aligned} &\beta\bar{\phi}_{\mathsf{xx}} + \bar{\phi}_{\mathsf{yy}} + \frac{\mu^2}{3}(1-\beta)\left(\bar{\phi}_{\mathsf{xxxx}} + \bar{\phi}_{\mathsf{yyyy}}\right) \\ &-\frac{1}{UL}(1-\beta)\left(3\bar{\phi}_{\mathsf{x}}\bar{\phi}_{\mathsf{xx}} + \bar{\phi}_{\mathsf{x}}\bar{\phi}_{\mathsf{yy}} + 2\bar{\phi}_{\mathsf{y}}\bar{\phi}_{\mathsf{xy}}\right) \approx 0 \, , \end{aligned} \tag{2.21}$$

or, to leading order in β,

$$\begin{aligned} &\beta\bar{\phi}_{\mathsf{xx}} + \bar{\phi}_{\mathsf{yy}} + \frac{\mu^2}{3}\left(\bar{\phi}_{\mathsf{xxxx}} + \bar{\phi}_{\mathsf{yyyy}}\right) \\ &-\frac{1}{UL}\left(3\bar{\phi}_{\mathsf{x}}\bar{\phi}_{\mathsf{xx}} + \bar{\phi}_{\mathsf{x}}\bar{\phi}_{\mathsf{yy}} + 2\bar{\phi}_{\mathsf{y}}\bar{\phi}_{\mathsf{xy}}\right) + O(\beta\mu^2\phi, \beta\phi^2) \approx 0 \, . \end{aligned} \tag{2.22}$$

The first thing that we notice about this equation is that, to leading order,

$$\bar{\phi}_{\mathsf{yy}} \approx 0 \, .$$

This means that near the critical speed the flow is nearly independent of y, i.e. one-dimensional in the $\mathsf{X}-$direction. This means that changes in the $\mathsf{y}-$direction are insignificant compared to changes in the $\mathsf{X}-$direction. Specifically, we can see from equation (2.22) that

$$\frac{\partial^2}{\partial \mathsf{y}^2} = O(\beta, \mu^2, \phi)\frac{\partial^2}{\partial \mathsf{X}^2} \; . \tag{2.23}$$

For moderately small β, we have

$$\frac{\partial^2}{\partial \mathsf{y}^2} = O(\beta)\frac{\partial^2}{\partial \mathsf{X}^2}$$

while for very small β,

$$\frac{\partial^2}{\partial \mathsf{y}^2} = O(\mu^2, \phi)\frac{\partial^2}{\partial \mathsf{X}^2} \; .$$

In any case, when β is small

$$\frac{\partial^2}{\partial \mathsf{y}^2} \ll \frac{\partial^2}{\partial \mathsf{X}^2} \; .$$

Therefore, the transcritical form of equation (2.21) is

$$\beta\bar{\phi}_{\mathsf{xx}} + \bar{\phi}_{\mathsf{yy}} + \frac{\mu^2}{3}\bar{\phi}_{\mathsf{xxxx}} - \frac{3}{UL}\bar{\phi}_{\mathsf{x}}\bar{\phi}_{\mathsf{xx}} \approx 0 \; .$$

In original unscaled variables, and letting ϕ be an approximation to the depth-averaged potential $\bar{\phi}$, we have the equation

$$\left(1 - F_h^2\right)\phi_{XX} + \phi_{yy} + \frac{1}{3}h^2\phi_{XXXX} - \frac{3}{U}\phi_X\phi_{XX} = 0 \; , \tag{2.24}$$

which was obtained by Mei (1976).

2.2.3 Dispersive or nonlinear theory?

Equation (2.24) has a wide range of validity, as it includes the leading order dispersive and nonlinear terms. It is a two-dimensional generalization of the one-dimensional Korteweg-deVries equation, which is known to work well for problems in which dispersion and nonlinearity are both important.

This two-dimensional version, however, is difficult to solve numerically in water of infinite lateral extent. Here we seek to gauge the relative importance of the dispersive and nonlinear terms, in order to see under which conditions either of them may be neglected.

Looking at the order of magnitude of the dispersive term in equation (2.24), we can write

$$\frac{1}{3}h^2\phi_{XXXX} = O\left(\left(\frac{h}{L}\right)^2\frac{\phi_X}{U}\right)\frac{U}{L}$$

while the nonlinear term has order

$$\frac{3}{U}\phi_X\phi_{XX} = O\left(\left(\frac{\phi_X}{U}\right)^2\right)\frac{U}{L} \; .$$

Comparing these, we can see that the nonlinear term may be neglected if

$$\phi_X/U \ll (h/L)^2 \tag{2.25}$$

while the dispersive term may be neglected if

$$\phi_X/U \gg (h/L)^2 \ . \tag{2.26}$$

These conditions are equivalent to the $\phi/UL - \mu^2$ comparisons made in §2.2.2.

Therefore, the relative importance of dispersion and nonlinearity depends on the size of the disturbance velocity in the $X-$direction. If the disturbance velocity is large, nonlinearity is more important, while if the disturbance velocity is small, dispersion is more important.

The size of the disturbance velocity is governed in part by the hull boundary condition. Matching the outer flow with an inner flow near the ship's hull as done by Tuck (1966) yields the boundary condition (2.2) for the outer potential ϕ. From this we can assess the magnitude of the velocity component in the $y-$direction:

$$\frac{\phi_y}{U} = O\left(\frac{S'(X)}{2h}\right) = O\left(\frac{S_{\max}}{Lh}\right) \tag{2.27}$$

where $S_{\max}$ is the maximum hull section area.

When F_h is close to 1, the velocity component in the $X-$direction is of a different magnitude to that in the $y-$direction. We saw in §2.2.2 that in this case the flow is nearly one-dimensional, such that $\phi_y \ll \phi_X$. Specifically, from the relation (2.23) we have

$$\frac{\partial^2}{\partial y^2} = O\left(\beta, \mu^2, \frac{\phi_X}{U}\right) \frac{\partial^2}{\partial X^2} \ .$$

Here we have returned to unscaled coordinates and used the fact that ϕ was considered scaled with respect to the standard potential UL.

Since it is the maximum of β, μ^2 and ϕ_X/U that governs the ordering, we shall write this as

$$\frac{\partial^2}{\partial y^2} \sim \max\left\{\beta, \mu^2, \frac{\phi_X}{U}\right\} \frac{\partial^2}{\partial X^2}$$

where "$\sim$" means "is of the same order as".

The velocity component ϕ_y is therefore smaller than ϕ_X by a factor

$$\phi_y \sim \max\left\{\beta^{\frac{1}{2}}, \mu, \left(\frac{\phi_X}{U}\right)^{\frac{1}{2}}\right\} \phi_X \ . \tag{2.28}$$

When F_h is very close to 1

Let us consider the case when F_h is very close to 1, such that β is not greater than both μ^2 and ϕ_X/U. Equation (2.28) then states that ϕ_y is of the order

$$\frac{\phi_y}{U} \sim \max\left\{\mu\frac{\phi_X}{U}, \left(\frac{\phi_X}{U}\right)^{\frac{3}{2}}\right\} .$$

We shall now use this along with the condition (2.27) to find the magnitude of ϕ_X/U. Substituting for ϕ_y gives

$$\frac{S_{\max}}{Lh} \sim \max\left\{\mu\frac{\phi_X}{U}, \left(\frac{\phi_X}{U}\right)^{\frac{3}{2}}\right\} .$$

Inverting this gives the magnitude of ϕ_X/U:

$$\frac{\phi_X}{U} \sim \min\left\{\frac{1}{\mu}\frac{S_{\max}}{Lh}, \left(\frac{S_{\max}}{Lh}\right)^{\frac{2}{3}}\right\} . \tag{2.29}$$

Firstly, let us consider the case when

$$\frac{\phi_X}{U} \sim \left(\frac{S_{\max}}{Lh}\right)^{\frac{2}{3}}$$

which corresponds to the nonlinear term in (2.24) being more important. The conditions for this to occur are that

$$\left(\frac{S_{\max}}{Lh}\right)^{\frac{2}{3}} < \frac{1}{\mu}\frac{S_{\max}}{Lh}$$

from (2.29). This simplifies to

$$\frac{S_{\max}}{h^2} > \left(\frac{h}{L}\right)^2 . \tag{2.30}$$

Substituting ϕ_X/U into the condition (2.26) tells us that dispersion may be neglected if

$$\left(\frac{S_{\max}}{Lh}\right)^{\frac{2}{3}} \gg \mu^2 .$$

Rearranging this gives

$$\frac{S_{\max}}{h^2} \gg \left(\frac{h}{L}\right)^2 \tag{2.31}$$

which is of the same form as condition (2.30). Therefore if condition (2.31) is satisfied, with F_h very close to 1 (i.e. $\beta < \mu^2$ and $\beta < \phi_X/U$) we may neglect the dispersive term in our governing equation (2.24).

Now let us return to the relation (2.29) and consider the case when

$$\frac{\phi_X}{U} \sim \frac{1}{\mu}\frac{S_{\max}}{Lh}$$

which corresponds to the dispersive term in (2.24) being more important. The conditions for this to occur are that

$$\frac{1}{\mu}\frac{S_{\max}}{Lh} < \left(\frac{S_{\max}}{Lh}\right)^{\frac{2}{3}}$$

from (2.29). This simplifies to

$$\frac{S_{\max}}{h^2} < \left(\frac{h}{L}\right)^2 . \tag{2.32}$$

Substituting ϕ_X/U into the condition (2.25) tells us that nonlinearity may be neglected if

$$\frac{1}{\mu}\frac{S_{\max}}{Lh} \ll \mu^2 .$$

Rearranging this gives

$$\frac{S_{\max}}{h^2} \ll \left(\frac{h}{L}\right)^2 \tag{2.33}$$

which, again, is of the same form as condition (2.32). Therefore if condition (2.33) is satisfied, with F_h very close to 1, we may neglect the nonlinear term in our governing equation (2.24).

When F_h is moderately close to 1

If F_h is not in the immediate vicinity of 1, so that $\beta > \mu^2$ and $\beta > \phi_X/U$, we have from the relation (2.28) that

$$\frac{\phi_y}{U} \sim \beta^{\frac{1}{2}}\frac{\phi_X}{U} .$$

Substituting for ϕ_y using equation (2.27) tells us that

$$\frac{S_{\max}}{Lh} \sim \beta^{\frac{1}{2}}\frac{\phi_X}{U}$$

so that ϕ_X/U has magnitude

$$\frac{\phi_X}{U} \sim \beta^{-\frac{1}{2}}\frac{S_{\max}}{Lh} .$$

From this we see that ϕ_X/U and therefore the nonlinear term in (2.24) increase in magnitude as $\beta \to 0$.

Using the condition (2.26) we can see that the dispersive term in (2.24) can be neglected if

$$\frac{S_{\max}}{h^2} \gg \beta^{\frac{1}{2}}\frac{h}{L} .$$

Using the condition (2.25), the nonlinear term in (2.24) can be neglected if

$$\frac{S_{\max}}{h^2} \ll \beta^{\frac{1}{2}}\frac{h}{L} . \tag{2.34}$$

This analysis is still valid when $\beta = O(1)$. In that case we need

$$\frac{S_{\max}}{h^2} \ll \frac{h}{L} \tag{2.35}$$

for the nonlinear term to be neglected, which is less restrictive than the condition (2.33). Provided that the condition (2.35) is satisfied, nonlinearity can be neglected whenever

$$\beta \gg \left(\frac{SL}{h^3}\right)^2$$

from condition (2.34).

As $\beta \to 0$ the nonlinear term increases in magnitude and the condition for nonlinearity to be neglected tends towards (2.33).

2.2.4 The linear transcritical equation

The nonlinear but dispersionless form of equation (2.24), namely

$$\left(1 - F_h^2\right)\phi_{XX} + \phi_{yy} - \frac{3}{U}\phi_X\phi_{XX} = 0\ . \tag{2.36}$$

was studied by Lea & Feldman (1972). They used local linearization to approximately solve the equation, and gave results for the trim and bow sinkage of a spheroidal hull in open water. Results were found for $0.8 \leq F_h \leq 1.2$. As there were no experimental results available for this simplified hull shape, it is difficult to judge the accuracy of the theory. However, in the plot of trim as a function of F_h, we do not witness the peak at $F_h \approx 1$ that was consistently present in the experimental results of Graff et al (1964). It is difficult to gauge the form of the midship sinkage, since bow sinkage was plotted by Lea & Feldman, which includes the effect of trim.

Trim and bow sinkage were found for the same hull as was considered by Graff et al (1964) at the exact critical Froude number $F_h = 1$. These were claimed to be similar to the experimental results, although it was not stated which value of h/L was being considered.

Further solutions of this nonlinear but non-dispersive equation were obtained by Ang (1993). He considered steady flow past a ship in a channel, and therefore found that no solution existed when F_h was close to 1. Although the nonlinear flow in a channel can be solved using finite-difference methods, this method is difficult to apply in open water because of the large $y-$domain needed when F_h is close to 1.

In §2.2.3 we found conditions under which the nonlinear term was of much smaller order than the dispersive term in equation (2.24). In summary, this was true if

$$\frac{S_{\max}}{h^2} \ll \frac{h}{L}$$

when $\beta = O(1)$, or

$$\frac{S_{\max}}{h^2} \ll \beta^{\frac{1}{2}} \frac{h}{L}$$

for small β such that $\beta > \mu^2$ and $\beta > \phi_X/U$. When F_h is very close to 1, nonlinearity could only be neglected if

$$\frac{S_{\max}}{h^2} \ll \left(\frac{h}{L}\right)^2 .$$

All of these conditions are quite restrictive for practical ships, and it could be said that it is hard to justify neglecting the nonlinear term in (2.24). However, in this Chapter we shall be doing just that, for the following reasons:

* Nonlinearity is usually included in one-dimensional KdV equations by necessity, as a steepening agent to provide a balance to the broadening effect of the dispersive term in ϕ_{XXXX}. However, here there is an adequate balance instead with the two-dimensional term in ϕ_{yy}.
* We saw from the conditions above that nonlinearity becomes less important away from $F_h = 1$. Our most important reason for studying transcritical flow is to determine the maximum sinkage, which occurs at $F_h \approx 0.9$. The actual flow in the immediate vicinity of $F_h = 1$ is relatively unimportant, as we know from experiment that the sinkage is small in this region.
* It is mainly dispersion that is responsible for limiting the subcritical sinkage; nonlinearity tends to steepen unidirectional waves and leads to breaking unless limited by dispersion in one dimension. However, such steepening effects are of less concern in fully two-dimensional situations where this breaking either does not occur at all, or occurs only in a small region of the (X, y) plane. This is particularly so in water of infinite width as assumed here.
* In finite-width channels, disturbances are larger, transcritical effects are amplified and the flow is more nearly unidirectional. In this case nonlinearity is necessary to describe the flow, as it predicts the onset of unsteadiness and production of solitons. In water of infinite width, no solitons are produced and the flow is steady, so nonlinearity is of less importance.
* The full nonlinear equation (2.24) is difficult and expensive to solve in two dimensions for open water. We wish to be able to provide results over a wide range of Froude numbers, which does not seem feasible using an accurate nonlinear method.
* We have shown that the linear theory is valid for very slender ships. As in other physical problems, it may be true that the linear theory gives good results outside of its expected range of validity. We will see when comparing results to experimental values that this is indeed the case here for predictions of maximum sinkage.

Therefore, by neglecting the nonlinear term in equation (2.24), we only need solve the linear equation

$$\beta\phi_{XX} + \phi_{yy} + \gamma\phi_{XXXX} = 0 \tag{2.37}$$

where we have defined the constant $\gamma = h^2/3$. This is to be solved subject to the same boundary condition (2.2), and will hereafter be referred to as transcritical shallow-water theory (TSWT).

This equation was suggested by Mei (1976) who used it to calculate the resistance of a slender ship at transcritical speeds.

2.3 Transcritical shallow-water theory (TSWT)

Here we solve the transcritical shallow-water equation and show how sinkage and trim can be calculated for a hull of general shape. We then consider the special case of fore-aft symmetric hulls, which gives us a good analytical insight into the nature of the solution. It is then briefly shown how the linear dispersive method can be extended to channels of finite width.

2.3.1 Solution by Fourier transform

The TSWT equation (2.37) can be solved for the potential ϕ by Fourier transform. Because of the symmetry of the problem, we shall here consider the region $y \geq 0$, with the solution being mirrored for $y \leq 0$. Using the Fourier transform

$$\Psi(k, y) = \int_{-\infty}^{\infty} \phi\,(X, y)\; e^{ikX} dX$$

and taking the transform of the partial differential equation (2.37), we obtain

$$-\beta k^2 \Psi + \Psi_{yy} + \gamma k^4 \Psi = 0\,. \tag{2.38}$$

This can be written as

$$\Psi_{yy} = \lambda^2 \Psi \tag{2.39}$$

with $\lambda^2 = \beta k^2 - \gamma k^4$. λ may be either pure real or pure imaginary.

Equation (2.39) has the general solution

$$\Psi = C(k) e^{-\lambda y} + D(k) e^{\lambda y}\,. \tag{2.40}$$

The boundary condition for ϕ as $X, y \to \infty$ states that ϕ must either tend towards zero or behave like an outgoing wave. In either case it must be bounded. Therefore as $y \to \infty$ the Fourier transform $\Psi(k, y)$ must also be bounded.

If $\lambda^2 > 0$, this will only be true if the coefficient of $e^{|\lambda| y}$is zero. Therefore when $\lambda^2 > 0$ we can write

$$\Psi = C(k) e^{-\lambda y} \tag{2.41}$$

with λ defined as the positive square root of λ^2 in this case, i.e.

$$\lambda = \sqrt{\beta k^2 - \gamma k^4} \qquad \text{for } \beta k^2 - \gamma k^4 > 0\,. \tag{2.42}$$

When $\lambda^2 < 0$, λ is imaginary and equation (2.40) represents two wave-like solutions for Ψ. Only one of these will represent outgoing rather than incoming waves. Without loss of generality we can represent Ψ using equation (2.41), and then choose the sign of λ in order to satisfy the "outgoing wave" radiation condition.

In this case, letting $\lambda = i\alpha$, where $\alpha = \pm\sqrt{\gamma k^4 - \beta k^2}$, gives the solution

$$\Psi = C(k)e^{-i\alpha y} \ .$$

Taking the inverse transform then gives the corresponding solution for ϕ:

$$\phi = \frac{1}{2\pi}\int_{-\infty}^{\infty} C(k)e^{-i\alpha y}e^{-ikX}dk \ .$$

In terms of earth-fixed coordinates (x, y), where $x = X - Ut$, this reads

$$\phi = \frac{1}{2\pi}\int_{-\infty}^{\infty} C(k)e^{-ikx}e^{-i\alpha\left(y+\frac{kU}{\alpha}t\right)}dk \ .$$

In order that this represents only outgoing waves in the $y-$direction, the sign of α must be opposite to that of k.

Combining this result with (2.42), we can define λ for all values of k, β, γ as follows:

$$\lambda = \begin{cases} \sqrt{\beta k^2 - \gamma k^4} & \text{for} \quad \beta k^2 - \gamma k^4 > 0 \\ -i\sqrt{\gamma k^4 - \beta k^2} & \text{for} \quad \beta k^2 - \gamma k^4 < 0 \text{ and } k > 0 \\ +i\sqrt{\gamma k^4 - \beta k^2} & \text{for} \quad \beta k^2 - \gamma k^4 < 0 \text{ and } k < 0 \ . \end{cases} \tag{2.43}$$

At subcritical Froude numbers, when $\beta > 0$, this becomes

$$\lambda = \begin{cases} \sqrt{\beta k^2 - \gamma k^4} & \text{for} \quad -\sqrt{\beta/\gamma} < k < \sqrt{\beta/\gamma} \\ -i\sqrt{\gamma k^4 - \beta k^2} & \text{for} \quad k > \sqrt{\beta/\gamma} \\ +i\sqrt{\gamma k^4 - \beta k^2} & \text{for} \quad k < -\sqrt{\beta/\gamma} \ , \end{cases} \tag{2.44}$$

whereas at supercritical Froude numbers, with $\beta < 0$, λ is given by

$$\lambda = \begin{cases} -i\sqrt{\gamma k^4 - \beta k^2} & \text{for} \quad k > 0 \\ +i\sqrt{\gamma k^4 - \beta k^2} & \text{for} \quad k < 0 \ . \end{cases} \tag{2.45}$$

With these definitions for λ, the solution for Ψ is universally represented by equation (2.41).

We can now apply the boundary condition (2.2) which comes from matching with the inner solution. For $y \geq 0$ this reads

$$\phi_y\left(X, 0\right) = \frac{US'(X)}{2h} \ .$$

Taking the Fourier transform yields

$$\Psi_y\left(k, 0\right) = -\frac{Uik\bar{S}(k)}{2h} \tag{2.46}$$

where $\bar{S}(k)$ is the Fourier transform of $S(X)$, i.e.

$$\bar{S}(k) = \int_{-\ell}^{\ell} S(X) e^{ikX} dX$$

Matching the derivative of equation (2.41) to the condition (2.46) determines $C(k)$:

$$-\lambda C(k) = -\frac{Uik\bar{S}(k)}{2h} .$$

Therefore the solution for Ψ is

$$\Psi = \frac{Uik\bar{S}(k)}{2h\lambda} e^{-\lambda y} . \tag{2.47}$$

Taking the inverse transform of this gives us the velocity potential ϕ:

$$\phi(X, y) = \frac{Ui}{4\pi h} \int_{-\infty}^{\infty} \frac{k\bar{S}(k)}{\lambda} e^{-\lambda y} e^{-ikX} dk \tag{2.48}$$

where λ is defined by equations (2.44) and (2.45). For subcritical flow, the integrand in (2.48) has singularities at $k = \pm\sqrt{\beta/\gamma}$. However, as the integrand behaves like $1/\sqrt{k \mp \beta/\gamma}$ near these singularities, they are integrable.

2.3.2 Pressure, forces, and squat

Since the TSWT is a linear theory, we shall use the fixed-ship method to solve for sinkage and trim, as described in Chapter 1. This states that the flow field can be solved with the ship in its rest position rather than in its (as yet unknown) squatted position. To do this we shall introduce the "hydrodynamic" pressure p, which is the pressure excess above hydrostatic

$$p = P + \rho g z .$$

From Bernoulli's equation for the leading term $\phi(X, y)$

$$\frac{p}{\rho} + \frac{1}{2}\left(U + \phi_X\right)^2 + \phi_y^2 = \frac{1}{2}U^2 ,$$

the hydrodynamic pressure is given by

$$p = -\rho U \phi_X \tag{2.49}$$

to leading order. Matching with the inner flow (Tuck 1966) gives the leading order pressure on the hull as

$$p = -\rho U \phi_X|_{y=0} , \tag{2.50}$$

so that p is a function of X only. Once this pressure is known we can find the upward force Z and trim moment M on the ship's hull. The upward force is given as in Chapter 1 by

$$Z = -\rho g \Delta + \int\int^{\zeta} -P \, d\mathbf{S}.\hat{\mathbf{z}} ,$$

submerged part of the hull up to the free surface $z = \zeta$. In linearized flow this free surface height is small; in addition, the hull walls are almost vertical at the waterline, meaning that the pressure produces little upward force near the waterline. If the hull walls make a small angle ω with the vertical, the vertical force can be linearized to

$$Z = -\rho g \Delta + \int\int^{0} -P \; d\mathbf{S}.\hat{\mathbf{z}} + O(P\zeta\omega) \; .$$

undisturbed free surface level $z = 0$, which will simplify the equation. Since P is of the same asymptotic order as ζ, the error is second order even for $\omega = O(1)$, and can be neglected. Therefore in terms of the hydrodynamic pressure, the vertical force is given by

$$\begin{aligned} Z &= -\rho g \Delta + \int\int^{0} (-p(X) + \rho g z) \; d\mathbf{S}.\hat{\mathbf{z}} \\ &= -\rho g \Delta + \oint (-p(X) + \rho g z) \; d\mathbf{S}.\hat{\mathbf{z}} - \int\int (-p(X) + \rho g z)_{z=0} \; dy \, dX \\ &= -\rho g \Delta + \int\int\int \frac{\partial}{\partial z} (-p(X) + \rho g z) \; dV + \int\int_{z=0} p(X) \, dy \, dX \end{aligned}$$

using the divergence theorem. The volume integral is evaluated over that part of the hull lying beneath $z = 0$, with the volume element $dV = dX \, dy \, dz$.

This expression reduces to

$$Z = \int_{-\ell}^{\ell} p(X) B(X) dX \; . \tag{2.51}$$

Since the upward force on any thin cross-sectional slice of thickness dX at station X is $dZ = p(X)B(X) \, dX$, the bow-up trim moment

$$M = -\int_{-\ell}^{\ell} X \, dZ$$

is given by

$$M = -\int_{-\ell}^{\ell} X \, p(X) B(X) dX \; . \tag{2.52}$$

Substituting the expression (2.48) for ϕ into equation (2.50) for the hydrodynamic pressure p, we obtain

$$p(X) = -\frac{\rho U^2}{4\pi h} \lim_{y \to 0} \int_{-\infty}^{\infty} \frac{k^2 \bar{S}(k)}{\lambda} \, e^{-\lambda y} \, e^{-ikX} \, dk \; .$$

The upward force Z on the ship as given by expression (2.51) is now

$$Z = -\frac{\rho U^2}{4\pi h} \int_{-\infty}^{\infty} \frac{k^2}{\lambda} \bar{S}(k) \bar{B}^*(k) dk \; . \tag{2.53}$$

Similarly the bow-up trim moment becomes

$$M = \frac{\rho U^2}{4\pi h} \int_{-\infty}^{\infty} \frac{k^2}{\lambda} \bar{S}(k) \overline{XB}^*(k) dk \; . \tag{2.54}$$

In these two expressions we have introduced the Fourier transforms of $B(X)$ and $XB(X)$, namely

$$\begin{aligned} \bar{B}(k) &= \int_{-\ell}^{\ell} B(X) e^{ikX} dX \\ \overline{XB}(k) &= \int_{-\ell}^{\ell} XB(X) e^{ikX} dX \ . \end{aligned} \tag{2.55}$$

In each case an asterisk denotes the complex conjugate.

Mei (1976) expressed the transcritical force in a form similar to (2.3), where the logarithm is replaced by a kernel involving Bessel and Struve functions. He did not attempt to calculate it numerically. Here we prefer to use the Fourier-transformed version (2.53) for computational purposes.

We note using the identity

$$\frac{1}{2} \int_{-\infty}^{\infty} |k| \bar{S}(k) \bar{B}^*(k) dk = - \int\int B'(X) S'(\xi) \log |X - \xi| \ dX \ d\xi \tag{2.56}$$

that the TSWT vertical force (2.53) agrees with the SWT result (2.3) in the limit as $\gamma \to 0$, i.e. when transcritical dispersion effects are negligible. In performing this limit, we must scale γ using the ship's length L, so that we are in essence taking the limit as $h/L \to 0$. Similarly the trim moment (2.54), and therefore actual sinkage and trim, all agree with SWT in the limit $h/L \to 0$.

Once the vertical force and trim moment are known, we can solve for sinkage and trim in a similar manner to that of Chapter 1, using the equilibrium equations

$$\begin{aligned} Z + \rho g \int_{-\ell}^{\ell} \{ s + X\theta \} \, B(X) \, dX &= 0 \\ M - \rho g \int_{-\ell}^{\ell} X \, \{ s + X\theta \} \, B(X) \, dX &= 0 \ . \end{aligned} \tag{2.57}$$

These can be solved simultaneously for the (downward) midship sinkage s and bow-up trim angle θ:

$$\begin{aligned} s &= \frac{1}{\rho g} \left\{ \frac{M_{\rm W} M + I_{\rm W} Z}{M_{\rm W}^2 - A_{\rm W} I_{\rm W}} \right\} \\ \theta &= \frac{1}{\rho g} \left\{ \frac{A_{\rm W} M + M_{\rm W} Z}{A_{\rm W} I_{\rm W} - M_{\rm W}^2} \right\} \ . \end{aligned} \tag{2.58}$$

As in Chapter 1, the hull parameters $A_{\rm W}, M_{\rm W}, I_{\rm W}$ are defined as

$$\begin{aligned} A_{\rm W} &= \int_{-\ell}^{\ell} B(X) \, dX \\ M_{\rm W} &= \int_{-\ell}^{\ell} X \, B(X) \, dX \\ I_{\rm W} &= \int_{-\ell}^{\ell} X^2 \, B(X) \, dX \ . \end{aligned} \tag{2.59}$$

2.3.3 Numerical method

In order to calculate the integrals (2.53) and (2.54) for a general hull shape, we discretize the $k-$variable into the discrete values $k_j = j\,\delta_k$ for integer values of j. The Fourier transforms $\bar{S}(k)$, $\bar{B}(k)$ and $\overline{XB}(k)$ are evaluated at these points k_j using Filon quadrature (see e.g. Abramowitz & Stegun p. 890). This is a method for taking Fourier transforms whereby the original function is approximated by a parabola over each pair of subintervals, using the functional values at the three discrete points k_j. The transform of this parabola is taken exactly, so that the method is accurate even when k is large and the integrand is highly oscillatory.

Although for clarity we have not introduced scaled variables here, in the computations $B(X)$ and $S(X)$ were scaled with respect to their maximum values; distances in the $X-$direction were scaled with respect to the shiplength L; and as a consequence k was scaled with respect to $1/L$. The range of scaled $k-$values was chosen to be [-100,100] for the computations; because of the linearity this was independent of ship dimensions. In both integrals, k^2/λ is bounded for large k, while $\bar{S}(k)$, $\bar{B}(k)$ and $\overline{XB}(k)$ all tend rapidly to zero for large k. For all Froude numbers the integrands were negligible for scaled values of $|k| > 60$. Redoing the calculations with a scaled k range of [-1000,1000] made negligible difference to Z or M.

The step size used in the scaled variable was $\delta_k = 0.1$, except in the special cases which we shall discuss. Redoing the calculations with $\delta_k = 0.01$ made negligible difference to Z or M.

The integrals (2.53) and (2.54) are treated differently depending on whether F_h is greater than or less than 1. We shall describe each case separately.

Supercritical

When $\beta < 0$, λ is given by equation (2.45) and the integrands in (2.53) and (2.54) are non-singular. Therefore we can evaluate them simply using Simpson's method. This approximates the integrand by a parabola over each pair of subintervals, using the value of the integrand at the three discrete points k_j. This parabola is then integrated exactly over each pair of subintervals.

Adding up all of these contributions yields the expression

$$Z = -\frac{\rho U^2}{4\pi h} \sum_{j=-N}^{N} w_j \frac{k_j^2}{\lambda_j} \bar{S}(k_j)\bar{B}^*(k_j)\,\delta_k \,. \tag{2.60}$$

Here we have defined the total number of subintervals as $2N$. If we choose N to be even, the weights w_j are 4/3 when j is odd and 2/3 when j is even; at the endpoints $j = \pm N$, $w_j = 1/3$.

A similar expression is used for the moment M, with $\bar{B}$ being replaced by $-\overline{XB}$.

Subcritical

When $\beta > 0$, λ is given by equation (2.44); we see that $\lambda = 0$ when $k = \pm\sqrt{\beta/\gamma}$. Therefore the integrands in (2.53) and (2.54) have singularities at these points, which must be treated carefully.

As previously stated, these singularities are integrable. Therefore we shall integrate the singular part of the integral exactly in the vicinity of the singularities.

Firstly, we choose our step size δ_k so that both singularities lie at discrete points k_j. The number of subintervals in $[0,\sqrt{\beta/\gamma}]$ is defined as N_1, while for $k > \sqrt{\beta/\gamma}$ there are N_2 subintervals. Similar partitions exist for $k < 0$. For simplicity we shall make both N_1 and N_2 even integers.

When $\sqrt{\beta/\gamma}$ is large, we can make $\delta_k \approx 0.1$ by choosing N_1 to be the closest even integer to $\sqrt{\beta/\gamma}/0.1$. The step size is then

$$\delta_k = \frac{\sqrt{\beta/\gamma}}{N_1} \; .$$

To keep an approximate $k-$range of [-100,100] we choose in this case

$$N_2 = 1000 - N_1 \; .$$

If $\sqrt{\beta/\gamma}$ is small, we need a smaller step size in the range $|k| < \sqrt{\beta/\gamma}$, where the integrand changes rapidly. We choose

$$N_1 = 10 \qquad \text{for} \quad \sqrt{\beta/\gamma} \leq 1.0$$

so that

$$\delta_k = \frac{\sqrt{\beta/\gamma}}{N_1}$$

again. In order to keep the approximate $k-$range of [-100,100] we choose N_2 as the closest even integer to $(100/\delta_k)$ here.

We now break up the integral (2.53) into different parts on each side of the singularities. When k is within two gridpoints of the singularities, we integrate the singular part exactly; otherwise, we use Simpson's rule as we did for supercritical Froude numbers. The expression (2.53) for Z is written

$$\begin{aligned} Z = \; - \; & \frac{\rho U^2}{4\pi h} \Bigg\{ \sum_{j=-N_1-N_2}^{-N_1-2} w_j \frac{k_j^2}{\lambda_j} \bar{S}(k_j)\bar{B}^*(k_j)\,\delta_k \\ + \; & \int_{-\sqrt{\beta/\gamma}-2\delta_k}^{-\sqrt{\beta/\gamma}} \frac{k^2}{i\sqrt{\gamma}} \frac{1}{\sqrt{k^2\,(k^2-\beta/\gamma)}} \bar{S}(k)\bar{B}^*(k)dk \\ + \; & \int_{-\sqrt{\beta/\gamma}}^{-\sqrt{\beta/\gamma}+2\delta_k} \frac{k^2}{\sqrt{\gamma}} \frac{1}{\sqrt{k^2\,(\beta/\gamma-k^2)}} \bar{S}(k)\bar{B}^*(k)dk + \sum_{j=-N_1+2}^{N_1-2} w_j \frac{k_j^2}{\lambda_j} \bar{S}(k_j)\bar{B}^*(k_j)\,\delta_k \end{aligned}$$

$$+ \int_{\sqrt{\beta/\gamma}-2\delta_k}^{\sqrt{\beta/\gamma}} \frac{k^2}{\sqrt{\gamma}} \frac{1}{\sqrt{k^2\,(\beta/\gamma - k^2)}} \bar{S}(k)\bar{B}^*(k)dk$$

$$+ \int_{\sqrt{\beta/\gamma}}^{\sqrt{\beta/\gamma}+2\delta_k} \frac{k^2}{-i\sqrt{\gamma}} \frac{1}{\sqrt{k^2\,(k^2 - \beta/\gamma)}} \bar{S}(k)\bar{B}^*(k)dk + \sum_{j=N_1+2}^{N_1+N_2} w_j \frac{k_j^2}{\lambda_j} \bar{S}(k_j)\bar{B}^*(k_j)\,\delta_k \Bigg\} .$$

As in the supercritical case, w_j is equal to $4/3$ when j is odd, $2/3$ when j is even and $1/3$ at the end points of *each* summation interval.

In order to evaluate the integrals near the singularities, we use the indefinite integrals

$$\int \frac{k}{\sqrt{k^2 - \beta/\gamma}}\, dk = \sqrt{k^2 - \beta/\gamma}$$

$$\int \frac{k}{\sqrt{\beta/\gamma - k^2}}\, dk = -\sqrt{\beta/\gamma - k^2}$$

and approximate $\bar{S}(k)\bar{B}^*(k)$ by a constant over each small interval, equal to its value at the centre of that interval. We can now evaluate the integrals to yield

$$\begin{aligned} Z = \; - \; & \frac{\rho U^2}{4\pi h} \Bigg\{ \sum_{j=-N_1-N_2}^{-N_1-2} w_j \frac{k_j^2}{\lambda_j} \bar{S}(k_j)\bar{B}^*(k_j)\,\delta_k \\ & + \frac{\bar{S}(k_{-N_1-1})\bar{B}^*(k_{-N_1-1})}{i\sqrt{\gamma}} \left[-\sqrt{k^2 - \beta/\gamma}\right]_{-\sqrt{\beta/\gamma}-2\delta_k}^{-\sqrt{\beta/\gamma}} \\ & + \frac{\bar{S}(k_{-N_1+1})\bar{B}^*(k_{-N_1+1})}{\sqrt{\gamma}} \left[\sqrt{\beta/\gamma - k^2}\right]_{-\sqrt{\beta/\gamma}}^{-\sqrt{\beta/\gamma}+2\delta_k} + \sum_{j=-N_1+2}^{N_1-2} w_j \frac{k_j^2}{\lambda_j} \bar{S}(k_j)\bar{B}^*(k_j)\,\delta_k \\ & + \frac{\bar{S}(k_{N_1-1})\bar{B}^*(k_{N_1-1})}{\sqrt{\gamma}} \left[-\sqrt{\beta/\gamma - k^2}\right]_{\sqrt{\beta/\gamma}-2\delta_k}^{\sqrt{\beta/\gamma}} \\ & + \frac{\bar{S}(k_{N_1+1})\bar{B}^*(k_{N_1+1})}{-i\sqrt{\gamma}} \left[\sqrt{k^2 - \beta/\gamma}\right]_{\sqrt{\beta/\gamma}}^{\sqrt{\beta/\gamma}+2\delta_k} + \sum_{j=N_1+2}^{N_1+N_2} w_j \frac{k_j^2}{\lambda_j} \bar{S}(k_j)\bar{B}^*(k_j)\,\delta_k \Bigg\} \end{aligned}$$

or

$$\begin{aligned} Z = \; - \; & \frac{\rho U^2}{4\pi h} \Bigg\{ \sum_{j=-N_1-N_2}^{-N_1-2} w_j \frac{k_j^2}{\lambda_j} \bar{S}(k_j)\bar{B}^*(k_j)\,\delta_k \\ & + \frac{\bar{S}(k_{-N_1-1})\bar{B}^*(k_{-N_1-1})}{i\sqrt{\gamma}} \sqrt{4\delta_k\,(\beta/\gamma) + 4\delta_k^2} \\ & + \frac{\bar{S}(k_{-N_1+1})\bar{B}^*(k_{-N_1+1})}{\sqrt{\gamma}} \sqrt{4\delta_k\,(\beta/\gamma) - 4\delta_k^2} + \sum_{j=-N_1+2}^{N_1-2} w_j \frac{k_j^2}{\lambda_j} \bar{S}(k_j)\bar{B}^*(k_j)\,\delta_k \\ & + \frac{\bar{S}(k_{N_1-1})\bar{B}^*(k_{N_1-1})}{\sqrt{\gamma}} \sqrt{4\delta_k\,(\beta/\gamma) - 4\delta_k^2} \\ & - \frac{\bar{S}(k_{N_1+1})\bar{B}^*(k_{N_1+1})}{i\sqrt{\gamma}} \sqrt{4\delta_k\,(\beta/\gamma) + 4\delta_k^2} + \sum_{j=N_1+2}^{N_1+N_2} w_j \frac{k_j^2}{\lambda_j} \bar{S}(k_j)\bar{B}^*(k_j)\,\delta_k \Bigg\} . \end{aligned}$$

A similar expression is used to compute M, with $\bar{B}$ replaced by $-\overline{XB}$. Once Z and M are computed, the sinkage and trim are found from equation (2.58).

2.3.4 Symmetric hulls

Let us illustrate analytically some properties of the transcritical shallow-water theory, by considering the special case of ships with fore-aft symmetry. In that case, $B(X)$ and $S(X)$ are both even functions of X. Since

$$\bar{B}(k) = \int_{-\ell}^{\ell} B(X)\, \cos(kX)\, dX + i \int_{-\ell}^{\ell} B(X)\, \sin(kX)\, dX \ ,$$

and similarly for $\bar{S}(k)$, the imaginary parts of $\bar{B}(k)$ and $\bar{S}(k)$ vanish. As such, the star is unnecessary in equation (2.54). In addition, the real-valued $\bar{B}(k)$ and $\bar{S}(k)$ are even functions of k.

On the other hand, $X\,B(X)$ is odd in X, so that $\overline{XB}(k)$ is pure imaginary and odd in k. In addition to these simplifications to the force and moment expressions (2.53) and (2.54), the hydrostatic coupling between sinkage and trim vanishes for fore-aft symmetry. In this case the expressions (2.58) become

$$\begin{aligned} s &= -\frac{Z}{\rho g A_{\mathrm{W}}} \\ \theta &= \frac{M}{\rho g I_{\mathrm{W}}} \ . \end{aligned} \tag{2.61}$$

We shall now look at the simplified sinkage and trim for supercritical and subcritical flow.

Supercritical

At supercritical Froude numbers, λ as given by equation (2.45) is odd in k. Therefore the integrand of the force integral (2.53) is also odd in k, and Z vanishes. Using equation (2.61), the supercritical sinkage is thus identically zero for fore-aft symmetric hulls. Although this result is not quite true for non-symmetric hulls, we shall see that the theory still predicts a very small supercritical sinkage. This is in agreement with the simple shallow-water theory (SWT) described in §2.1, which also predicts zero supercritical sinkage for fore-aft symmetric hulls.

The integrand in the moment expression (2.54) is even in k, so that we can write

$$M = \frac{\rho U^2}{2\pi h} \int_0^{\infty} \frac{ik}{\sqrt{\gamma k^2 - \beta}} \bar{S}(k) \overline{XB}(k) dk \ , \tag{2.62}$$

whereupon the trim angle θ is given from equation (2.61) by

$$\theta = \frac{F_h^2}{2\pi I_{\mathrm{W}}} \int_0^{\infty} \frac{ik}{\sqrt{\gamma k^2 - \beta}} \bar{S}(k) \overline{XB}(k) dk \ . \tag{2.63}$$

This amounts to a significant bow-up trim in the supercritical Froude number range, in agreement with SWT. Here, however, the trim is finite as $F_h \to 1$.

Subcritical

When $\beta > 0$, λ is given by equation (2.44). We see that λ is even in k for $|k| < \sqrt{\beta/\gamma}$ and odd in k for $|k| > \sqrt{\beta/\gamma}$. Therefore the force integrand (2.53) is also even for $|k| < \sqrt{\beta/\gamma}$ and odd for $|k| > \sqrt{\beta/\gamma}$, so that it reduces to

$$Z = -\frac{\rho U^2}{2\pi h} \int_0^{\sqrt{\beta/\gamma}} \frac{k}{\sqrt{\beta - \gamma k^2}} \bar{S}(k)\bar{B}(k)\, dk \,. \tag{2.64}$$

Using the relation (2.61), the sinkage is given by

$$s = \frac{F_h^2}{2\pi A_{\mathrm{W}}} \int_0^{\sqrt{\beta/\gamma}} \frac{k}{\sqrt{\beta - \gamma k^2}} \bar{S}(k)\bar{B}(k)\, dk \,. \tag{2.65}$$

This force is non-singular as $\beta \to 0$. In fact, we can show how it behaves asymptotically as $\beta \to 0$:

$$\begin{aligned}
s &\sim \frac{1}{2\pi A_{\mathrm{W}}\sqrt{\gamma}} \int_0^{\sqrt{\beta/\gamma}} \frac{k}{\sqrt{\beta/\gamma - k^2}} \bar{S}(k)\bar{B}(k)\, dk \\
&\sim \frac{\bar{S}(0)\bar{B}(0)}{2\pi A_{\mathrm{W}}\sqrt{\gamma}} \int_0^{\sqrt{\beta/\gamma}} \frac{k}{\sqrt{\beta/\gamma - k^2}}\, dk \\
&= \frac{\bar{S}(0)\bar{B}(0)}{2\pi A_{\mathrm{W}}\sqrt{\gamma}} \left[-\sqrt{\frac{\beta}{\gamma} - k^2} \right]_0^{\sqrt{\beta/\gamma}} \\
&= \frac{\Delta A_{\mathrm{W}}}{2\pi A_{\mathrm{W}}\sqrt{\gamma}} \sqrt{\frac{\beta}{\gamma}} \\
&= \frac{\Delta\sqrt{1 - F_h^2}}{2\pi\gamma} \,.
\end{aligned}$$

We see that the subcritical sinkage tends towards zero in a square-root manner as $F_h \to 1$.

The moment integrand in equation (2.54) is odd for $|k| < \sqrt{\beta/\gamma}$ and even for $|k| > \sqrt{\beta/\gamma}$, so that the trim moment reduces to

$$M = \frac{\rho U^2}{2\pi h} \int_{\sqrt{\beta/\gamma}}^{\infty} \frac{ik}{\sqrt{\gamma k^2 - \beta}} \bar{S}(k)\overline{XB}(k)\, dk \,, \tag{2.66}$$

giving a trim angle

$$\theta = \frac{F_h^2}{2\pi I_{\mathrm{W}}} \int_{\sqrt{\beta/\gamma}}^{\infty} \frac{ik}{\sqrt{\gamma k^2 - \beta}} \bar{S}(k)\overline{XB}(k)\, dk \,. \tag{2.67}$$

The subcritical trim is non-zero according to this theory; it increases as $\beta \to 0$ but remains finite. As $\gamma \to 0$ the trim tends towards zero at all subcritical Froude numbers, in accordance with SWT.

2.3.5 Finite-width channel

We now solve the TSWT equation (2.37) for a ship moving along the centre of a channel. We expect that the steady linear theory will be of limited validity in this case, because it is well known that unsteady effects are important in finite-width channels. In fact, as we saw in Chapter 1, it is only by including nonlinearity that the onset of unsteadiness can be predicted; this linear theory will furnish a steady solution even when F_h is close to 1.

For Froude numbers not too close to 1, or in wide channels, the flow is still steady and this theory could be used. When the true flow is unsteady, the theory would serve only as an approximation to the time-averaged unsteady flow.

As we shall see, although the resulting equations are simple, their solution is extremely difficult. We put this theory forward mainly for mathematical interest rather than practical use.

Fourier transform solution

As was done in §2.3.1, we solve the problem by Fourier transform. The same equation (2.39) for the transformed variable Ψ applies, except that the boundary condition as $|y| \to \infty$ is here replaced by a wall boundary condition on the channel walls $y = \pm w/2$. Again, we shall solve the flow in the region $y \geq 0$, with the solution being mirrored for $y \leq 0$.

The wall boundary condition is

$$\phi_y|_{y=w/2} = 0$$

which, on taking the Fourier transform, becomes

$$\Psi_y|_{y=w/2} = 0\,. \tag{2.68}$$

The general solution of equation (2.39) can be written in the form

$$\Psi = C_1(k)\cosh\left\{\lambda\left(y - \frac{w}{2}\right)\right\} + D_1(k)\sinh\left\{\lambda\left(y - \frac{w}{2}\right)\right\}\,.$$

Applying the boundary condition (2.68) requires that $D_1(k) = 0$. Therefore

$$\Psi = C_1(k)\cosh\left\{\lambda\left(y - \frac{w}{2}\right)\right\}\,. \tag{2.69}$$

Since we are considering a finite domain in the $y-$direction, there is no need for a radiation condition in this direction. As such, we can choose λ to be either $\pm\sqrt{\beta k^2 - \gamma k^4}$. We can see from the solution (2.69), which is even in λ, that the sign of λ is irrelevant even when λ is imaginary. We shall see later that a radiation condition must instead be applied in the $X-$direction for this case of a ship in a channel.

In order to determine $C_1(k)$ we use the same transformed hull boundary condition (2.46), which becomes

$$\lambda C_1(k) \sinh\left\{-\frac{\lambda w}{2}\right\} = -\frac{Uik\bar{S}(k)}{2h} .$$

Using this in equation (2.69), the solution for Ψ is

$$\Psi = \frac{Uik\bar{S}(k)}{2h\lambda \sinh\left\{\frac{\lambda w}{2}\right\}} \cosh\left\{\lambda\left(y - \frac{w}{2}\right)\right\} . \tag{2.70}$$

Taking the inverse transform gives the velocity potential ϕ:

$$\phi = \frac{Ui}{4\pi h}\int_{-\infty}^{\infty} \frac{k\bar{S}(k)}{\lambda \sinh\left\{\frac{\lambda w}{2}\right\}} \cosh\left\{\lambda\left(y - \frac{w}{2}\right)\right\} e^{-ikX}\, dk . \tag{2.71}$$

The hull pressure as given by equation (2.50) has the form

$$p = -\frac{\rho U^2}{4\pi h} \lim_{y\to 0} \int_{-\infty}^{\infty} \frac{k^2\bar{S}(k)}{\lambda} \coth\left\{\frac{\lambda w}{2}\right\} e^{-\lambda y}\, e^{-ikX}\, dk . \tag{2.72}$$

The upward force and bow-up trim moment are now given from equations (2.51) and (2.52) as

$$\begin{aligned} Z &= -\frac{\rho U^2}{4\pi h}\int_{-\infty}^{\infty} \frac{k^2}{\lambda} \coth\left\{\frac{\lambda w}{2}\right\} \bar{S}(k)\bar{B}^*(k)dk \\ M &= \frac{\rho U^2}{4\pi h}\int_{-\infty}^{\infty} \frac{k^2}{\lambda} \coth\left\{\frac{\lambda w}{2}\right\} \bar{S}(k)\overline{XB}^*(k)dk . \end{aligned} \tag{2.73}$$

We see that these differ from the open-water expressions (2.53) and (2.54) only by the factor of $\coth(\lambda w/2)$ in the integrand. However, this factor has a profound effect on the form of the integrand.

In the subcritical case, λ is real for $|k| < \sqrt{\beta/\gamma}$ and the integrand is non-singular, as it is for open water. However, the singularity at $|k| = \sqrt{\beta/\gamma}$ is now of a different form, since $\coth(\lambda w/2)$ is also singular at this point. As $|k| \to \sqrt{\beta/\gamma}$, $\lambda \to 0$, so that

$$\coth(\lambda w/2) \to \frac{1}{(\lambda w/2)}$$

and

$$\begin{aligned} \frac{k^2}{\lambda} \coth\left\{\frac{\lambda w}{2}\right\} &\to \frac{2k^2}{w\lambda^2} \\ &= -\frac{2}{w\gamma\left(k + \sqrt{\beta/\gamma}\right)\left(k - \sqrt{\beta/\gamma}\right)} . \end{aligned} \tag{2.74}$$

This result applies whether λ is real or imaginary, i.e. whether $|k|$ is less than or greater than $\sqrt{\beta/\gamma}$. Therefore this point is a *simple pole.*

When λ is imaginary, further singularities exist whenever $\lambda w/2 = n\pi$ for integer values of n. This is true for both subcritical and supercritical flow. Rearranging using $\lambda^2 = \beta k^2 - \gamma k^4$ tells us that these occur at the points k_n, defined by

$$k_n^2 = \begin{cases} \frac{\beta}{2\gamma}\left(1 + \sqrt{1 + \frac{4n^2\pi^2\gamma}{w^2\beta^2}}\right) & \text{if} \quad \beta > 0 \\ \frac{\beta}{2\gamma}\left(1 - \sqrt{1 + \frac{4n^2\pi^2\gamma}{w^2\beta^2}}\right) & \text{if} \quad \beta < 0\,. \end{cases} \tag{2.75}$$

The case $n = 0$ corresponds in the subcritical case to the double point $k_0 = \pm\sqrt{\beta/\gamma}$, while in the supercritical case it corresponds to $k_0 = 0$.

To see the form of the singularities for arbitrary n (excluding $n = 0$ for $\beta > 0$, which we have already considered), we let $\lambda = i\alpha$, where α is real. Using $\coth(i\alpha) = -i\cot(\alpha)$, this gives

$$\frac{k^2}{\lambda}\coth\left\{\frac{\lambda w}{2}\right\} = -\frac{k^2}{\alpha}\cot\left\{\frac{\alpha w}{2}\right\}\,.$$

The singularities occur at $\alpha_n = 2n\pi/w$; we can expand in a Taylor series around these points to give

$$\begin{aligned} \tan\left\{\frac{\alpha w}{2}\right\} &\sim \tan\left\{\frac{\alpha_n w}{2}\right\} + \frac{w}{2}\sec^2\left\{\frac{\alpha_n w}{2}\right\}(\alpha - \alpha_n) \\ &= \frac{w}{2}(\alpha - \alpha_n) \end{aligned}$$

so that

$$\frac{k^2}{\lambda}\coth\left\{\frac{\lambda w}{2}\right\} \sim -\frac{2k^2}{w\alpha_n}\,\frac{1}{\alpha - \alpha_n} \tag{2.76}$$

when α is close to α_n.

Also, since $\alpha^2 = \gamma k^4 - \beta k^2$, we have

$$\alpha\, d\alpha = \left(2\gamma k^3 - \beta k\right) dk$$

so that, around α_n,

$$\alpha_n(\alpha - \alpha_n) \sim \left(2\gamma k_n^3 - \beta k_n\right)(k - k_n)\,.$$

Therefore, from the relation (2.76), we have

$$\frac{k^2}{\lambda}\coth\left\{\frac{\lambda w}{2}\right\} \sim -\frac{2k_n^2}{w\left(2\gamma k_n^3 - \beta k_n\right)}\,\frac{1}{k - k_n} \tag{2.77}$$

near each singularity k_n. $2\gamma k_n^3 - \beta k_n$ can only equal zero when $|k| = \beta/(2\gamma)$, which is outside the range of λ being imaginary for either subcritical or supercritical flow. The point $k_0 = 0$, for supercritical flow, is non-singular because of the factor of k^2 in the numerator. Therefore all of the singularities at the points given by expression (2.75) are *simple poles.*

The path of integration in the complex $k-$plane must pass around all of these poles, and it is in deciding which way to pass around the poles that the radiation condition is used. This is contrary to the open-water case, in which the two singularities were of

inverse-square-root type. In that case it did not matter whether the path of integration passed above or below the singularities, as the arc integral is zero and we only needed to evaluate the Cauchy principal value part of the integral.

When the path of integration in the complex $k-$plane passes either above or below a pole, k has either a positive or a negative imaginary part respectively. Suppose in this case

$$k = k_r + ik_i \ .$$

Then, looking at the velocity potential (2.71), we can see that he sign of k_i will influence the behaviour as $X \to -\infty$. Specifically, the e^{-ikX} term now has the form

$$e^{-ikX} = e^{-ik_rX} e^{k_iX} \ .$$

The radiation condition used here is that there should be no disturbance as $X \to -\infty$; therefore we must choose $k_i > 0$, so that the path of integration must pass *above* the poles in the complex $k-$plane. This applies whether k is positive or negative.

The force and moment expressions (2.73) must therefore each be evaluated as a Cauchy principal value integral plus a sum of arc integrals passing above each of the singularities. Looking specifically at the upward force Z, the sum of arc integrals has the form

$$-\frac{\rho U^2}{4\pi h} \sum_{n=-\infty}^{\infty} \bar{S}(k_n)\bar{B}^*(k_n).\,(-\pi i)\,\mathrm{res}\left(\frac{k^2}{\lambda}\coth\left\{\frac{\lambda w}{2}\right\}\ ;\ k_n\right) \ .$$

For subcritical flow, the residue at the double point $n = 0$ (i.e. $k = \pm\sqrt{\beta/\gamma}$ is evaluated using the relation (2.74) to be

$$-\frac{4}{w\sqrt{\gamma\beta}}\,\mathrm{sgn}\,k \ .$$

For all of the other points k_n we can use the expression (2.77) to find the residues, giving

$$-\frac{2k_n^2}{w\,(2\gamma k_n^3 - \beta k_n)} \ .$$

The sum of arc integrals for supercritical flow now has the form

$$\frac{\rho U^2 i}{4h} \sum_{n=-\infty}^{\infty} \bar{S}(k_n)\bar{B}^*(k_n)\frac{2k_n^2}{w\,(2\gamma k_n^3 - \beta k_n)}$$

where the points k_n are given by equation (2.75). In the subcritical case we must add the contributions around $k = \pm\sqrt{\beta/\gamma}$, namely

$$\frac{\rho U^2 i}{wh\sqrt{\gamma\beta}}\left[\bar{S}(-\sqrt{\frac{\beta}{\gamma}})\bar{B}^*(-\sqrt{\frac{\beta}{\gamma}}) - \bar{S}(\sqrt{\frac{\beta}{\gamma}})\bar{B}^*(\sqrt{\frac{\beta}{\gamma}})\right] \ .$$

In calculating the trim moment M, we replace $\bar{B}$ by $-\overline{XB}$ in the above expressions.

Summing up these residues for a ship of general shape is relatively straightforward, as they die away to zero quite quickly as $|k|$ increases. In the special case of fore-aft symmetric

hulls, where $\bar{S}(k)$ and $\bar{B}(k)$ are real and even in k, the residues are odd in k and their sum is zero.

However, numerical evaluation of the Cauchy principal value part of (2.73) is complicated, due to the infinite number of unequally spaced poles. Even for symmetric hulls there is no cancellation for $|k| > \sqrt{\beta/\gamma}$; the integrand in that case is even in k, whereas in open water (§2.3.4) it is odd. The integration over a small region either side of each singularity can be handled analytically, and we shall do this in Appendix B.2. However, the difficulty in separately computing the integral over each non-singular region deterred us from giving numerical results for this theory.

2.4 Finite-depth theory (FDT)

The TSWT just described is a shallow-water theory which includes the dispersive term of leading order in the small quantity h/L.

We shall now look at a theory which is *fully-dispersive*; that is, no assumption about shallowness is made whatsoever. As such, the variation of linear wave speed with wavelength and water depth is exact according to this theory. It is equally valid for any depth of water, even in the limit of infinite depth.

The method was introduced by Tuck & Taylor (1970), who derived the basic formulae that we shall reproduce here. Because of the complexity of the resulting integrals, they only gave limited numerical results for symmetric hulls. Here we study the integrals in more detail and use the theory to predict the midship sinkage of a ship of general shape.

2.4.1 The original equations

Tuck & Taylor considered the linearized flow around a slender ship moving in an arbitrary depth of water. They found that the vertical force and trim moment are each the sum of two components, i.e.

$$\begin{aligned} Z &= Z_\infty + Z_d \\ M &= M_\infty + M_d \,. \end{aligned} \tag{2.78}$$

Here Z_∞ and M_∞ are the force and moment on the lower half of an equivalent double body in an unbounded fluid; Z_d and M_d are a correction due to the finite depth of water.

In Appendix B.3 and with numerical results we show that the corrections Z_d and M_d tend to the TSWT expressions (2.53) and (2.54) as $h/L \to 0$. Since these expressions are inversely proportional to the depth, and Z_∞, M_∞ are independent of depth, Z_d and M_d formally dominate Z_∞ and M_∞ as $h/L \to 0$.

The calculation of Z_∞ and M_∞ is a well-known but difficult problem. At practical h/L values, Z_∞ is still appreciable and must be included in the force computations.

Here we approximate Z_∞ using the analytic formula of Havelock (1939) for a spheroid, and approximate each hull as an equivalent slender spheroid of the same length and displacement, as done by Tuck & Taylor (1970). This gives for Z_∞

$$Z_\infty = \rho U^2 A_W \epsilon^2 \left(\log \frac{\epsilon}{2} + \frac{3}{2} - \epsilon \right) \tag{2.79}$$

with A_W again the waterplane area. The slenderness ϵ is equal to the beam/length ratio of the equivalent spheroid; for a general hull this is given by

$$\epsilon = \sqrt{\frac{12}{\pi} C_\forall} \; . \tag{2.80}$$

Here $C_\forall$ is the volumetric coefficient Δ / L^3, with Δ the displaced volume. The linearized flow furnished by this theory is of leading order in the small quantity ϵ.

For fore-aft symmetric ships, M_∞ is identically zero. Since the hull shapes that we are considering are close to fore-aft symmetric, we shall not attempt the difficult calculation of M_∞, assuming instead that it is small enough to be neglected for midship sinkage calculations.

The depth corrections Z_d and M_d were found by Tuck & Taylor to satisfy

$$\begin{aligned} Z_d &= -\frac{\rho U^2}{4\pi^2} \int_{-\infty}^{\infty} k^2 \bar{S}(k) \bar{B}^*(k) \Omega(k) dk \\ M_d &= \frac{\rho U^2}{4\pi^2} \int_{-\infty}^{\infty} k^2 \bar{S}(k) \overline{XB}^*(k) \Omega(k) dk \; , \end{aligned} \tag{2.81}$$

where $\Omega(k)$ is given by

$$\Omega(k) = -2 \int_{|k|}^{\infty} \frac{1}{\sqrt{q^2 - k^2}} \left[1 - \frac{q}{q \tanh(qh) - F_h^2 k^2 h} \right] dq \; . \tag{2.82}$$

Apart from the complicated integral defining $\Omega(k)$, these Fourier-transformed expressions are similar to the TSWT expressions (2.53) and (2.54).

2.4.2 Studying the $\Omega(k)$ integral

The integrand in (2.82) has a singularity at $q = q_0$, where

$$q_0 h \, \tanh(q_0 h) = F_h^2 k^2 h^2 \; . \tag{2.83}$$

Taking a Taylor expansion of $q \tanh(qh) - F_h^2 k^2 h$ around this point tells us that

$$q \tanh(qh) - F_h^2 k^2 h \sim \left(\tanh(q_0 h) + q_0 h \, \mathrm{sech}^2(q_0 h) \right) (q - q_0) \qquad \text{near } q = q_0$$

so that the singular point q_0 is a simple pole.

In determining $\Omega(k)$, the path of integration must pass around this pole in the complex $q-$plane. It is in deciding whether to pass above or below the pole that the radiation

condition is used. The Fourier-transformed velocity potential which involves $\Omega(k)$ must be inverted to find the velocity potential ϕ ; as seen in Tuck & Taylor this expression for ϕ therefore involves a factor of e^{-ikX} in the integrand (similar to the TSWT expression (2.48). As we showed in §2.3.5, the imaginary part of k while traversing the pole must be positive for there to be no disturbance as $X \to -\infty$. This is true whether the real part of k is positive or negative.

We can use the fact that the path of integration must pass above the pole in the complex $k-$plane, to work out which side of the pole the path of integration should pass in the complex $q-$plane. The variable q comes about through a substitution

$$q = \sqrt{k^2 + \nu^2} \tag{2.84}$$

where the variable ν is the Fourier transform variable in the $y-$direction (i.e. the inverse transform for ϕ involves a $\Psi(\nu)e^{-i\nu y}d\nu$ integration). Therefore, letting

$$q = q_r + iq_i$$

$$k = k_r + ik_i$$

allows us to find whether q_i should be positive or negative. Substituting into equation (2.84) and squaring, we have

$$q_r^2 - q_i^2 + 2q_r q_i i = k_r^2 - k_i^2 + 2k_r k_i i + \nu^2 \ .$$

Equating imaginary parts requires that

$$q_r q_i = k_r k_i \ .$$

Since the range of integration is over positive values of q_r and the radiation condition states that k_i should be positive, the sign of q_i must be the same as that of k_r. Therefore the path of integration in the complex $q-$plane must pass *above* the pole when $k > 0$ and *below* the pole when $k < 0$. This was not noticed by Tuck & Taylor.

The integrand in (2.82) is pure real. Therefore the real part of $\Omega(k)$ is obtained by calculating the Cauchy principal value integral, while the imaginary part is evaluated from the residue at the pole. This gives for the imaginary part

$$\begin{aligned} \mathrm{Im}\{\Omega(k)\} &= -\pi \,\mathrm{sgn}(k) \frac{-2}{\sqrt{q_0^2 - k^2}} \,\mathrm{res}\left(\frac{-q}{q\tanh(qh) - F_h^2 k^2 h} \,;\, q_0 \right) \\ &= \frac{-2\pi q_0 \,\mathrm{sgn}(k)}{\sqrt{q_0^2 - k^2}\left(q_0 h \,\mathrm{sech}^2(q_0 h) + \tanh(q_0 h) \right)} \ , \end{aligned} \tag{2.85}$$

again different to the Tuck & Taylor result.

We note that $\mathrm{Re}\{\Omega(k)\}$ is even and $\mathrm{Im}\{\Omega(k)\}$ is odd (as they must be for Z_d and M_d to be pure real in the expressions (2.81)). Hence we only need to discuss the solution of equation (2.82) for $k > 0$.

The pole in equation (2.82) will only occur in the range of integration if $q_0 > k$. Using the fact that

$$\tanh(x) < x \qquad \text{for } x > 0$$

we can state that

$$q_0 h \tanh(q_0 h) < (q_0 h)^2 .$$

Using the definition (2.83) for q_0 tells us that

$$F_h^2 k^2 h^2 < (q_0 h)^2$$

or

$$q_0 > F_h k .$$

Therefore we can say immediately that q_0 will always be greater than k when $F_h > 1$.

If $F_h < 1$, we can still have $q_0 > k$ if k is in the correct range. Let us first suppose that $q_0 = k$ at some k value which we shall call k_0. Substituting this into the definition (2.83) gives

$$k_0 h \tanh(k_0 h) = F_h^2 k_0^2 h^2$$

or

$$\frac{\tanh(k_0 h)}{k_0 h} = F_h^2 . \tag{2.86}$$

Since

$$0 < \frac{\tanh(x)}{x} < 1 \qquad \text{for } x > 0 ,$$

equation (2.86) will always have a solution for k_0 when $F_h < 1$. As F_h increases from zero to one, k_0 decreases from infinity to zero.

We shall now show that when $F_h < 1$, $q_0 > k$ for all $k > k_0$. Because $\tanh(x)/x$ is a decreasing function of x, for $k > k_0$ we have

$$\frac{\tanh(kh)}{kh} < \frac{\tanh(k_0 h)}{k_0 h} ,$$

or, using the definition (2.86) for k_0,

$$\frac{\tanh(kh)}{kh} < F_h^2 .$$

We now substitute in the definition (2.83) for q_0 to give

$$\frac{\tanh(kh)}{kh} < \frac{\tanh(q_0 h)}{q_0 h} .$$

Again, since $\tanh(x)/x$ is a decreasing function of x, this implies $q_0 > k$ whenever $k > k_0$.

$\Omega(k)$ has a non-zero imaginary part whenever $q_0 > k$; this is true for all $k > 0$ if $F_h > 1$, or for all $k > k_0$ if $F_h < 1$, with k_0 defined by equation (2.86). Remember that we are only considering positive $k-$values here, since we know that $\mathrm{Im}\{\Omega(-k)\} = -\mathrm{Im}\{\Omega(k)\}$.

The imaginary part of $\Omega(k)$ for $F_h < 1$ was overlooked by Tuck & Taylor, leading to the incorrect conclusion of zero subcritical trim for fore-aft symmetric hulls.

We note from the expression (2.85) that the imaginary part of $\Omega(k)$ is non-zero but finite for all k if $F_h > 1$, since q_0 is always greater than k in this case. In the subcritical case, since $q_0 = k$ when $k = k_0$, equation (2.85) is singular around $k = k_0$. Similarly, the Cauchy principal value integral in (2.82) is unbounded when q_0 and k coincide, as the denominator acts like $(q-k)^{-3/2}$ around $q = k$. The full (q, k) double integrals in the force and moment expressions (2.81) do still exist; we must, however, take care in evaluating them around $(q, k) = (q_0, k_0)$.

2.4.3 Numerical method

In order to evaluate Z_d and M_d according to equation (2.81), we discretize the $k-$variable in the same way as was done in §2.3.3. For each value of k we evaluate the integral (2.82) by making the substitution $q = k \sec\vartheta$ to remove the singularity at $q = k$ (here also we shall only consider $k > 0$).

The integral then becomes

$$\Omega(k) = -2\int_0^{\frac{\pi}{2}} \left[1 - \frac{q}{q\tanh(qh) - F_h^2 k^2 h}\right] \frac{d\vartheta}{\cos\vartheta} \,. \tag{2.87}$$

This has a simple pole at $\vartheta = \vartheta_0$, defined by $q_0 = k\sec\vartheta_0$. In order to evaluate it, we split off the singular part using the method

$$\int_0^{\frac{\pi}{2}} \frac{f(\vartheta)}{\vartheta - \vartheta_0}\, d\vartheta = \int_0^{\frac{\pi}{2}} \frac{f(\vartheta) - f(\vartheta_0)}{\vartheta - \vartheta_0}\, d\vartheta + f(\vartheta_0)\log_e\left|\frac{\frac{\pi}{2} - \vartheta_0}{\vartheta_0}\right|$$

and then evaluate the remaining non-singular integral by numerical quadrature.

For values of k not equal to k_0, this method worked well for dealing with the singularity at $q = q_0$. However, the singularity when $(q, k) = (q_0, k_0)$ proved difficult to deal with because of its two-dimensional nature. We attempted doing the $k-$integral before the $q-$integral but this did not help matters, and no simple substitution could be found to avoid the problem. In the end the best that could be done was to use the midpoint method to evaluate $\Omega(k)$, with a finely-spaced grid; the resulting discrete values were then used in the force and moment integrals (2.81) despite their inverse-square-root singularity. As such, Z_d and M_d were slightly oscillatory functions of F_h when F_h was close to 1, because the singularity at $k = k_0$ moved into the range where the integrand was appreciable. In presenting graphs of the results we have smoothed them slightly over this small region close to $F_h = 1$.

2.5 Scaling

The TSWT force (2.53) and moment (2.54) were derived in terms of dimensional variables. However, they may be written in dimensionless form, since they and the TSWT and FDT theories described are all linear. For a given shape of ship, the dimensionless products

$$\frac{Z}{\rho g S_{\max} B_{\max}} \qquad \text{and} \qquad \frac{M}{\rho g S_{\max} B_{\max} L} \tag{2.88}$$

are functions only of F_h and h/L. Solving (2.57) then tells us that

$$\begin{aligned} \frac{s}{L} &= C_\forall \;\; f\left(F_h, \frac{h}{L}\right) \\ \theta &= C_\forall \;\; m\left(F_h, \frac{h}{L}\right) \end{aligned} \tag{2.89}$$

where the functions f, m depend only on the shape of ship.

Therefore, for a given shape of ship, h/L ratio and Froude number, the ship may be stretched in the streamwise or transverse directions, with the only influence on s/L coming from $C_\forall$. In particular, s/L is independent of scale, if the ship's proportions are kept constant. This allows us to justifiably "scale up" model test results according to this theory. Since the trim angle θ is independent of scale, the bow and stern sinkages are also proportional to shiplength for constant values of h/L and F_h.

In FDT, only the force and moment corrections Z_d and M_d (2.81) can be written so as to allow stretching in the transverse directions. Z_∞ and M_∞ both have complicated dependence upon beam and section area and so cannot be scaled in this way. However, the total FDT force and moment can still be written as dimensionless products like (2.88), provided that the proportions of the ship remain constant. Therefore s/L and θ are still independent of scale in FDT, and can be justifiably scaled up with increasing ship size.

2.6 Results

2.6.1 Comparing TSWT and FDT

In order to compare TSWT and FDT numerically, we first consider a fore-aft symmetric hull with parabolic waterplane and section area curves, i.e.

$$\begin{aligned} B(X) &= B_{\max}\left(1 - \frac{X^2}{\ell^2}\right) \\ S(X) &= S_{\max}\left(1 - \frac{X^2}{\ell^2}\right) \end{aligned} \tag{2.90}$$

for $X \in [-\ell, \ell]$. The maximum beam and section area are chosen to be in the same proportions as the Taylor A3 hull, which will be discussed later. Therefore we have chosen $L/B_{\max} = 10.8$ and $L^2/S_{\max} = 378.3$ for these results.

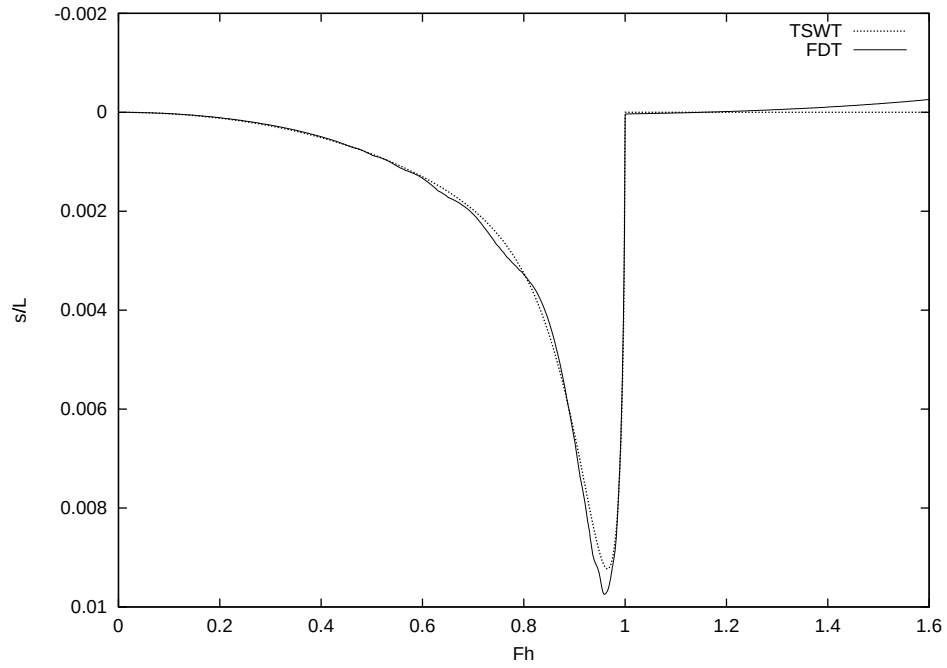

Figure 2.1: Sinkage (as a fraction of shiplength) as a function of F_h for parabolic hull, using TSWT and FDT.

Figure 2.1 shows the scaled midship sinkage s/L as a function of F_h for this hull, with $h/L = 0.125$, as calculated using both transcritical theories. We see that, at this relatively small value of h/L, the two theories produce very similar results. The sinkage in each case rises to a maximum at $F_h = 0.965$ before tending sharply back toward zero. This is consistent with the result of §2.3.4 that the TSWT sinkage as a function of F_h tends to zero in a square-root manner as $F_h \to 1$ and is identically zero for $F_h > 1$. FDT has similar properties, although there is an apparent small but non-zero supercritical sinkage which we believe to be spurious (see later).

We notice that the maximum sinkage according to FDT ($s/L = 0.0097$) is slightly higher than according to TSWT ($s/L = 0.0092$).

Whereas TSWT gives a smooth monotone increase in the sinkage until it reaches the maximum, FDT is slightly oscillatory in slope. This is a property of the governing equations and not of the numerical method, as the graph was reproduced exactly with different grid spacings in each of the variables. Being fully dispersive, FDT retains some bow-stern wave interference effects that are familiar in classical ship hydrodynamics, and which for example lead to analogous oscillations in wave resistance curves for ships.

The present FDT results can be compared with those of Tuck & Taylor (1970). The maximum sinkage given there for one particular value of h/L agrees moderately well (within 10%) with our predictions, although their sinkage curve is more oscillatory at lower Froude numbers. This may have been due to the computations in Tuck & Taylor (1970) not handling the singularity in $\Omega(k)$ for $F_h < 1$ with adequate numerical precision.

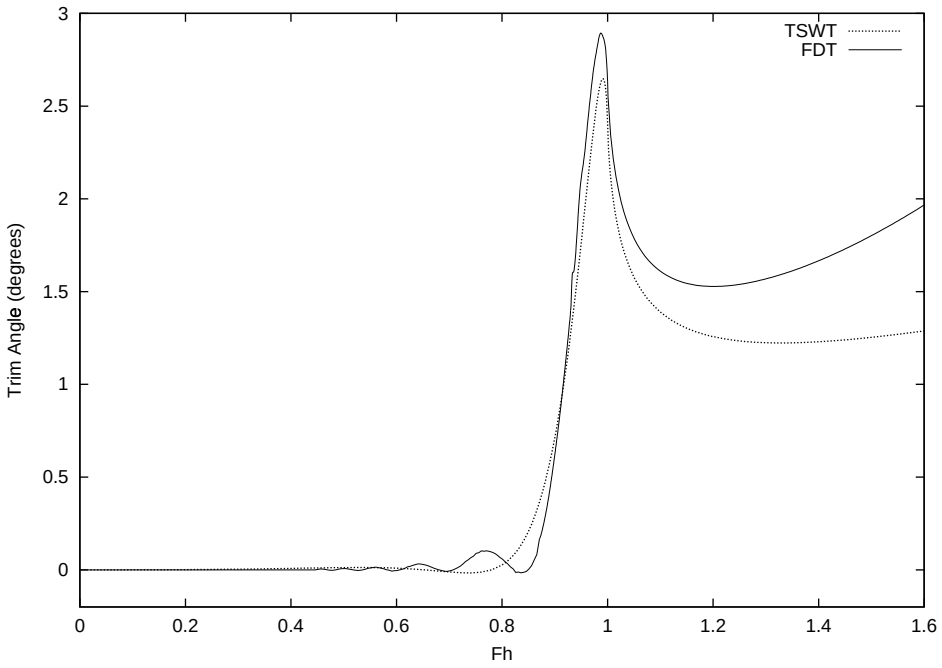

Figure 2.2: Bow-up trim angle (in degrees) as a function of F_h for parabolic hull with $h/L = 0.125$, using TSWT and FDT.

A problem with FDT is an anomalous behaviour at large Froude numbers. The infinite-depth force contribution F_∞ increases in proportion to U^2; if the theory is to agree with TSWT in the shallow-water limit, F_∞ should be cancelled by the correction F_d at high Froude numbers, leading to a net force that tends to zero at infinite speed. However, any error in approximating either F_∞ or F_d will ultimately produce a total force that is erroneously quadratic in U for large F_h. This is already beginning to be apparent at the right side of Figure 2.1, and the present FDT results (especially with use of the Havelock approximation to F_∞) are not to be considered accurate at large F_h.

Figure 2.2 shows the corresponding trim angles for the same hull, according to the two theories. According to both theories, the ship will have a large bow-up trim angle in the neighbourhood of $F_h = 1$. The maximum trim occurs at $F_h = 0.99$ according to both theories, which is slightly higher than the Froude number at which the maximum sinkage occurs ($F_h = 0.965$).

As is the case with sinkage, the maximum trim according to FDT (2.88 degrees) is slightly higher than according to TSWT (2.65 degrees). Also, the TSWT curve is smooth, while the FDT is oscillatory at lower Froude numbers. The discrepancy for large Froude numbers cannot be due to an error in approximating M_∞, since this is identically zero. We suspect that the correction M_d may be quite sensitive for large Froude numbers, and place more faith in the TSWT in this range.

2.6.2 Comparison with experimental results

We have used both the TSWT and FDT to compute the midship sinkage of a "Taylor standard series" hull (Gertler 1954), which corresponds to a slightly non-fore-aft-symmetric ship. A model hull of that shape designated A3 by Graff et al (1964) was used; this has $L/B = 10.8$, $L/T = 32.4$ (with T the draught) and volumetric coefficient $C_\forall = 0.0017$. The experimental results of Graff et al (1964) for the same hull are reproduced here for comparison.

Shallow water

Figure 2.3 shows the midship sinkage as a function of Froude number for the A3 hull, travelling in water of scaled depth $h/L = 0.125$. As an example, this would correspond to a 200 metre ship, with a draught of 6.2 metres, travelling in water of depth 25 metres. The sinkage is calculated using TSWT and FDT theories, with the experimental results also shown.

We see that both theories are reasonable in accuracy. In particular, the maximum sinkage determined experimentally ($s/L = 0.0089$) lies in between that predicted by TSWT ($s/L = 0.0081$) and by FDT ($s/L = 0.0094$). There is a difference in the Froude number at which this maximum sinkage occurs, being at $F_h = 0.89$ experimentally, although we predict it at $F_h = 0.965$, according to both theories.

The rising of the ship in the water, for F_h slightly greater than 1, is not predicted by either of the theories. However, for larger F_h, the predicted sinkage is very close to zero, in accordance with the experimental results. Since this ship is not quite fore-aft symmetric, TSWT gives a very small but non-zero sinkage for $F_h > 1$, which agrees reasonably with the experimental results. The quadratic-type error in FDT again becomes apparent for large F_h.

Deeper water

Figure 2.4 shows the midship sinkage for the same ship travelling in twice the depth of water, i.e. $h/L = 0.25$. This corresponds to a depth of 50 metres for our example hull of length 200 metres and draught 6.2 metres. In this case we see that TSWT greatly underestimates the maximum sinkage, as the shallow-water assumption of h/L being small is no longer acceptable. FDT, however, gives a maximum sinkage of $s/L = 0.0066$ at $F_h = 0.86$, which is close to the experimental maximum of $s/L = 0.0068$ at $F_h = 0.88$.

2.6.3 Trim and stern sinkage

The trim of the A3 hull, as predicted using TSWT, was also compared to experimental results. This is shown in Figure 2.5. There is fair agreement in this case, despite the predicted peak being sharper and higher than the experimental results.

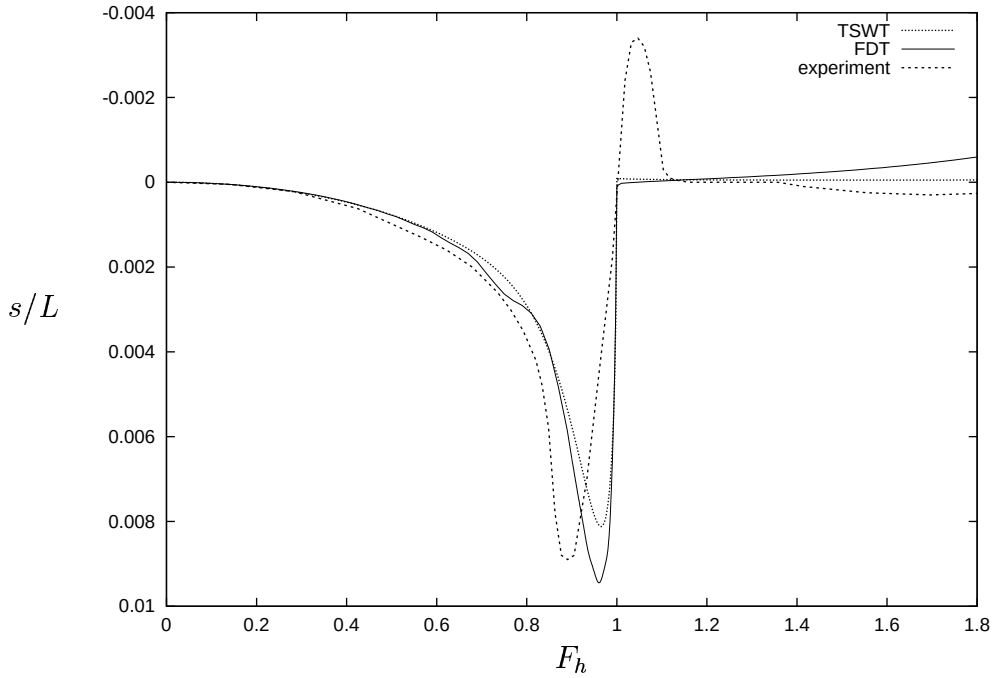

Figure 2.3: Sinkage (as a fraction of shiplength) as a function of F_h for Taylor Series hull, with $h/L = 0.125$. TSWT, FDT and experimental results.

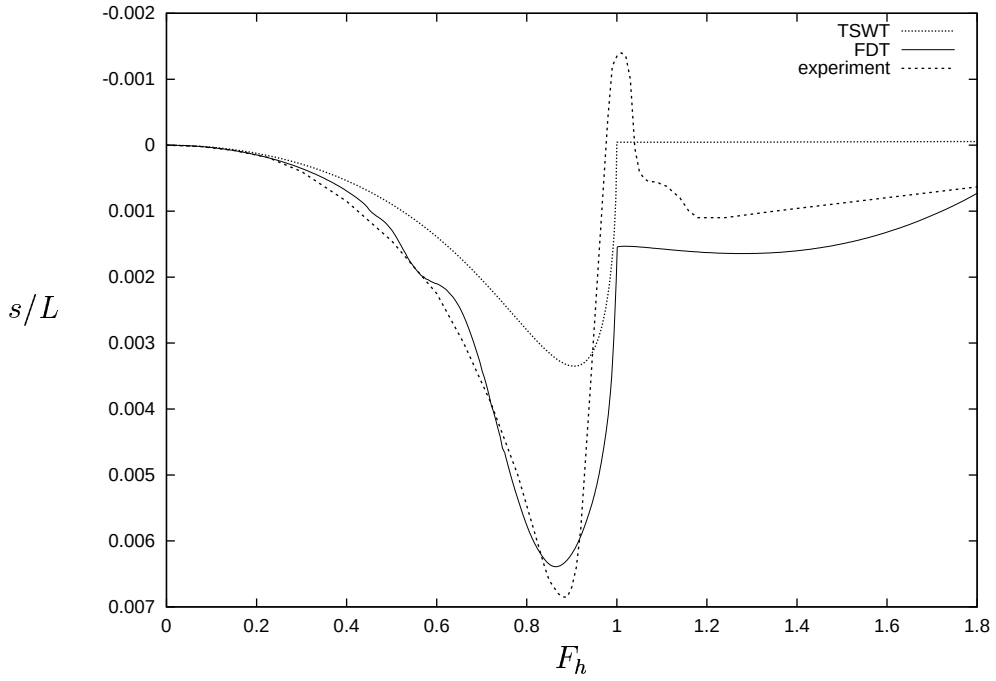

Figure 2.4: Sinkage (as a fraction of shiplength) as a function of F_h for Taylor Series hull, with $h/L = 0.25$. TSWT, FDT and experimental results.

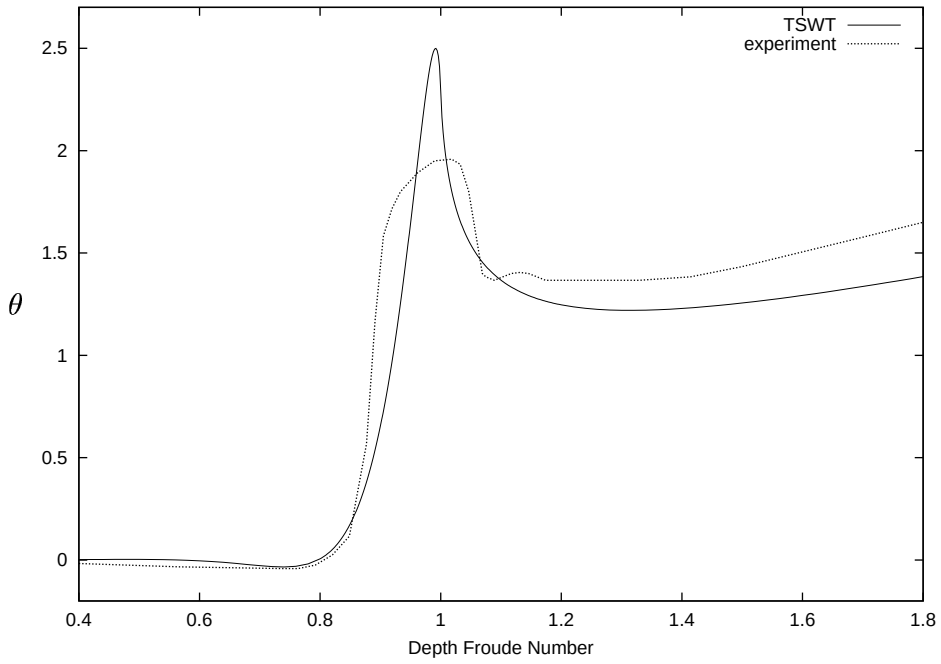

Figure 2.5: Bow-up trim angle (in degrees) as a function of F_h for Taylor Series hull, with $h/L = 0.125$. Comparison of TSWT with experiment.

The large bow-up trim experienced by ships in the transcritical speed range means that the ship's stern is particularly vulnerable to grounding. Since the maximum midship sinkage and maximum trim occur at almost the same Froude number, the stern sinkage will be very large around this Froude number.

In Figure 2.6 we have plotted the scaled stern sinkage s_{stern}/L (given by $s/L+\theta/2$) for the A3 and parabolic hulls. This is found using TSWT and plotted as a function of Froude number. We see that for the A3 hull the maximum stern sinkage is $s_{\text{stern}}/L = 0.0285$. The experimental results give a smaller maximum of $s_{\text{stern}}/L = 0.0228$, the difference mainly being due to the difference in trim angles.

For the parabolic hull, which has a larger $C_\forall$, the stern sinkage reaches $s_{\text{stern}}/L = 0.0308$. For a 200 metre ship, these results correspond to a predicted stern sinkage of 5.7 metres for the A3 hull (compared to 4.56 metres according to the experimental results) and 6.16 metres for the parabolic hull.

2.6.4 Maximum sinkage

We have seen that when midship and stern sinkage are plotted against F_h for a fixed value of h/L, they both reach a maximum just below $F_h = 1$. In fact, at very high supercritical Froude numbers, the stern sinkage may reach a higher value than in the transcritical range; however, the speeds required for this to occur are not realistic for most displacement hulls.

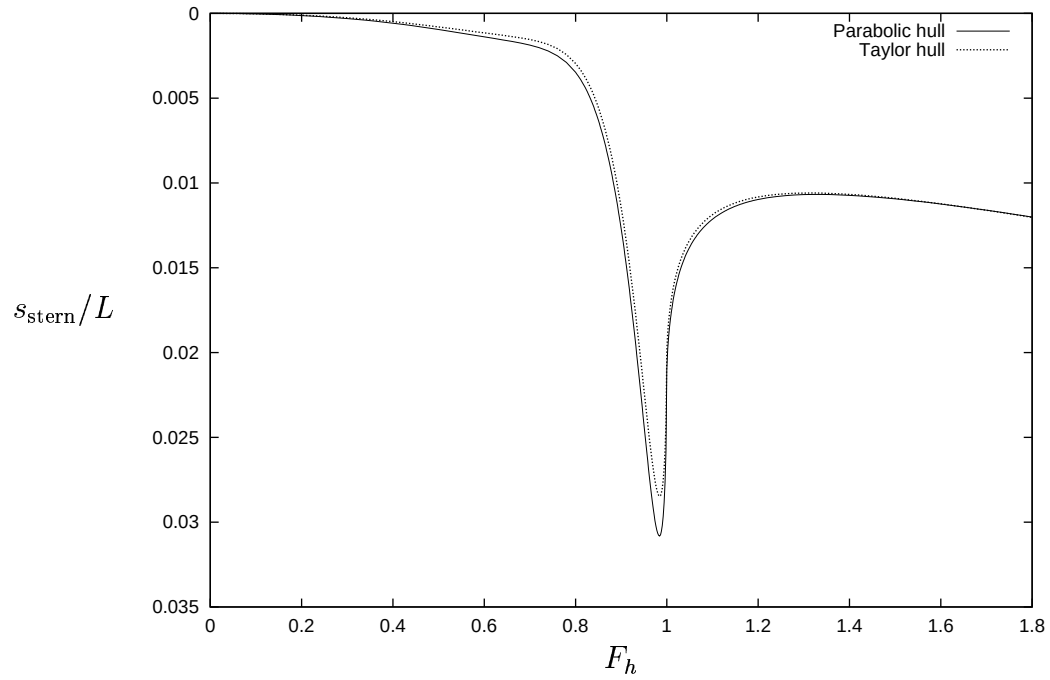

Figure 2.6: Stern sinkage (as a fraction of shiplength) as a function of F_h for parabolic and Taylor Series hull, with $h/L = 0.125$. Calculated using TSWT.

By finding the maximum sinkage with respect to F_h for each value of h/L, we can plot the maximum midship and stern sinkage as a function of h/L. This is shown in Figure 2.7 for the Taylor hull. The at-rest underkeel clearance (UKC) is also shown for each depth.

Where the maximum sinkage is larger than the UKC, there exists a range of Froude numbers for which the ship is predicted to scrape the sea floor. Therefore, where the UKC line crosses the maximum stern sinkage curve gives the value of h/L for which the stern is predicted to just touch the sea floor at one particular Froude number. If the ship were unable to trim, the midship would touch the sea floor at the value of h/L for which the maximum midship sinkage curve crosses the UKC line.

Therefore we see that for the Taylor hull the stern is at risk of grounding for $h/L < 0.078$, which corresponds to $h/T < 2.52$. Similarly, if trim were not taken into account, the midship would be at risk of grounding for $h/L < 0.052$, which corresponds to $h/T < 1.68$. These are large at-rest clearances that are needed for ships which intend to travel at transcritical Froude numbers.

2.7 Conclusions

We have used two slender-body methods to solve for the sinkage and trim of a ship travelling at arbitrary Froude number, including the transcritical region.

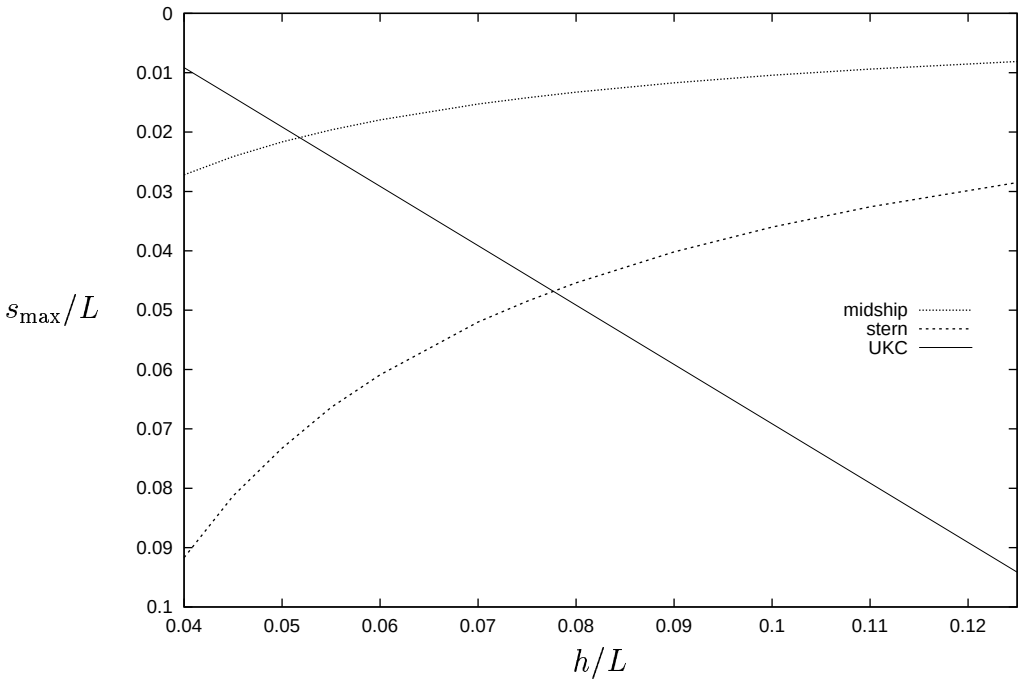

Figure 2.7: Maximum midship and stern sinkage (as a fraction of shiplength) as a function of h/L for Taylor Series hull, as calculated using TSWT. At-rest underkeel clearance (UKC) also shown for each depth.

The transcritical shallow-water theory (TSWT) developed by Mei (1976) has been extended and exploited numerically using Fourier transform methods to give sinkage and trim. This theory has also been extended to the case of a ship moving in a channel of finite width; however, the numerical difficulty in computing the resulting force integral, and its limited validity, mean that the open-water theory is more practically useful.

The finite-depth theory (FDT) developed by Tuck and Taylor (1970) has also been improved and used for general hull shapes. This theory gives a sinkage force and trim moment that are slightly oscillatory in F_h. Since the theory involves summing infinite-depth and finite-depth contributions, both of which vary with U^2 at high Froude numbers, any error will grow approximately quadratically with U. Therefore we cannot use this theory at large supercritical Froude numbers. Also, the difficulty in finding the infinite-depth contributions numerically, as well as the extra integral needed to compute the force and moment, make FDT more difficult to implement than TSWT.

When compared to the experimental results of Graff et al (1964) , both theories were seen to give good results for the maximum midship sinkage at $h/L = 0.125$. At $h/L = 0.25$, as expected, only FDT gave good results for maximum midship sinkage.

In practice, scenarios in which ships are at risk of grounding will normally have $h/L < 0.125$. Since TSWT is a shallow-water theory and it works well at $h/L = 0.125$, we expect that it will give even better results at smaller, practically useful values of h/L. Unfortunately, $h/L = 0.125$ is the smallest value for which experimental data are available to check the theory.

The main discrepancies between the theoretical and experimental results were:

* The trim predicted using TSWT has a sharper, higher peak than was found experimentally.
* The maximum sinkage was predicted to occur at a slightly higher Froude number than was observed experimentally.
* Neither of the theories predicted the rise of the ship in the water that was observed experimentally at low supercritical Froude numbers.

The two likely reasons for these discrepancies are:

1. Although the experiments were performed in a very wide tank, it is possible that unsteadiness and production of solitons may have altered the transcritical flow from what would be observed in open water.
2. The nonlinear term that was neglected in the derivation of TSWT may need to be included when F_h is close to 1.

Further experimental and numerical work are required to resolve these discrepancies.

In any case, the results for maximum sinkage furnished by this theory were impressively close to the experimental values, and it is this maximum sinkage which is of most importance. The bodily rise of the ship in the water at supercritical Froude numbers is not of concern with regard to ship grounding.

Another interesting departure from the experimental results was the lesser angle of trim predicted by TSWT at supercritical Froude numbers. Although sinkage is basically an inviscid phenomenon, it is thought that viscosity may affect the trim; separation near the stern would tend to decrease the pressure there and increase the bow-up trim moment.

Since, in the transcritical range, the ship experiences a large bow-up trim moment, the maximum transcritical sinkage occurs at the stern. By calculating this stern sinkage for our two example hulls, we showed that the stern sinkage can be remarkably large at transcritical Froude numbers.

Part II

Non-uniform Depth

Chapter 3

Unsteady Squat in a Narrow Channel

We shall now extend the results of Chapter 1 to the case of a ship moving in a channel of non-uniform depth. This will be done by developing an unsteady hydraulic theory in earth-fixed coordinates. Some of this work has appeared in Gourlay & Tuck (1998a).

3.1 Problem formulation

The formulation for water of non-uniform depth is similar to the case of constant depth. The following quantities are defined in the same way as in Chapter 1: the free surface height ζ, local beam B, hull section area S and area taken up by the water A. The channel may still have a cross-section of any shape; here, however, the cross-section may also vary along the channel. The same assumptions discussed in Appendix B.1 apply for the non-uniform channel.

The main difference in the theoretical treatment is a switch to the earth-fixed coordinate x, which is shown in Figure 3.1. Defining again the average depth over any channel cross-section as h, we have $h = h(x)$ in this coordinate system. Similarly, the waterline channel width w may also be a function of x. In this way, the method is valid for either rectangular-sectioned or arbitrarily-shaped channels.

The benefit of using the earth-fixed coordinate system lies in the fact that h and w are independent of time t at fixed x. The drawback is that the ship parameters $S(X)$ and $B(X)$ do depend on t in the new coordinate system.

Having chosen the position of the origin $x = 0$, we choose the origin in t to be the time at which the centre of the ship passes $x = 0$. The transformation between the two sets of coordinates is therefore $x = X - Ut$, with t the same for each coordinate system. Hence we write $S(X) = S(x + Ut)$ in the new coordinate system, and similarly for $B(X)$. Both of these quantities have non-zero x and t derivatives.

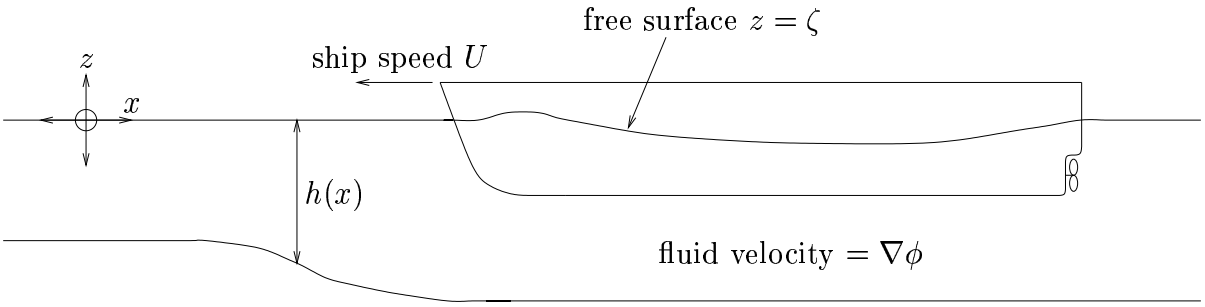

Figure 3.1: Earth-fixed frame of reference

The velocity potential in earth-fixed coordinates is ϕ, which is the same as the disturbance velocity potential in body-fixed coordinates (as used in Chapter 2). According to the hydraulic theory, this is a function of x and t only. The streamwise velocity component ϕ_x will be designated as u, which is the same as the velocity perturbation in body-fixed coordinates used in §1.4. In the unsteady theory, the time-derivatives of ϕ are also needed.

Since we shall be concentrating ultimately on linearized flow, the ship will be considered vertically fixed in its rest position.

3.2 The unsteady hydraulic equations

In terms of the cross-sectional area A taken up by the water, the unsteady continuity equation can be written (Stoker 1957 p. 453) as

$$\frac{\partial A}{\partial t} + \frac{\partial}{\partial x}(Au) = 0 \tag{3.1}$$

where, as in §1.2, $A(x,t) = S_0 - S + (w - B)\zeta$. Here $S_0 = wh$ is a function of x only, and we assume that the ship and channel walls are vertical at the waterline.

Using the change of variables $X = x + ut$, the x and t derivatives of $S(X)$ become

$$\begin{aligned} \frac{\partial S}{\partial x} &= S'(X) \\ \frac{\partial S}{\partial t} &= US'(X)\ . \end{aligned} \tag{3.2}$$

Henceforth $S'(X)$ will be abbreviated to S', and similarly for $B'(X)$. Expanding equation (3.1) gives for the unsteady continuity equation

$$\begin{aligned} -US' + (w - B)\,\zeta_t - UB'\zeta + (S_0 - S + (w - B)\,\zeta)\,u_x \\ +u\,(S_{0x} - S' + (w - B)\,\zeta_x + (w_x - B')\,\zeta) = 0\ . \end{aligned} \tag{3.3}$$

The unsteady Bernoulli equation in earth-fixed coordinates is

$$g\zeta + \frac{1}{2}u^2 + \phi_t = 0\ . \tag{3.4}$$

Since $u = \phi_x$, the continuity equation (3.3) and Bernoulli equation (3.4) define two simultaneous equations for the unknowns $\phi(x,t)$ and $\zeta(x,t)$. We can eliminate ζ by rearranging (3.4) to give

$$\begin{aligned} \zeta &= -\frac{1}{g}\left(\frac{1}{2}u^2 + \phi_t\right) \\ \zeta_t &= -\frac{1}{g}\left(uu_t + \phi_{tt}\right) \\ \zeta_x &= -\frac{1}{g}\left(uu_x + u_t\right) \ . \end{aligned} \tag{3.5}$$

Substituting these into the continuity equation (3.3) yields the nonlinear equation of unsteady hydraulic flow:

$$\begin{aligned} -US' &- \frac{w-B}{g}\left(uu_t + \phi_{tt}\right) + \frac{UB'}{g}\left(\frac{1}{2}u^2 + \phi_t\right) + \left(S_0 - S - \frac{w-B}{g}\left(\frac{1}{2}u^2 + \phi_t\right)\right)u_x \\ &+ u\left(S_{0x} - S' - \frac{w-B}{g}\left(uu_x + u_t\right) - \frac{w_x - B'}{g}\left(\frac{1}{2}u^2 + \phi_t\right)\right) = 0 \ . \end{aligned} \tag{3.6}$$

This is a rather complicated nonlinear differential equation in two variables. A series of attempts to solve it using a centred finite-difference method proved unsuccessful, due to stability problems in solving the tridiagonal system. In any case, it is inconsistent to solve the nonlinear problem unless we are also allowing the ship to squat (see §1.6) and this would be very laborious in the unsteady case.

We shall prefer to concentrate here on the linearized form of the equation, which is applicable to ships and channels for which B/w and S/S_0 are small quantities. In this case u, ϕ_t and ζ are also small, so that we may neglect terms of second order in any of these quantities. The method is similar to that used in §1.4 for steady flow. Again, the ship and channel walls need not be vertical at the waterline for linearized flow, but they should not be excessively sloping.

The linearized version of the unsteady hydraulic equation (3.6) becomes

$$-US' - \frac{w}{g}\phi_{tt} + S_0 u_x + uS_{0x} = 0$$

or

$$\frac{\phi_{tt}}{g} - \frac{1}{w}\left(S_0\phi_x\right)_x = -\frac{US'}{w} \tag{3.7}$$

which is a one-dimensional wave equation with a forcing term. Therefore we expect that travelling waves may be produced when depth changes are encountered by the ship. The boundary conditions for this equation are that ϕ_x and ϕ_t should both vanish as $x \to \pm\infty$.

In this chapter we shall only consider channels that have constant waterline width w but varying depth h. In that case equation (3.7) simplifies to

$$\frac{\phi_{tt}}{g} - \left(h\phi_x\right)_x = -\frac{US'}{w} \ . \tag{3.8}$$

Alternatively, this can be written in terms of the fluid speed u by differentiating with respect to x, giving

$$\frac{u_{tt}}{g} - (hu)_{xx} = -\frac{US''}{w} \,. \tag{3.9}$$

We shall now consider the application of this theory to the simple case of a step depth change, and then outline a numerical method for dealing with general $h(x)$.

3.3 Analytic solution for a step depth change

The simplest non-uniform depth problem is that of a ship passing from a region of constant depth into another region of a different constant depth. This situation is depicted in Figure 3.2 for a ship moving into shallower water.

We take the step to be at $x = 0$ and choose the origin in time as when the ship's midsection passes the step. t is therefore negative up until the ship's midsection passes the step. The region $x > 0$ is denoted region 1, such that $h = h_1$, $\phi = \phi_1$ and $F_h = F_1$ here. Similarly, $h = h_2$, $\phi = \phi_2$ and $F_h = F_2$ for $x < 0$.

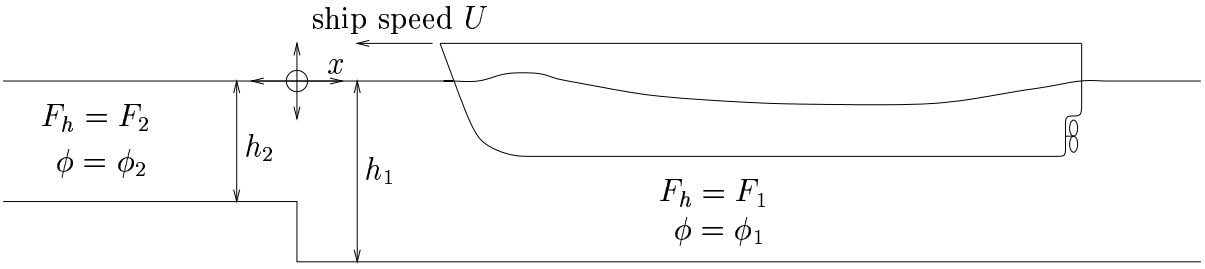

Figure 3.2: Ship passing a step depth change

Note that one of the assumptions of hydraulic theory, that of slowly-varying channel dimensions, is violated at the step. However, the resulting error in the flow occurs only in a very small region either side of $x = 0$. Lamb (1932, p. 262) showed that, provided the flux hu and free surface height ζ are continuous across the step, the flow is still accurate outside of the immediate vicinity of the step. We may justifiably use the theory therefore for overall outputs such as sinkage and trim.

For this problem we shall solve the flow analytically by first considering separately the flow on each side of the step.

For either $x > 0$ or $x < 0$, h is constant and equation (3.8) is a simple wave equation. This has the particular solution

$$\phi = \frac{UV(x + Ut)}{hw\,(1 - F_h^2)} \,,$$

where $V(X)$ is related to the ship's volume such that $V'(X) = S(X)$. This is the linearized steady-state solution that was found in §1.4.

The general solution also allows waves of arbitrary shape that travel at speed $\sqrt{gh}$ and remain unchanged in form. Therefore in each region of constant depth, the most general solution of (3.8) is

$$\phi(x,t) = \frac{UV(x+Ut)}{hw\,(1-F_h^2)} + Uf^+(x-\sqrt{gh}\,t) + Uf^-(x+\sqrt{gh}\,t)\ . \tag{3.10}$$

Here f^- and f^+ are arbitrary functions; these waves must travel unchanged in form until they hit the boundaries at $x = 0$ or $x = \pm\infty$.

We assume that the ship has started an infinite distance from the step, at which stage the flow is perfectly steady with respect to the ship. Therefore there can be no wave travelling in the $-x$ direction for $x > 0$, since it would have to have originated at $x = \infty$; here we know the flow is steady with no mechanism for producing radiating waves. Similarly, there cannot possibly be any waves produced at $x = -\infty$, and hence there cannot be any waves travelling in the $+x$ direction for $x < 0$. Hence we may write

$$\begin{aligned}
\phi_1(x,t) &= \frac{UV(x+Ut)}{h_1 w\,(1-F_1^2)} + Uf_1(x-\sqrt{gh_1}\,t) \\
\phi_2(x,t) &= \frac{UV(x+Ut)}{h_2 w\,(1-F_2^2)} + Uf_2(x+\sqrt{gh_2}\,t)\ .
\end{aligned} \tag{3.11}$$

At this stage f_1 and f_2 are still arbitrary functions whose form must be determined from the matching conditions at the step. These matching conditions are that the flux $h\phi_x$ and free surface height ζ must be continuous at $x = 0$. The conditions must hold for all values of the time t. Note that the resulting fluid speed u and free surface slope ζ_x are actually discontinuous across the step.

Using equations (3.11) to match the flux $h\phi_x$ from each region at $x = 0$ gives the condition that

$$\frac{S(Ut)}{w\,(1-F_1^2)} + h_1 f_1'(-\sqrt{gh_1}\,t) = \frac{S(Ut)}{w\,(1-F_2^2)} + h_2 f_2'(\sqrt{gh_2}\,t)\ . \tag{3.12}$$

The linearized free surface height can be seen from equation (3.5) to be proportional to ϕ_t. Matching this from each region at $x = 0$ gives

$$\frac{U^2 S(Ut)}{wh_1\,(1-F_1^2)} - U\sqrt{gh_1}\,f_1'(-\sqrt{gh_1}\,t) = \frac{U^2 S(Ut)}{wh_2\,(1-F_2^2)} + U\sqrt{gh_2}\,f_2'(\sqrt{gh_2}\,t)\ . \tag{3.13}$$

These two conditions can be solved simultaneously to give

$$f_1'(-\sqrt{gh_1}\,t) = \frac{(F_1-F_2)S(Ut)}{wh_1(1-F_1^2)(1+F_2)}$$

and

$$f_2'(\sqrt{gh_2}\,t) = \frac{(F_1-F_2)S(Ut)}{wh_2(1-F_2^2)(1-F_1)}\ .$$

Integrating yields the form of the travelling waves as

$$\begin{aligned} f_1(x-\sqrt{gh_1}\,t) &= \frac{(F_2-F_1)\,V\left(-F_1(x-\sqrt{gh_1}\,t)\right)}{wh_1F_1\,(1-F_1^2)\,(1+F_2)} \\ f_2(x+\sqrt{gh_2}\,t) &= \frac{(F_1-F_2)\,V\left(F_2(x+\sqrt{gh_2}\,t)\right)}{wh_2F_2\,(1-F_2^2)\,(1-F_1)} \end{aligned} \tag{3.14}$$

for $x > 0$ and $x < 0$ respectively. These waves have the same shape as that produced by the ship (proportional to $V(x+Ut)$), but have different length, amplitude and velocity. With f_1 and f_2 defined in this way, the flow field is now known for all x and t and can be used to determine sinkage and trim.

In the analysis we have made no assumptions about whether the Froude numbers F_1 and F_2 need to be greater than or less than 1. In fact, the theory is equally valid for all Froude numbers, excepting the singularity at $F_h = 1$. Therefore the flow may be subcritical on both sides of the step, supercritical on both sides of the step, or subcritical on one side and supercritical on the other.

This linear one-dimensional theory predicts waves travelling away from the step that remain unchanged in form. In practice, these waves will normally either disperse or break as they move away from the step. However, we might expect that this should occur some time after the ship is passing the step, so that they will not then affect the ship's sinkage and trim.

3.3.1 Results for a simple hull

In order to compare these analytic results with the numerical method that is shortly to be introduced, we shall consider a symmetric cusped hull whose local beam and section area are given by

$$\begin{aligned} S(X) &= S_{\max}\left(1-\frac{X^2}{\ell^2}\right)^3 \\ B(X) &= B_{\max}\left(1-\frac{X^2}{\ell^2}\right) . \end{aligned} \tag{3.15}$$

Figure 3.3 shows the fluid flux uh for such a ship that has just passed a step depth change to shallower water. The step is at $x = 0$ and the ship is moving from right to left. In this case the flow is subcritical on both sides of the step. The large peak is the accelerated flow around the ship, and is basically the steady flow. However, superimposed on this are the two travelling waves, each radiating out from the step in opposite directions.

Each of these waves produces a retardation in flow speed u, which corresponds to the troughs in the graph. The waves start being formed when the bow passes the step and are completed when the stern passes the step. Therefore, while the ship is passing over the step, the waves act to decrease the flow speed past the ship. Even once the ship's

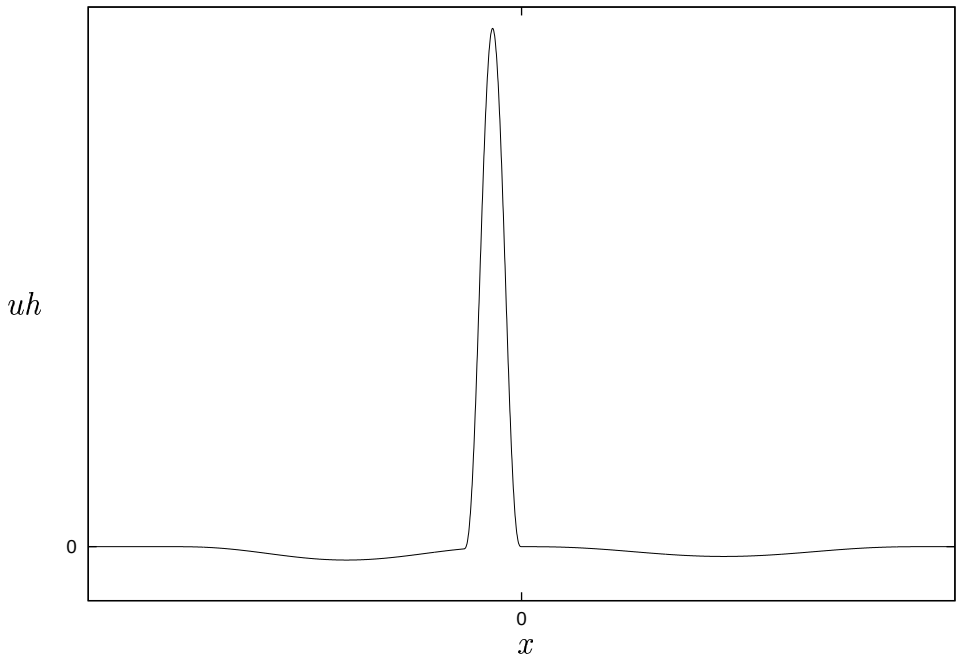

Figure 3.3: Fluid flux uh as a function of x for a ship that has just passed a step depth change to shallower water

stern is past the step, u is still affected until the wave travelling in $x < 0$ completely overtakes the ship.

In Figure 3.4 the ship is passing a similar depth change but from shallow to deeper water. We see that the waves are still radiating out from the step, but are crests rather than troughs in this case. Therefore they act to increase the flow speed past the ship while it is passing the step.

Results were also obtained for cases when the flow on one or both sides was supercritical. For example, for a step depth change to shallower water with $F_1 < 1$ and $F_2 > 1$, the ship will now be travelling faster than the radiating wave in $x < 0$. Also, this wave will now be of opposite sign. When F_1 and F_2 are both supercritical, a positive wave is radiated for $x > 0$ and a negative wave, still travelling slower than the ship, is radiated for $x < 0$.

Once the flow field is determined, we can calculate the transient vertical force and trim moment on the ship. Since we are using the fixed-ship method, these are found in the same way as was done in §2.3.2, i.e.

$$\begin{aligned} Z &= \int_{-\ell}^{\ell} p\, B(X)\, dX \\ M &= -\int_{-\ell}^{\ell} X\, p\, B(X)\, dX\ . \end{aligned} \tag{3.16}$$

In earth-fixed coordinates, with $x = X - Ut$, Z and M become

$$Z = \int_{-\ell-Ut}^{\ell-Ut} p\, B(x+Ut)\, dx$$

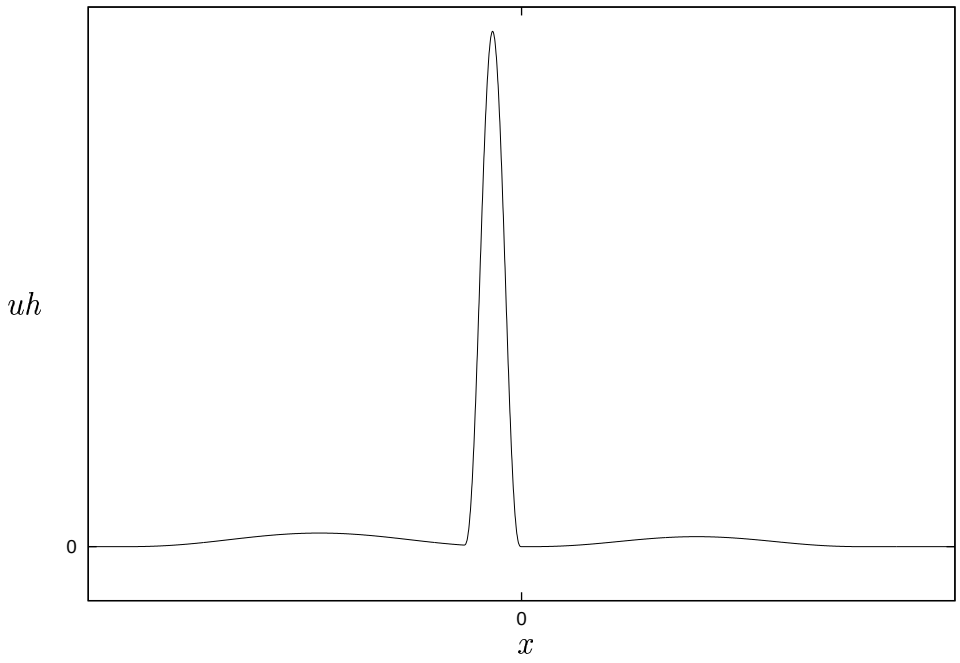

Figure 3.4: Fluid flux uh as a function of x for a ship that has just passed a step depth change to deeper water

$$M \;=\; -\int_{-\ell-Ut}^{\ell-Ut} (x+Ut)\, p\, B(x+Ut)\, dx \;. \tag{3.17}$$

The unsteady hydrodynamic hull pressure p is found from Bernoulli's equation in earth-fixed coordinates

$$\frac{p}{\rho} + \frac{1}{2}u^2 + \phi_t = 0 \;,$$

giving, in linearized form,

$$p = -\rho\phi_t \;. \tag{3.18}$$

Using the solution (3.11) and (3.14), the hydrodynamic pressure has the analytic solution

$$p = \begin{cases} -\frac{\rho U^2}{w}\left[\frac{S(x+Ut)}{h_1 w(1-F_1^2)} + \frac{(F_2-F_1)S\left(-F_1(x-\sqrt{gh_1}\,t)\right)}{wh_1F_1\left(1-F_1^2\right)(1+F_2)}\right] & \text{for} \quad x>0 \\ -\frac{\rho U^2}{w}\left[\frac{S(x+Ut)}{h_2 w(1-F_2^2)} + \frac{(F_1-F_2)S\left(F_2(x+\sqrt{gh_2}\,t)\right)}{wh_2F_2\left(1-F_2^2\right)(1-F_1)}\right] & \text{for} \quad x<0 \;. \end{cases} \tag{3.19}$$

This is used in equations (3.17) to determine the vertical force and trim moment.

Figure 3.5 shows the transient vertical force on the ship as it passes a step depth change to shallower water. For these results we have used $F_1 = 0.143$, $F_2 = 0.165$ and $w/h_1 = 1$. The axes are scaled so that the results are valid for any values of the other quantities.

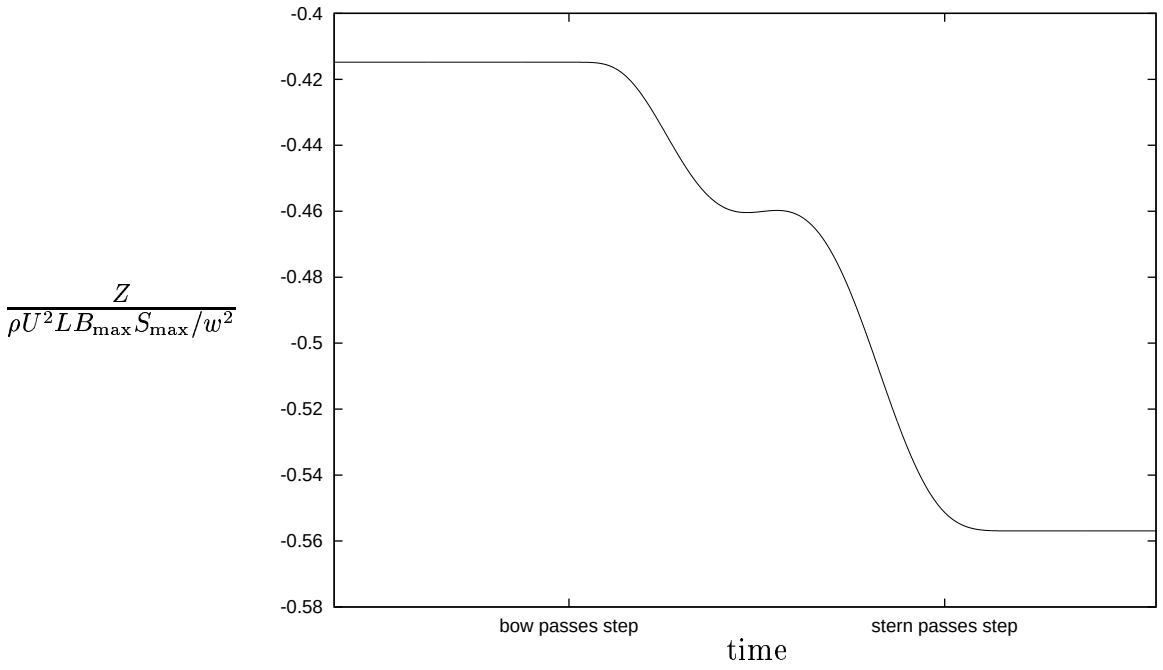

Figure 3.5: Scaled vertical force on a ship passing a step depth change to shallower water

We can see here the effect that the radiating waves have on the vertical force upon the ship. Rather than trending smoothly from the steady deep water value to the larger-magnitude steady shallow-water value, there is a lag which results from the flow retardation due to the two waves. This means that the vertical force does not reach the shallow steady value until after the ship's stern passes the step. More importantly, it at no stage "overshoots" the shallow water value.

The transient trim moment (Figure 3.6) shows a strong bow-up trim as the ship is passing the step. This means that the ship's bow is unlikely to run aground while passing over the step. The trim moment returns to zero slightly after the stern passes the step.

If changes in vertical force and trim moment happen slowly, we can assume the ship to remain in static equilibrium. In that case the results of §2.3.4 apply for the midship sinkage and trim of a symmetric hull, i.e.

$$\begin{aligned} Z &= -\rho g A_{\mathrm{W}} s \\ M &= \rho g I_{\mathrm{W}} \theta \, . \end{aligned}$$

Therefore, Figures 3.5 and 3.6 are proportional to the transient midship sinkage and trim of the ship as it passes the step. The vertical axis of Figure 3.5 represents

$$\frac{s}{-\frac{3}{2}\frac{U^2}{g}\frac{S_{\max}}{w^2}}$$

while the vertical axis of Figure 3.6 represents

$$\frac{\theta}{30\frac{U^2}{gL}\frac{S_{\max}}{w^2}} \, .$$

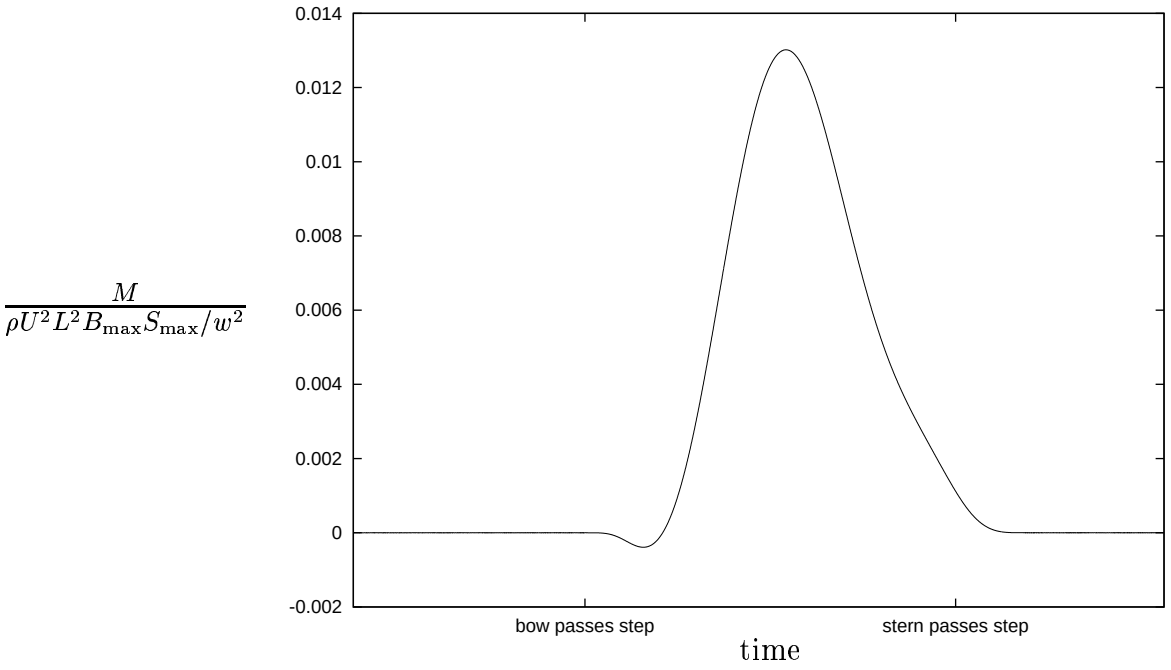

Figure 3.6: Scaled bow-up trim moment on a ship passing a step depth change to shallower water

We can use this midship sinkage and trim to find the bow and stern sinkage of the hull, which are shown in Figure 3.7. The strongly bow-up trim is evident, with the bow having quite a small sinkage while the step is being passed. The trim moment has almost returned to zero by the time the stern passes the step, so that the stern is only slightly more likely to ground in the shallow water than when the ship is in its steady-state condition.

Although the static equilibrium method will normally give a fair approximation to the transient sinkage and trim, for a step depth change the variations are quite rapid and we should include dynamical effects. Knowing the force and moment as a function of time, the heave and pitch of the ship can be determined by added-mass ship motion methods, although we shall not do this here.

Experiments in which the author participated were undertaken to study this phenomenon at the Australian Maritime College (see Duffield 1997). These were to study both the vertical force and trim moment for a fixed ship, and the sinkage and trim of a ship free to squat, for the case (among others) of a step depth change.

The results were in general agreement with those shown here, with the ship experiencing a considerable bow-up trim while passing a step depth change to shallower water. In most cases neither the bow nor stern was more likely to run aground than in the shallow-water steady-state condition. In fact, the vertical force took longer to reach steady state than was predicted using this theory. The few cases where the stern or bow sinkage exceeded the steady-state values were due to dynamical oscillations.

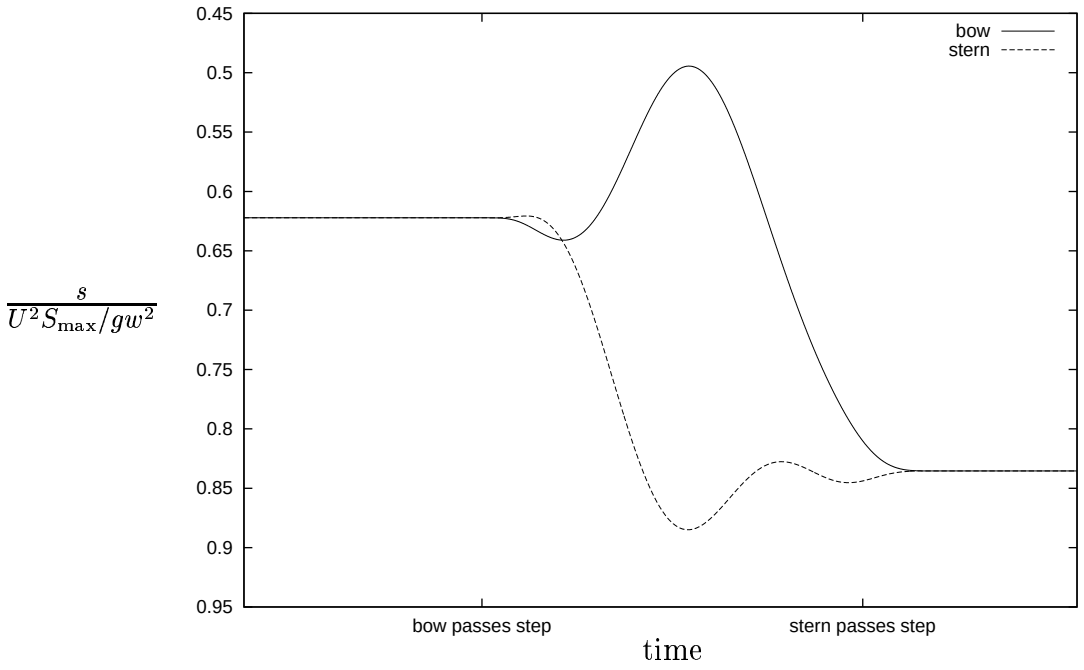

Figure 3.7: Bow and stern sinkage for a ship passing a step depth change to shallower water

For the case of a ship passing a step depth change to deeper water, the calculated vertical force and bow-up trim moment are almost the mirror image of the deep-to-shallow case. That is, the ship experiences a bow-down trim moment while it is passing into the deeper water, and the magnitude of the vertical force slowly decreases to the steady-state value.

3.4 Numerical method for general depth profiles

We now outline a finite-difference method for solving the partial differential equation (3.8) for general $h(x)$.

Because of the first derivative term in $h_x\phi_x$, centred-difference schemes to solve for ϕ are unstable according to the Neumann criterion (Shashkov 1996 p. 155–158). The same is true when solving for u in equation (3.9).

To overcome this difficulty, we write equation (3.9) in the form

$$(uh)_{tt} - gh\,(uh)_{xx} = -\frac{gUh}{w}S''(x+Ut) \tag{3.20}$$

and use centred differencing to solve for the flux uh. In this way the first derivative terms are effectively removed. Writing $f = uh$ for convenience, and defining $f_j^n = f(x_j, t_n)$, centred differencing produces the three-level equation

$$f_j^{n+1} = (2-2s_j)f_j^n - f_j^{n-1} + s_j(f_{j+1}^n + f_{j-1}^n) - \frac{gUh_j(\delta t)^2}{w}S''(x_j+Ut_n)\,. \tag{3.21}$$

Here $h_j = h(x_j)$, δt is the time step, δx is the x step and $s_j = gh_j(\delta t/\delta x)^2$. If we know the values of f_j^n at the first two time levels, we can use equation (3.21) as a time-stepping method. A Neumann stability analysis shows that the method will be numerically stable provided that $s_j \leq 1$.

The condition on s_j is effectively an upper limit on the size of the time step δt. Since the condition must be satisfied everywhere in the computation region, and s_j has its maximum value when h is at its maximum, the limiting size of the time step will be governed by the maximum depth $h_{\max}$ in the region of computation. The maximum possible time step is then given by $\delta x/\sqrt{gh_{\max}}$.

The region of computation is chosen large enough that waves cannot propagate to the boundaries by the time the final time step is reached. Therefore we use the boundary conditions that $f = 0$ at the upstream and downstream edges of the computation region.

In the case where the ship starts in water of constant depth, we can use the steady solution

$$f(x,t) = \frac{US(x+Ut)}{w\,(1-F_h^2)} \tag{3.22}$$

(see §1.4) as our initial condition at the first two time levels. If the ship starts in water of non-uniform depth, the expression (3.22), with $h = h(x)$ in $F_h = U/\sqrt{gh}$, provides a reasonable quasi-steady estimate to the initial flow.

With the fluid flux $f = uh$ calculated at each time level, we now know the fluid speed u as a function of x and t. In this case we find it easiest to switch to body-fixed coordinates in order to find the vertical force and trim moment as a function of time.

The unsteady Bernoulli equation in body-fixed coordinates is

$$\frac{p}{\rho} + \frac{1}{2}\,(U+u)^2 + \phi_t = \frac{1}{2}U^2$$

which gives the linearized hydrodynamic pressure p as

$$p = -\rho\,(Uu + \phi_t) \tag{3.23}$$

Note that the time derivative ϕ_t is taken at constant X, rather than at constant x as is the case in the earth-fixed coordinate system.

Substituting the expression (3.23) into equation (3.16) for the vertical force Z gives

$$Z = -\rho U \int_{-\ell}^{\ell} u\,B(X)\,dX - \rho \int_{-\ell}^{\ell} \phi_t\,B(X)\,dX$$

In order to evaluate the ϕ_t part of the integral, we define the hull parameter

$$\mathcal{B}(X) = \int_{-\ell}^{X} B(\xi)d\xi$$

and integrate by parts. This gives

$$Z = -\rho U \int_{-\ell}^{\ell} u\,B(X)\,dX - \rho\,[\mathcal{B}\phi_t]_{-\ell}^{\ell} + \rho \int_{-\ell}^{\ell} u_t\mathcal{B}(X)\,dX$$

or

$$Z = -\rho U \int_{-\ell}^{\ell} u\, B(X)\, dX - \rho \int_{-\ell}^{\ell} u_t \left[\mathcal{B}(X) - \mathcal{B}(\ell)\right]\, dX \ . \tag{3.24}$$

In a similar manner, the bow-up trim moment (from equation (3.17)) is given by

$$M = \rho U \int_{-\ell}^{\ell} u\, X\, B(X)\, dX + \rho \int_{-\ell}^{\ell} u_t \left[\mathcal{M}(X) - \mathcal{M}(\ell)\right]\, dX \tag{3.25}$$

with

$$\mathcal{M}(X) = \int_{-\ell}^{X} \xi B(\xi)\, d\xi \ .$$

3.4.1 Step depth change solution

As a test of the accuracy of this numerical method, solutions were obtained for a step depth change and compared with the analytic results. One of the benefits of solving for the flux $f = uh$, instead of the fluid speed u, is that continuity of flux is automatically satisfied at step depth changes. The other condition, that ϕ_t be continuous, is satisfied if we require that $(uh)_x$ is continuous, as can be seen from equation (3.8).

In the course of performing computations for general-shaped hulls passing a step depth change, it came to light that the finite difference method was given to producing spurious waves radiating ahead of and behind the ship. These are a natural feature of the partial differential equation, but should not be produced in steady-state flow.

A careful analysis of the finite-difference equation (3.21) shows how this can occur. Suppose that the ship's bow lies at a position x slightly less than x_{j+1} at time t_n. According to hydraulic theory in constant depth, there should be no disturbance ahead of the bow, that is, $f_j^n = f_{j-1}^n = 0$. Since the bow has not yet arrived at $x = x_j$, S'' is also zero there. For subcritical flow, since $U < \sqrt{gh}$ and $gh_j(\delta t/\delta x)^2 \leq 1$, the ship moves a distance less than δx in each time step. Therefore f_j^{n+1} should also be zero.

However, according to equation (3.21), f_j^{n+1} is given by $s_j f_{j+1}^n$ in this case. This starts a wave travelling ahead of the ship that will continue to propagate as time goes on. A similar wave is also generated travelling behind the ship.

For the wave ahead of the ship to be eliminated, S'' must exactly cancel the contributions from each of the gridpoints in equation (3.21). This does happen in the limit as $\delta x \to 0$, but is difficult to achieve at finite values of δx. For general-shaped mathematically-defined hulls, less spurious waves were produced when using a finite-difference method for S'' than when using the exact second derivative. This was because the finite-difference method gave a smooth extension to the values of S'' ahead of the bow, which helped to eliminate the forward-propagating waves.

It was in order to circumvent the problem of waves radiating away from the ship in the steady state that we used a cusped hull with $S'' = 0$ at the bow and stern. However, another idiosyncrasy of the finite-difference method was also revealed: that of numerical drift.

Suppose that the finite-difference method is to be solved in a region of constant depth h. Summing both sides of equation (3.21) over all values of j yields

$$\sum_j f_j^{n+1} = 2\sum_j f_j^n - \sum_j f_j^{n-1} - \frac{gUh(\delta t)^2}{w\delta x}\sum_j S''\delta x \; . \tag{3.26}$$

As $\delta x \to 0$, $\sum_j S''\delta x \to \int S''(X)\, dX$ which is zero for our cusped hull.

The sum of f values over all x gridpoints should be the same for each time level, since the flow is steady. However, if for any reason this is not true, so that

$$\sum_j f_j^{n-1} = k$$

and

$$\sum_j f_j^n = (1+\epsilon)k \; ,$$

equation (3.26) tells us that

$$\sum_j f_j^{n+1} = (1+2\epsilon)k \; .$$

In other words, the results will have a drift that increases linearly with time. For a ship passing a step depth change, this effect was observed in each region of constant depth, with output quantities having a linearly increasing drift away from their steady-state values. In order to correct for this, while the ship was entirely in a region of constant depth, the sum $\sum_j f_j^{n+1}$ would be calculated at the new time level. Each value of f_j^{n+1} would then be scaled so as to keep a constant sum at each time level.

Having dealt with these numerical difficulties, the finite-difference solution for the vertical force and trim moment agreed with the analytic solution for a step depth change. With the method thus verified, we shall now look at the case of a ship travelling in smoothly shelving water, and then two constant depths joined by a ramp.

3.4.2 Smoothly shelving sea floor

The case of a ship travelling in a channel whose floor is shelving at a small constant slope ϑ is depicted in Figure 3.8.

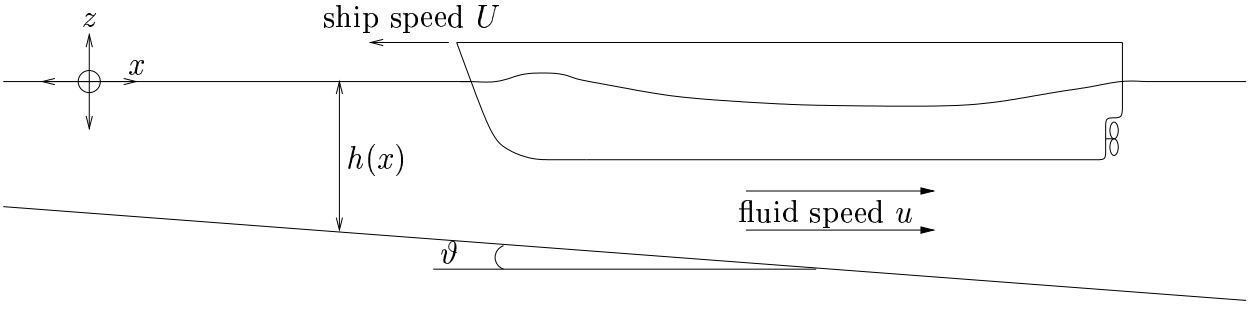

Figure 3.8: Smoothly shelving sea floor

The program was run using the initial condition given in equation (3.22), that is, the quasi-steady approximation $\bar{u}$, given by

$$\bar{u} = \frac{US(x+Ut)}{wh(1-F_h^2)} = \frac{US(x+Ut)}{w\left(h - \frac{U^2}{g}\right)} \tag{3.27}$$

where $h = h(x)$. Values of ϑ up to 15 degrees were considered.

It was found that even after running the ship from quite deep water until it touched the bottom, the velocity profile as given by the finite-difference method was almost indistinguishable from the quasi-steady approximation (3.27). Therefore we conjecture that, for a sloping channel with constant gradient, the quasi-steady approximation provides an accurate and simple estimate of the velocity profile.

Using this approximation to the fluid speed u, the vertical force (3.24) becomes, in body-fixed coordinates,

$$Z = -\frac{\rho U^2}{w}\int_{-\ell}^{\ell} \frac{B(X)S(X)}{h - \frac{U^2}{g}} - \rho\int_{-\ell}^{\ell} u_t\left[\mathcal{B}(X) - \mathcal{B}(\ell)\right] dX \tag{3.28}$$

From equation (3.27), we have, in body-fixed coordinates,

$$u_t = u_h\, h_t = -\frac{US(X)\, h_t}{w\left(h - \frac{U^2}{g}\right)^2}\,.$$

In body-fixed coordinates, $h_t = -Uh_X$, so that Z now becomes

$$Z = -\frac{\rho U^2}{w}\int_{-\ell}^{\ell} \frac{B(X)S(X)}{h - \frac{U^2}{g}} + \frac{\left(\mathcal{B}(\ell) - \mathcal{B}(X)\right) S(X)h_X}{\left(h - \frac{U^2}{g}\right)^2}\, dX\,. \tag{3.29}$$

In a similar manner, the bow-up trim moment (from equation (3.25)) is given by

$$M = \frac{\rho U^2}{w}\int_{-\ell}^{\ell} \frac{XB(X)S(X)}{h - \frac{U^2}{g}} + \frac{\left(\mathcal{M}(\ell) - \mathcal{M}(X)\right) S(X)h_X}{\left(h - \frac{U^2}{g}\right)^2}\, dX\,. \tag{3.30}$$

Equations (3.29) and (3.30) give the vertical force and trim moment as predicted using the quasi-steady approximation (3.27). This is valid for any depth function $h(x)$, although we expect that it will be more accurate for slowly-varying depth functions. Note that the expression (3.27) is still a function of time, and the time derivative terms must still be included in the force and moment calculations.

We shall now see how these simplified expressions compare to the finite-difference results for a more general depth function.

3.4.3 Ramp between two constant depths

Here we consider the bottom topography of two constant depths joined by a ramp at a constant angle. In the first case this ramp is three times the length of the ship, while in the second case it is the same length as the ship. The same hull and constant depths as in §3.3.1 are used.

Figures 3.9 and 3.10 show the vertical force and trim moment on the ship as it passes the long ramp. These are calculated using both the finite-difference method and the quasi-steady approximation described in §3.4.2.

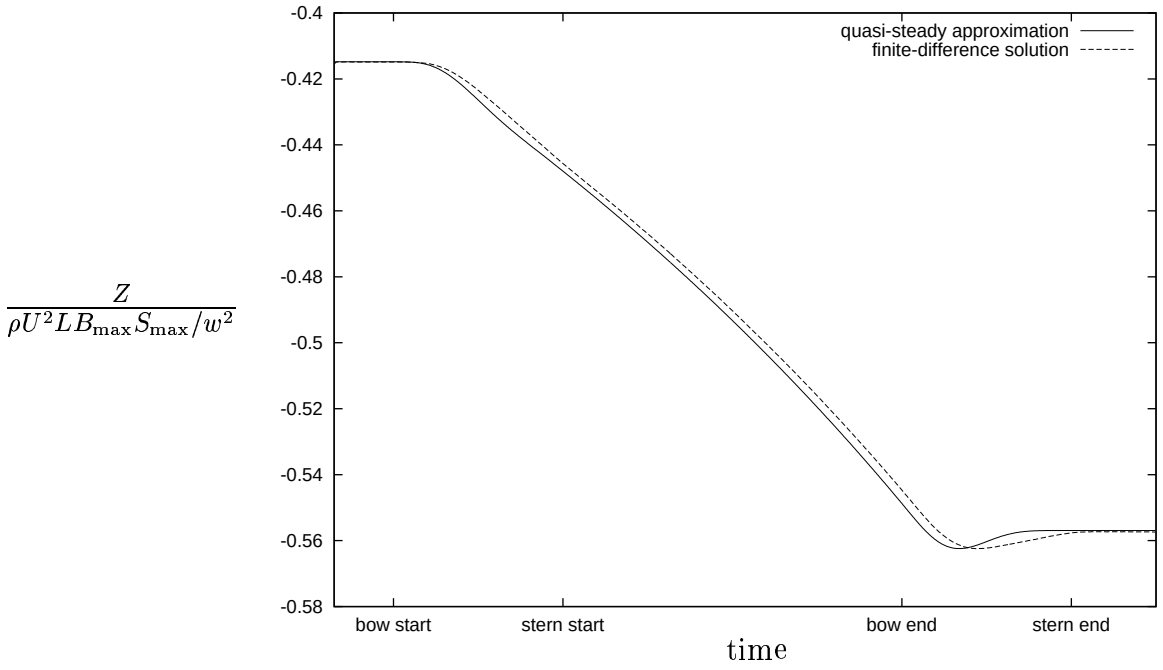

Figure 3.9: Scaled vertical force on a ship moving between two constant depths joined by a long ramp. Plotted as a function of time, with the points at which the bow or stern passes the start or end of the ramp indicated.

We see that for this gently-sloping bottom topography, the quasi-steady solution is quite close to the finite-difference solution. Both predict a gradual transition between the two steady-state vertical forces, with a slight overshoot that was not predicted for the step depth change. The bow-up trim is also quite similar according to both methods. We notice by comparing the trim graph to Figure 3.6 that the trim moment is much smaller for the ramp than for the step depth change.

For the short ramp case (Figures 3.11 and 3.12), there is less agreement between the quasi-steady and finite-difference results, showing that the quasi-steady approximation becomes less accurate when rapid depth changes occur. We notice that a slightly greater overshoot is observed in the vertical force than for the long ramp. The magnitude of the trim moment is larger than for the long ramp (Figure 3.10) and smaller than for the step (Figure 3.6).

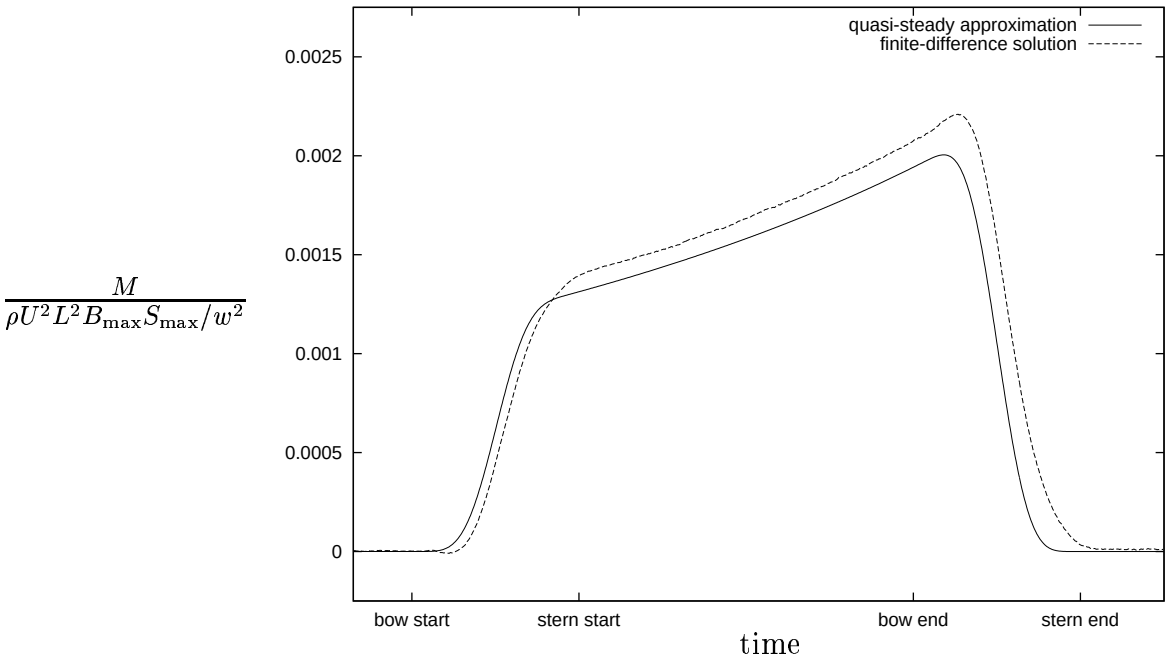

Figure 3.10: Scaled bow-up trim moment on a ship moving between two constant depths joined by a long ramp. Plotted as a function of time, with the points at which the bow or stern passes the start or end of the ramp indicated.

Experimental results (Duffield 1997) for a ship passing a ramp showed more of a lag in the vertical force reaching the steady-state value than was predicted here. No overshoot was witnessed.

3.5 Conclusions

We have developed an unsteady hydraulic theory that describes the flow past a ship in a channel of non-uniform depth. Since the full nonlinear theory proved difficult to solve, effort was focussed on the linear theory. This was solved analytically in the case of a step depth change, and an analytic quasi-steady solution was given for general $h(x)$. A numerical finite-difference method was developed to solve the linearized equation for general $h(x)$.

For a smoothly-shelving sea floor, the finite-difference results were almost identical to those predicted using the quasi-steady theory. The results were also similar for a long ramp between two constant depths, showing that the quasi-steady solution provides a reasonably accurate solution to the unsteady hydraulic equation for slowly-varying $h(x)$.

The results from the finite-difference method agreed with the analytic results for a step depth change. These showed a lag in the vertical force in reaching the new steady state, and a strong bow-up trim while the ship was passing a step depth change to shallower water. A lag was also predicted in the vertical force for a ship moving into deeper water,

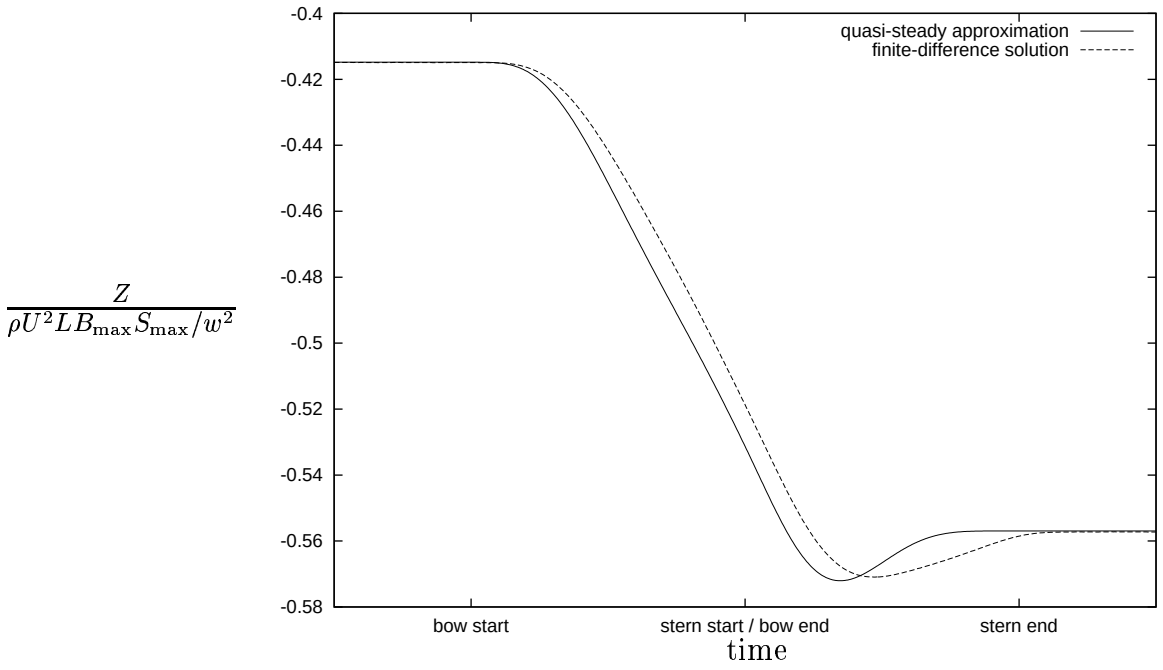

Figure 3.11: Scaled vertical force on a ship moving between two constant depths joined by a short ramp. Plotted as a function of time, with the points at which the bow or stern passes the start or end of the ramp indicated.

with a bow-down trim in that case.

The experimental results of Duffield (1997) also showed a significant bow-up trim for a ship passing a step depth change to shallower water. However, the vertical force, for both step and ramp depth changes, showed more of a lag in reaching the new steady-state value. This may have been due to the channel being too wide for hydraulic theory to be valid; however, we shall see in the following chapter that quite similar results are obtained using a fully two-dimensional slender-body shallow-water theory. Another possibility is that the experimental lag in the vertical force may have been due to viscous effects. During the time that the ship is passing a sudden depth change, rapid flow changes occur which may not be adequately described by inviscid theory.

In any case, both the theoretical and experimental results showed that ships are only marginally more at risk of grounding when moving into or out of shallow water than when they are in the shallow-water steady-state condition.

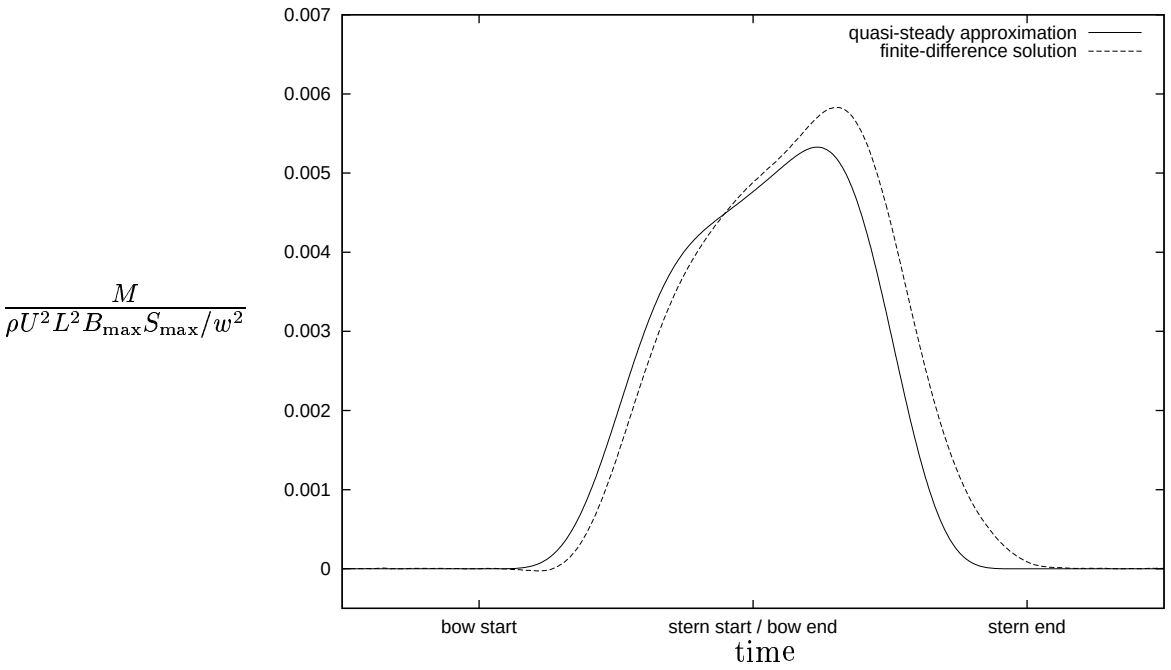

Figure 3.12: Scaled bow-up trim moment on a ship moving between two constant depths joined by a short ramp. Plotted as a function of time, with the points at which the bow or stern passes the start or end of the ramp indicated.

Chapter 4

Two-Dimensional Unsteady Squat

Here we develop an unsteady slender-body shallow-water theory. This theory is able to describe the flow around a ship travelling in open water or a channel of non-uniform depth. The theory and some preliminary results appeared in Gourlay & Tuck (1998b).

4.1 Unsteady slender-body shallow-water theory

Tuck (1964) developed a steady slender-body theory for ships travelling in an infinite depth of water. This method assumed that the ship's beam and draft were both small (order ϵ) multiples of the shiplength L.

The theory was then adapted to shallow water of constant depth (Tuck 1966) for unbounded fluid domains. In this case it was assumed that the water depth h was of the same order as the ship's draught, so that h/L was also of order ϵ. This shallowness assumption, along with the slenderness of the ship, greatly simplified the hydrodynamic equations. Later (Tuck 1967) the theory was extended to describe the flow around a ship travelling in a channel of constant width and depth.

In each case the problem was solved by matched asymptotic expansions, with the flow in an inner region close to the ship being matched to the far-field solution.

We now follow a similar approach, but use earth-fixed coordinates (x, y, z, t), with the ship moving at speed U in the $-x$ direction. The formulation is the same as that described in §3.1, with the extra spatial dimension y defined in the transverse direction (as in Figure 1.1) to form a right-handed (x, y, z) coordinate system.

The undisturbed depth is allowed to vary in both the x and y directions. For simplicity, however, we assume that if the depth varies in the $y-$direction it is symmetric about the $x-$axis, so that $h(x, y) = h(x, -y)$. To preserve this symmetry, if the ship is travelling in a channel it will be taken to be moving along the centre of the channel. With these simplifications, the flow can be solved in $y > 0$ and then mirrored in $y < 0$. The more

general problem not only requires solution in the entire domain, but also a more difficult non-symmetric matching of the inner and outer flows.

We shall start with the unsteady, nonlinear equations of inviscid, irrotational flow. These are Laplace's equation

$$\phi_{xx} + \phi_{yy} + \phi_{zz} = 0 \,, \tag{4.1}$$

the unsteady Bernoulli equation applied on the free surface

$$g\zeta + \frac{1}{2}\phi_x^2 + \frac{1}{2}\phi_y^2 + \frac{1}{2}\phi_z^2 + \phi_t = 0 \qquad \text{on } z = \zeta(x,y,t) \,, \tag{4.2}$$

the kinematic condition on the free surface

$$\phi_z = \phi_x\zeta_x + \phi_y\zeta_y + \zeta_t \qquad \text{on } z = \zeta(x,y,t) \tag{4.3}$$

and the kinematic condition on the sea floor

$$\phi_z = -\phi_x h_x - \phi_y h_y \qquad \text{on } z = -h(x,y) \,. \tag{4.4}$$

4.1.1 The outer expansion

In the outer region we assume that $x, y = O(L)$ while $z = O(\epsilon L)$, and expand ϕ in powers of ϵ:

$$\phi = \phi^{(1)} + \phi^{(2)} + \phi^{(3)} + ...$$

where each $\phi^{(n)}$ is $O(\epsilon^n)$. Equating like powers of ϵ in (4.1) tells us successively that

$$\begin{aligned} \phi^{(1)}_{zz} &= 0 \\ \phi^{(2)}_{zz} &= 0 \\ \phi^{(3)}_{zz} &= -\nabla^2_{xy}\phi^{(1)} \end{aligned} \tag{4.5}$$

where $\nabla^2_{xy} = \frac{\partial^2}{\partial x^2} + \frac{\partial^2}{\partial y^2}$.

Therefore $\phi^{(1)}_z$ and $\phi^{(2)}_z$ are constant in z. Equating powers of ϵ in the bottom condition (4.4) then tells us that these quantities are zero, so that $\phi^{(1)}$ and $\phi^{(2)}$ are both independent of z. We therefore have

$$\phi^{(1)} = \phi^{(1)}(x,y,t)$$

and

$$\phi^{(2)} = \phi^{(2)}(x,y,t) \,.$$

Equation (4.4) also tells us that

$$\phi^{(3)}_z = -\phi^{(1)}_x h_x - \phi^{(1)}_y h_y \qquad \text{on } z = -h(x,y) \,,$$

which, along with the Laplace equation (4.5), determines $\phi^{(3)}_z$ as follows:

$$\phi^{(3)}_z = -\nabla^2_{xy}\phi^{(1)}.(z+h) - \phi^{(1)}_x h_x - \phi^{(1)}_y h_y \,. \tag{4.6}$$

We now use the free surface conditions to find an expression for $\phi_z^{(3)}$ on $z = 0$. The Bernoulli equation (4.2) becomes, to leading order,

$$g\zeta + \phi_t^{(1)} = 0 \, . \tag{4.7}$$

If $h/L = O(\epsilon)$, we expect for linearized flow that $\zeta/L = O(\epsilon)^2$, and this can be shown as follows. The standard dimensions of ϕ_x are U, such that $\phi_x/U = O(\epsilon)$. Therefore the standard dimensions of ϕ_t are that of $\phi_x \, dx/dt$, so that $\phi_t/U^2 = O(\epsilon)$. Writing equation (4.7) as

$$\frac{\zeta}{L} = -F_h^2 \frac{h}{L} \frac{\phi_t}{U^2}$$

we see that, subject to the assumption that the Froude number F_h is asymptotically of $O(1)$, the free surface height is of second order, i.e.

$$\frac{\zeta}{L} = O(\epsilon^2) \, .$$

Hence, consistent to second order in ϵ, the leading terms in the kinematic condition (4.3) give

$$\phi_z^{(3)} = \zeta_t \qquad \text{on } z = 0 \, . \tag{4.8}$$

The linearized free surface conditions (4.7) and (4.8) combine to give the free surface condition

$$\phi_z^{(3)} = -\frac{\phi_{tt}^{(1)}}{g} \qquad \text{on } z = 0 \, .$$

Equating this with the expression (4.6) applied at $z = 0$ gives the unsteady slender-body shallow-water equation for the first-order outer velocity potential $\phi^{(1)}(x, y, t)$ (which we will simply call ϕ from now on), namely

$$\frac{\phi_{tt}}{g} = (h\phi_x)_x + (h\phi_y)_y \, . \tag{4.9}$$

This is a type of wave equation that describes two-dimensional wave propagation in a non-uniform medium characterized by $h(x, y)$. It is given by Stoker (1957, p. 419) for describing two-dimensional long waves in shallow water of non-uniform depth. It has been used, for example, to model tsunami propagation over non-uniform bottom topography (see Houston 1978, Tuck 1979). Although the differential equation is easily solved when h =constant, for general $h(x, y)$ complicated numerical methods are required.

In open water, the boundary condition for equation (4.9) is that the fluid velocity $\nabla\phi$ must either tend to zero or behave like an outgoing wave at infinity. On the other hand, if there are vertical side walls at $y = \pm\frac{1}{2}w(x)$, we must apply the wall boundary condition

$$\phi_y = \pm\frac{1}{2} w_x \phi_x \qquad \text{on } y = \pm\tfrac{1}{2}w(x) \, .$$

In this chapter, however, we shall only consider channels of constant width w, with the ship travelling along the centre of the channel. In this case, the wall boundary condition becomes

$$\phi_y = 0 \qquad \text{on } y = \pm w/2 \, . \tag{4.10}$$

4.1.2 The inner expansion and matching

In non-uniform depth, the inner flow analysis goes over virtually unchanged from that developed by Tuck (1966) for constant depth.

In the inner region, both y and z are $O(\epsilon L)$, while x is still $O(L)$. We assume a series solution for the inner velocity potential φ of the form

$$\varphi = \varphi^{(1)} + \varphi^{(2)} + \varphi^{(3)} + ...$$

where each $\varphi^{(n)}$ is $O(\epsilon^n)$. In this region the depth is a slowly varying function of the inner variable y/ϵ, provided that h has no discontinuities in y near $y = 0$. Therefore, to leading order, $h(x, y) = h(x, 0)$ over the entire inner region.

The inner flow is governed by the changing cross-sectional area S of the ship's hull, which causes water to pushed aside when S is increasing and pulled in when S is decreasing. The behaviour of this inner flow further from the hull provides a boundary condition which drives the outer flow.

The equations for the leading term $\varphi^{(1)}$ reduce to a 2-D Laplace equation in the (y, z) plane with Neumann (zero normal velocity) boundary conditions on the hull, sea floor and linearized free surface $z = 0$. Continuity then requires that there be zero net outflow at the outer edges of the inner region, where $y/\epsilon \to \pm\infty$. Because of the symmetry of the problem in the y-direction, there is no mechanism for producing any cross-flow in the y-direction either. Since $\varphi^{(1)}$ has zero normal derivative on all boundaries (including the artificial boundaries at the outer edges of the inner region), $\varphi^{(1)}$ is a constant in the (y, z) plane. Therefore $\varphi^{(1)} = \varphi^{(1)}(x, t)$.

The equations for $\varphi^{(2)}$ are also unaffected by the variable depth. The outflow due to the changing cross-sectional area of the hull, namely $US'(x+Ut)$, is channelled sideways into equal constant streams at the outer edges of the inner region (where h is still given by its value at $y = 0$), so that we have

$$\frac{\partial \varphi^{(2)}}{\partial y} \to \pm \frac{US'(x+Ut)}{2h(x,0)} \qquad \text{as } y/\epsilon \to \pm\infty \, . \tag{4.11}$$

Matching the inner and outer flows requires that the inner limit of $\phi(x, y, t)$ be equal to the leading inner term $\varphi^{(1)}(x, t)$:

$$\phi\,(x, 0, t) = \varphi^{(1)}(x, t) \, . \tag{4.12}$$

The $y-$derivative ϕ_y must also match across the two regions; this is given at the outer edge of the inner region by equation (4.11), and at the inner edge of the outer region by $\phi_y\,(x, 0_\pm, t)$. Equating these gives the "body" boundary condition on the plane $y = 0_\pm$ for the leading outer term $\phi(x, y, t)$

$$\phi_y\,(x, 0_\pm, t) = \pm \frac{US'\,(x+Ut)}{2h(x,0)} \, . \tag{4.13}$$

Therefore we need only solve equation (4.9), subject to the body boundary condition (4.13) and the boundary condition at infinity or on the channel walls, in order to know the entire leading-order flow field.

In the derivation of this theory, no assumptions have been made about the magnitude of the channel width; however, for the slender-body theory to be valid, the ship's beam must be small compared to the channel width. This same condition was required for the linearized unsteady hydraulic theory discussed in Chapter 3. We should therefore expect that in the limit as $w/L \to 0$ (with B/w still small) the two-dimensional theory should produce the same flow as predicted using the one-dimensional theory. In fact, the two theories do become identical in this limit, as is shown in Appendix B.4.

4.1.3 Vertical force, moment, sinkage and trim

In terms of the inner velocity potential φ near the ship's hull, the unsteady Bernoulli relation for the hydrodynamic pressure p reads

$$p + \frac{\rho}{2}\left(\varphi_x^2 + \varphi_y^2 + \varphi_z^2\right) + \rho\varphi_t = 0 \; .$$

To leading order this becomes

$$p = -\rho\varphi_t^{(1)} \; .$$

Using the matching condition (4.12), we can write this in terms of the outer potential ϕ as

$$p = -\rho\phi_t(x, 0, t) \; . \tag{4.14}$$

With the hull pressure p thus found, the unsteady vertical force Z and trim moment M can be found in the same way as was done in §3.3.1, by switching to body-fixed coordinates and using

$$\begin{aligned} Z &= \int_{-\ell}^{\ell} p\, B(X)\, dX \\ M &= -\int_{-\ell}^{\ell} X\, p\, B(X)\, dX \; . \end{aligned} \tag{4.15}$$

4.2 An analytic solution for a step depth change

In the case of a ship approaching a step depth change, equation (4.9) can be solved analytically using the method of images. This solution makes no allowance for waves being produced as the ship passes the step, so is of limited use thereafter. Only the flow in the time up until the ship meets the step is considered here. However, as we shall see, the theory may remain approximately valid even after the ship passes the step in the case of a wide channel or open water.

The problem formulation is the same as that described in §3.3, with the step at $x = 0$ and the ship moving from right to left. For $x > 0$ we have $h = h_1$, $\phi = \phi_1$ and $F_h = F_1$;

for $x < 0$, $h = h_2$, $\phi = \phi_2$ and $F_h = F_2$. It is assumed here that the flow is subcritical for $x > 0$, i.e. $F_1 < 1$. We shall initially consider the case of a step depth change in *open water*.

4.2.1 Constant depth solution

Let us first consider the special case where $h =$ constant, and the Froude number F_h is less than 1. In this case there are solutions to the governing equation (4.9) of the form $\phi(x, y, t) = \psi(X, Y)$, with $X = x + Ut$, $Y = \sqrt{1 - F_h^2}\, y$. The function $\psi(X, Y)$ then satisfies Laplace's equation

$$\psi_{XX} + \psi_{YY} = 0 \tag{4.16}$$

in these (X, Y) coordinates.

The solution of (4.16) for a single unit source at the origin in the (X, Y) plane is

$$\psi(X, Y) = \frac{1}{2\pi} \log \sqrt{X^2 + Y^2}\ . \tag{4.17}$$

Therefore, this is also the solution of (4.9) for a single unit source moving in the (x, y) plane, with $\phi(x, y, t) = \psi(X, Y)$, i.e.

$$\phi(x, y, t) = \frac{1}{2\pi} \log \sqrt{(x + Ut)^2 + (1 - F_h^2) y^2}\ . \tag{4.18}$$

For a line of sources of length $L = 2\ell$, centred on $X = 0$, the solution of (4.16) is

$$\psi(X, Y) = \frac{1}{2\pi} \int_{-\ell}^{\ell} Q(\xi) \log \sqrt{(X - \xi)^2 + Y^2}\, d\xi\ . \tag{4.19}$$

This transforms to a moving line of sources in the (x, y) plane, with $\phi(x, y, t) = \psi(X, Y)$, so that

$$\phi(x, y, t) = \frac{1}{2\pi} \int_{-\ell}^{\ell} Q(\xi) \log \sqrt{(x + Ut - \xi)^2 + (1 - F_h^2) y^2}\, d\xi\ . \tag{4.20}$$

The source strength $Q(X)$ can be found using the boundary condition (4.13). If we consider $y > 0$, differentiating equation (4.20) gives

$$\phi_y(x, 0, t) = \frac{\sqrt{1 - F_h^2}}{2} \lim_{y \to 0} \frac{1}{\pi} \int_{-\ell}^{\ell} \frac{Q(\xi) \sqrt{1 - F_h^2}\, y}{(X - \xi)^2 + (1 - F_h^2) y^2}\, d\xi\ .$$

The function

$$\frac{1}{\pi} \lim_{a \to 0} \frac{a}{x^2 + a^2}$$

is the delta function $\delta(x)$; it is zero everywhere except at the singular point $x = 0$. The delta function has the property

$$\int_{-\infty}^{\infty} \delta(x) f(x)\, dx = f(0)$$

for any bounded function $f(x)$ which is continuous at $x = 0$. Therefore

$$\phi_y(x, 0, t) = \frac{\sqrt{1 - F_h^2}\, Q(X)}{2}$$

which, on equating with equation (4.13), yields the source strength as

$$Q(X) = \frac{US'(X)}{h\sqrt{1 - F_h^2}} \,. \tag{4.21}$$

Using equation (4.20), the velocity potential for a slender ship moving in shallow water of constant depth is therefore

$$\phi(x, y, t) = \frac{U}{2\pi h\sqrt{1 - F_h^2}} \int_{-\ell}^{\ell} S'(\xi) \log \sqrt{(x + Ut - \xi)^2 + (1 - F_h^2)y^2}\, d\xi \,. \tag{4.22}$$

This is a simple derivation of the constant-depth slender-body shallow-water solution obtained by Tuck (1966).

We shall now exploit the fact that the ship acts like a line of sources on $y = 0$. The flow produced by each source as it approaches the step is considered, before using linear superposition to find the flow around the entire ship.

4.2.2 The method of images

In the case of a ship moving at constant speed towards a step depth change, we can use the method of images to find the flow on each side of the step. We first consider an isolated unit source moving at speed U in the $-x$ direction in $x > 0$ for $t < 0$, so that it will reach the origin at $t = 0$. If there were no step present, the flow would simply be given by (4.18). However, the step acts as a partially reflective barrier; the total flow $\phi = \phi_1$ in $x > 0$ is then that of the original source located at $x = -Ut$, plus that of an image source located the same distance away on the other side of the step (at $x = Ut$), in a fictitious extension to $x < 0$ with everywhere constant depth h_1. Thus

$$\begin{aligned} \phi_1(x, y, t) &= \frac{1}{2\pi} \log \sqrt{(x + Ut)^2 + (1 - F_1^2)y^2} \\ &+ \frac{\eta}{2\pi} \log \sqrt{(x - Ut)^2 + (1 - F_1^2)y^2} \end{aligned} \tag{4.23}$$

in $x > 0$. The image source strength η is yet to be determined.

In order to find η we must match this flow to that of the 'transmitted' flow in $x < 0$, where the depth is h_2. Because of the wave-like nature of equation (4.9), this flow is analogous to that of a wave partially reflecting and partially transmitting as it passes across the boundary between two different media. The flow $\phi = \phi_2$ in $x < 0$ will then appear to be generated by a source located in a fictitious extension to $x > 0$ with everywhere constant depth h_2. This moving source will be seen to have a different velocity, which we will call

U_*, and must be at position $x = -U_* t > 0$, so as to also arrive at the origin at $t = 0$. Its strength is written as ν, which is to be determined. Therefore the flow in $x < 0$ is

$$\phi_2(x, y, t) = \frac{\nu}{2\pi} \log \sqrt{(x + U_* t)^2 + (1 - F_*^2) y^2} \tag{4.24}$$

with $F_* = U_*/\sqrt{g h_2}$. Note that our present solutions are only valid when $F_1 < 1$ and $F_* < 1$; i.e. the flows produced by the ship at its speed U in its depth h_1, and by the image (at a different speed U_* in a different depth h_2) are both subcritical. Supercritical flows will not be considered here.

The matching conditions across the step require continuity of the free-surface elevation (proportional to ϕ_t) and flux $h\phi_x$ for all y and $t < 0$. These conditions determine the three unknowns η, ν and U_*.

Matching ϕ_t across the step requires that

$$\phi_{1t}(0_+, y, t) = \phi_{2t}(0_-, y, t) \ ,$$

or

$$\frac{2U^2 t(1 + \eta)}{U^2 t^2 + (1 - F_1^2) y^2} = \frac{2U_*^2 t \nu}{U_*^2 t^2 + (1 - F_*^2) y^2} \ .$$

If this is to be true for all y and $t < 0$ we must have

$$1 + \eta = \nu \tag{4.25}$$

and

$$\frac{1 - F_1^2}{U^2} = \frac{1 - F_*^2}{U_*^2} \ . \tag{4.26}$$

Matching the flux across the step requires that

$$h_1 \phi_{1x}(0_+, y, t) = h_2 \phi_{2x}(0_-, y, t) \ ,$$

or

$$\frac{2U t h_1 (1 - \eta)}{U^2 t^2 + (1 - F_1^2) y^2} = \frac{2U_* t h_2 \nu}{U_*^2 t^2 + (1 - F_*^2) y^2} \ .$$

If this is to be true for all y and $t < 0$ we need

$$\frac{h_1 (1 - \eta)}{U} = \frac{h_2 \nu}{U_*} \tag{4.27}$$

in addition to condition (4.26).

The three simultaneous equations (4.25), (4.26) and (4.27) can be solved to give the required expressions for η, ν, and U_*, namely

$$\eta = \frac{h_1 - h_2 \sqrt{1 + F_2^2 - F_1^2}}{h_1 + h_2 \sqrt{1 + F_2^2 - F_1^2}} \ , \tag{4.28}$$

$$\nu = \frac{2h_1}{h_1 + h_2\sqrt{1 + F_2^2 - F_1^2}} \tag{4.29}$$

and

$$U_* = \frac{U}{\sqrt{1 + F_2^2 - F_1^2}} \tag{4.30}$$

where $F_2 = U/\sqrt{gh_2}$. Note that the speed U in the definition of F_2 is that of the ship itself, and $F_2 \neq F_*$. Although we have assumed that $F_* < 1$, it is not necessary that $F_2 < 1$. In fact, analysis of equation (4.30) shows that $F_* < 1$ for all values of F_2 if $F_1 < 1$.

If $h_2 < h_1$ (i.e. the ship is moving towards shallower water) the source strength η is between 0 and 1, whereas if $h_2 > h_1$ we have $-1 < \eta < 0$. The transmissivity ν is always positive when $F_1 < 1$.

For a line distribution of sources, the same analysis applies, so that the velocity potential in $x > 0$ satisfies

$$\begin{aligned} \phi_1(x,y,t) &= \frac{1}{2\pi}\int_{-\ell}^{\ell} Q(\xi)\log\sqrt{(x+Ut-\xi)^2 + (1-F_1^2)y^2}\,d\xi \\ &+ \frac{\eta}{2\pi}\int_{-\ell}^{\ell} Q(\xi)\log\sqrt{(x-Ut+\xi)^2 + (1-F_1^2)y^2}\,d\xi \end{aligned} \tag{4.31}$$

where η is again given by equation (4.28). Note that the image line of sources is effectively reversed, as the image ship is also approaching the step bow-first, but from the opposite direction.

In order to satisfy the body boundary condition, the source strength $Q(X)$ must still be given by equation (4.21). Therefore ϕ_1 becomes

$$\begin{aligned} \phi_1(x,y,t) &= \frac{U}{2\pi h_1\sqrt{1-F_1^2}}\int_{-\ell}^{\ell} S'(\xi)\log\sqrt{(x+Ut-\xi)^2 + (1-F_1^2)y^2}\,d\xi \\ &+ \frac{\eta U}{2\pi h_1\sqrt{1-F_1^2}}\int_{-\ell}^{\ell} S'(\xi)\log\sqrt{(x-Ut+\xi)^2 + (1-F_1^2)y^2}\,d\xi\ . \end{aligned} \tag{4.32}$$

So long as the ship remains entirely in $x > 0$, this represents in $x > 0$ the flow created by the original ship and an image ship (of reduced strength η) both moving towards the step with speed U.

4.2.3 Vertical force and trim moment

In order to determine the fluid pressure on the hull, we find the inner velocity potential $\phi_1(x,0,t)$, which becomes

$$\phi_1(x,0,t) = \frac{U}{2\pi h_1\sqrt{1-F_1^2}}\int_{-\ell}^{\ell}\big[\log(x-\xi+Ut) + \eta\log(x+\xi-Ut)\big]S'(\xi)d\xi\ . \tag{4.33}$$

The hydrodynamic hull pressure p is then determined using equation (4.14), giving

$$p = -\frac{\rho U^2}{2\pi h_1 \sqrt{1-F_1^2}} \int_{-\ell}^{\ell} \left[\frac{1}{x-\xi+Ut} - \frac{\eta}{x+\xi-Ut} \right] S'(\xi) d\xi \; . \tag{4.34}$$

In order to calculate Z and M, we transfer to the body-fixed coordinate $X = x + Ut$, whereupon p becomes

$$p = -\frac{\rho U^2}{2\pi h_1 \sqrt{1-F_1^2}} \int_{-\ell}^{\ell} \left[\frac{1}{X-\xi} - \frac{\eta}{X+\xi-2Ut} \right] S'(\xi) d\xi \; . \tag{4.35}$$

Inserting this into the expression (4.15) for Z yields

$$Z = -\frac{\rho U^2}{2\pi h_1 \sqrt{1-F_1^2}} \int_{-\ell}^{\ell} \int_{-\ell}^{\ell} B(X) S'(\xi) \left[\frac{1}{X-\xi} - \frac{\eta}{X+\xi-2Ut} \right] \, dX d\xi \; . \tag{4.36}$$

This result may be written in alternative forms if we are considering a sharp-ended vessel, for which B and S vanish at the bow and stern. Integrating equation (4.36) by parts then yields the alternative forms

$$Z = \frac{\rho U^2}{2\pi h_1 \sqrt{1-F_1^2}} \int_{-\ell}^{\ell} \int_{-\ell}^{\ell} B(X) S(\xi) \left[\frac{1}{(X-\xi)^2} + \frac{\eta}{(X+\xi-2Ut)^2} \right] \, dX d\xi \tag{4.37}$$

and

$$Z = \frac{\rho U^2}{2\pi h_1 \sqrt{1-F_1^2}} \int_{-\ell}^{\ell} \int_{-\ell}^{\ell} B'(X) S'(\xi) \big[\log(X-\xi) - \eta \log(X+\xi-2Ut) \big] \, dX d\xi \; . \tag{4.38}$$

In each equation the first term in the square brackets gives the steady constant-depth vertical force. For equation (4.38) this is in the same form as that derived by Tuck (1966). The second term in each equation gives the additional force due to the presence of the approaching step, which is time-dependent.

It would interest us to know whether this additional force, which we will denote by Z_{step}, is positive or negative. Looking at equation (4.37) we see that when the distance of the centre of the ship from the step, $d = -Ut$, is large (remember $t < 0$) the integral

$$Z_{\text{step}} = \frac{\rho U^2 \eta}{2\pi h_1 \sqrt{1-F_1^2}} \int_{-\ell}^{\ell} \int_{-\ell}^{\ell} \frac{B(X) S(\xi)}{(X+\xi+2d)^2} \, dX d\xi \tag{4.39}$$

acts like

$$\frac{\rho U^2 \eta}{2\pi h_1 \sqrt{1-F_1^2}} \int_{-\ell}^{\ell} \int_{-\ell}^{\ell} \frac{B(X) S(\xi)}{4d^2} \, dX d\xi \; ,$$

which integrates to

$$Z_{\text{step}} \sim \frac{\rho U^2 \eta \Delta A_{\text{W}}}{8\pi h_1 d^2 \sqrt{1-F_1^2}} \tag{4.40}$$

when d is large. Here Δ is the ship's displacement and A_{W} is the waterline area in the horizontal plane.

Equation (4.40) tells us that, at least when the ship is more than several shiplengths away from the step, the vertical force correction Z_{step} is proportional to $1/d^2$. Z_{step} is positive for a ship moving towards shallower water ($\eta > 0$), and negative for a ship moving towards deeper water ($\eta < 0$). This means that the midship squat of the ship will be less than the steady-state value for a ship moving towards shallower water, and more than the steady-state value for a ship moving towards deeper water.

The bow-up trim moment M can be found in a similar manner to equation (4.36) as

$$M = \frac{\rho U^2}{2\pi h_1 \sqrt{1-F_1^2}} \int_{-\ell}^{\ell} \int_{-\ell}^{\ell} X\, B(X) S'(\xi) \left[\frac{1}{X-\xi} - \frac{\eta}{X+\xi-2Ut} \right] dX\, d\xi \; . \tag{4.41}$$

The first term in the square brackets gives the steady constant-depth trim moment, while the second term gives the additional moment

$$M_{\mathrm{step}} = -\frac{\rho U^2 \eta}{2\pi h_1 \sqrt{1-F_1^2}} \int_{-\ell}^{\ell} \int_{-\ell}^{\ell} \frac{X\, B(X) S'(\xi)}{X+\xi-2Ut}\, dX\, d\xi \; . \tag{4.42}$$

For sharp-ended vessels, this can be integrated by parts to give the large-d limit

$$M_{\mathrm{step}} \sim -\frac{\rho U^2 \eta \Delta M_{\mathrm{W}}}{8\pi h_1 d^2 \sqrt{1-F_1^2}} \; , \tag{4.43}$$

where

$$M_{\mathrm{W}} = \int_{-\ell}^{\ell} X\, B(X)\, dX \; .$$

For a fore-aft symmetric ship, $M_{\mathrm{W}} = 0$ and the trim moment correction given by (4.43) is zero. If $M_{\mathrm{W}} > 0$, as is most often the case, the ship will experience a slightly greater bow-down trim when moving towards shallower water.

When the ship comes closer to the step and the preceding asymptotic analysis is no longer valid, we may evaluate the integrals (4.39) and (4.42) numerically. Both of these integrals are non-singular if $d > \ell$, i.e. the ship's bow has not yet reached the step. This is in contrast to the steady-state contributions in equations (4.36) and (4.41), which are always singular.

The integrals may be evaluated using a two-dimensional Simpson method. This can also be used for the singular integrals if we integrate the singular part exactly in the vicinity of the singularity. Although results for open water are not shown here, the correction to the vertical force continues to increase as the ship approaches the step.

Although we have stated that the validity of the image method can only be ensured for a ship *approaching* a step depth change, it is possible that no radiating waves are produced when a ship passes a step depth change in open water. Numerical results for

wide channels seem to suggest that this is the case. If this is so, the image method could equally well be used after the ship has passed the step depth change. In this case we would also have to assume that $F_2 < 1$ for the analysis to be valid.

Alternatively, since nowhere in the above derivation have we assumed that $U > 0$, for a ship moving away from a step depth change we can change U to $-U$ and $S(X)$ to $S(-X)$ to obtain the flow field. The ship is then still in $x > 0$ but heading away from the step in the positive x-direction. We see from equation (4.39) that for a fore-aft symmetric ship, the vertical force here will be the same as if the ship were moving towards the step.

If radiating waves are not produced, it is also possible to use the image method when the ship is passing over the step. In this case we use the same analysis as previously for the stern section of the ship which lies in $x > 0$. The flow due to the bow in $x < 0$ and its image can then be considered separately, and the resulting velocity potentials added by linear superposition. However, this method is tedious and no numerical results were computed.

4.2.4 Finite-width channel

The steady solution of equation (4.9) for a unit source in a channel with walls at $y = \pm w/2$ can again be found by solving Laplace's equation (4.16) in (X, Y) coordinates. In these coordinates, the source is stationary in a channel with side walls at $Y = \pm\sqrt{1 - F_h^2}\, w/2$. The velocity potential $\psi(X, Y)$ for a unit source in these coordinates can then be found simply by the Schwarz-Christoffel transformation. It is given by Tuck (1997) and satisfies

$$\psi(X, Y) = \frac{1}{2\pi} \log \sqrt{\cosh\left(\frac{2\pi X}{w\sqrt{1 - F_h^2}}\right) - \cos\left(\frac{2\pi Y}{w\sqrt{1 - F_h^2}}\right)}\,. \tag{4.44}$$

Therefore, in a similar manner to the open-water case, the steady-state solution for a moving line of sources of strength such that (4.13) is satisfied can be found to be

$$\phi(x, y, t) = \frac{U}{2\pi h\sqrt{1 - F_h^2}} \int_{-\ell}^{\ell} S'(\xi) \log \sqrt{\cosh\left(\frac{2\pi}{w\sqrt{1 - F_h^2}}(x - \xi + Ut)\right) - \cos\left(\frac{2\pi y}{w}\right)}\, d\xi\,. \tag{4.45}$$

This is an alternative derivation of the steady slender-body shallow-water solution for a ship in a channel. It is in a different form to the Fourier-transformed solution given by Tuck (1967).

As for the open-water case, to find the flow field in the presence of a step at $x = 0$ we consider a single moving source and its image, so that for $x > 0$,

$$\begin{aligned} \phi_1(x, y, t) &= \frac{1}{2\pi} \log \sqrt{\cosh\left(\frac{2\pi}{w\sqrt{1 - F_1^2}}(x + Ut)\right) - \cos\left(\frac{2\pi y}{w}\right)} \\ &+ \frac{\eta}{2\pi} \log \sqrt{\cosh\left(\frac{2\pi}{w\sqrt{1 - F_1^2}}(x - Ut)\right) - \cos\left(\frac{2\pi y}{w}\right)} \end{aligned} \tag{4.46}$$

while for $x < 0$,

$$\phi_2(x,y,t) = \frac{\nu}{2\pi}\log\sqrt{\cosh\left(\frac{2\pi}{w\sqrt{1-F_*^2}}(x+U_*t)\right) - \cos\left(\frac{2\pi y}{w}\right)}\,. \tag{4.47}$$

Matching ϕ_t and $h\phi_x$ across $x = 0$ gives the same values of η, ν and U_* as in (4.28–4.30). The vertical force in this case is

$$Z = Z_{\text{steady}} + Z_{\text{step}}\ ,$$

with

$$Z_{\text{steady}} = -\frac{\rho U^2}{2h_1 w\,(1-F_1^2)}\int_{-\ell}^{\ell}\int_{-\ell}^{\ell} B(X)S'(\xi)\coth\left(\frac{\pi(X-\xi)}{w\sqrt{1-F_1^2}}\right)\,dX\,d\xi \tag{4.48}$$

and

$$Z_{\text{step}} = \frac{\rho U^2\eta}{2h_1 w\,(1-F_1^2)}\int_{-\ell}^{\ell}\int_{-\ell}^{\ell} B(X)S'(\xi)\coth\left(\frac{\pi(X+\xi-2Ut)}{w\sqrt{1-F_1^2}}\right)\,dX\,d\xi\ . \tag{4.49}$$

The first term Z_{steady} is the steady-state constant-depth solution, in a different form to the Fourier-transformed version derived by Tuck (1967). For sharp-ended vessels, the extra force Z_{step} due to the presence of the step can again be integrated by parts to give

$$Z_{\text{step}} = \frac{\rho U^2\pi\eta}{2h_1 w^2\,(1-F_1^2)^{\frac{3}{2}}}\int_{-\ell}^{\ell}\int_{-\ell}^{\ell}\frac{B(X)S(\xi)}{\sinh^2\left(\frac{\pi(X+\xi-2Ut)}{w\sqrt{1-F_1^2}}\right)}\,dX\,d\xi\ . \tag{4.50}$$

For large values of d this limits to

$$Z_{\text{step}} \sim \left(\frac{m}{\sinh m}\right)^2\frac{\rho U^2\eta\Delta A_{\text{W}}}{8\pi h_1 d^2\sqrt{1-F_1^2}} \tag{4.51}$$

with

$$m = 2\pi d/(w\sqrt{1-F_1^2})\ .$$

This differs from the open-water theory by the factor $(m/\sinh(m))^2$. This factor is positive, so the sign of Z_{step} is the same as in infinite width. We see also that the two theories agree in the infinite-width limit, since $m/\sinh(m) \to 1$ as $w \to \infty$.

We know from the results of Chapter 3 that radiating waves are produced when a ship passes a step depth change in a narrow channel. As we shall see in the following Section, these waves are still produced in wider channels, although their amplitudes are smaller than in narrow channels. Therefore we would expect the image method to be valid after the ship's bow passes the step only in the case of wide channels, for which radiated waves appear to be negligible. In this case the flow could be found in the same way as was discussed at the end of §4.2.2.

4.3 Numerical method

4.3.1 General depth profiles

The two-dimensional governing equation (4.9) can be solved in a similar manner to the one-dimensional model considered in §3.4, by writing it in finite-difference form.

If we write equation (4.9) in the form

$$\frac{\phi_{tt}}{g} = h\left(\phi_{xx} + \phi_{yy}\right) + h_x\phi_x + h_y\phi_y \tag{4.52}$$

and use a centred-difference method to solve for ϕ, a similar problem of numerical stability arises to that encountered in §3.4. According to the Neumann criterion, such a method will be unstable due to the presence of the first derivative terms ϕ_x and ϕ_y.

This difficulty was avoided in the one-dimensional case by solving for the flux $h\phi_x$; in the two-dimensional case, however, there are two flux components $h\phi_x$ and $h\phi_y$. It is possible to write two centred finite-difference equations to be solved jointly for the two flux components at each time level, although such a scheme also proved unstable.

By writing equation (4.52) in the form

$$\frac{(h\phi)_{tt}}{g} = h\nabla^2(h\phi) - (h\phi)\nabla^2 h\ , \tag{4.53}$$

a stable centred-difference method was found by solving instead for the single quantity $h\phi$. Because of the $\nabla^2 h$ term in equation (4.53), this method is clearly more suited to smooth depth functions $h(x, y)$. However, it can be modified for discontinuous depth functions, as we shall see.

The boundary conditions on the differential equation (4.53) in open water are that ϕ_x, ϕ_y and ϕ_t all vanish or behave like an outgoing wave far away from the ship. If we are solving the finite-difference equation in open water we must create artificial boundaries at a sufficient distance from the ship. Ideally, these boundaries will be outside of the domain of influence of the ship, so that we can set all ϕ derivatives to zero without any risk of numerical reflection from the boundaries. Since the domain of influence becomes larger as time increases, the boundaries also must be further from the ship if we wish to study the flow at larger times.

For the case of a ship in a channel, we can instead specify the boundary condition of zero fluid velocity normal to the channel walls. This limits the size of the computational domain that is needed in the $y-$direction. As such, finite-width channels present less numerical difficulty than open water; we shall prefer to concentrate on finite-width channels for the numerical results.

Once the velocity potential is determined at each time level, the hydrodynamic pressure is best found by switching to body-fixed coordinates, in order to more simply evaluate Z

and M. The Bernoulli relation in body-fixed coordinates, namely

$$p + \frac{\rho}{2}\left(\phi_X^2 + \phi_y^2 + \phi_z^2\right) + \rho\phi_t + \rho U\phi_X = 0\,,$$

can be expanded in the inner region to give the leading-order hydrodynamic pressure on the hull

$$p = -\rho\left(\frac{\partial}{\partial t} + U\frac{\partial}{\partial X}\right)\varphi^{(1)}$$

which, using (4.12), becomes

$$p = -\rho\left(\frac{\partial}{\partial t} + U\frac{\partial}{\partial X}\right)\phi|_{y=0}\,. \tag{4.54}$$

With this expression for p in body-fixed coordinates, the vertical force Z and trim moment M can be simply evaluated using the expressions (4.15). In fact, to determine the overall quantities Z and M, it is better to bypass the evaluation of p in order to avoid unnecessary numerical differentiation. For example, the expression for Z becomes

$$\begin{aligned} Z &= -\rho\left\{\int_{-\ell}^{\ell} B(X)\,\phi_t|_{y=0}\,dX + U\int_{-\ell}^{\ell} B(X)\,\phi_X|_{y=0}\,dX\right\} \\ &= -\rho\left\{\frac{\partial}{\partial t}\int_{-\ell}^{\ell} B(X)\,\phi|_{y=0}\,dX - U\int_{-\ell}^{\ell} B'(X)\,\phi|_{y=0}\,dX\right\}\,, \end{aligned} \tag{4.55}$$

where we have moved the $t-$differentiation outside the first integral and integrated by parts in the second, assuming $B(\ell) = 0$. A similar method is used for the trim moment M:

$$M = \rho\left\{\frac{\partial}{\partial t}\int_{-\ell}^{\ell} X\,B(X)\,\phi|_{y=0}\,dX - U\int_{-\ell}^{\ell}(XB)'\,\phi|_{y=0}\,dX\right\}\,. \tag{4.56}$$

4.3.2 Step depth change

In the case of a step depth discontinuity, we use the constant-depth form of the governing equation (4.52) and apply suitable matching conditions at the step. As previously, these postulate that both $h\phi_x$ and ϕ_t are continuous across the step. Continuity of ϕ_t is guaranteed by requiring that ϕ itself be continuous across the step at all times.

The constant-depth form of equation (4.52) is

$$\phi_{tt} = gh\left(\phi_{xx} + \phi_{yy}\right) \tag{4.57}$$

which is the ordinary constant-coefficient wave equation. Writing $\phi_{j,k}^n = \phi(x_j, y_k, t_n)$, we may centre difference this to obtain the three-level time-stepping method

$$\phi_{j,k}^{n+1} = s_x\left(\phi_{j+1,k}^n + \phi_{j-1,k}^n\right) + s_y\left(\phi_{j,k+1}^n + \phi_{j,k-1}^n\right) + 2\left(1 - s_x - s_y\right)\phi_{j,k}^n - \phi_{j,k}^{n-1}\,. \tag{4.58}$$

Here s_x and s_y are defined by $s_x = gh\,(\delta t)^2 / (\delta x)^2$, $s_y = gh\,(\delta t)^2 / (\delta y)^2$, with δx, δy and δt the grid spacings in the x, y and t variables. s_x and s_y are constant in each region of constant depth.

This method will be stable according to the Neumann criterion provided that $s_x + s_y \leq 1$. This is more restrictive than the criterion for one-dimensional flow ($s_x \leq 1$).

The grid is so chosen that gridpoints lie on the lines $y = 0$, $y = w/2$ and $x = 0$. Because of the symmetry of the problem we only need to consider the region $y > 0$.

The boundary conditions for ϕ_y on the boundaries $y = 0$ and $y = w/2$ are enforced by creating fictitious gridpoints outside the boundaries. These are then used to evaluate the finite-difference form of the derivative ϕ_y on the boundary. The finite-difference equation (4.58) can now be applied on the boundaries as well as within the computational domain.

However, since there is a line of gridpoints on the depth discontinuity at $x = 0$, we cannot apply the finite-difference equation on $x = 0$; the relevant equation here comes from matching the flux $h\phi_x$ across the step. Matching ϕ across the step is automatically satisfied since the gridpoints at $x = 0$ belong to both regions.

In order to match the flux across the step we equate the three-point finite difference forms for $h\phi_x$ in each region:

$$h_1 \left(\frac{-3\phi_{0,k} + 4\phi_{1,k} - \phi_{2,k}}{2\delta x} \right) = h_2 \left(\frac{3\phi_{0,k} - 4\phi_{-1,k} + \phi_{-2,k}}{2\delta x} \right) . \tag{4.59}$$

This relation is then rearranged to find the value of $\phi_{0,k}$ at the new time level, using the neighbouring values which have already been found from equation (4.58).

In the case of a step depth change, it is not necessary to have a very large domain in the $x-$direction, which would be required if we wanted to set $\nabla\phi = 0$ at the outer boundaries. Since the waves produced while the ship is passing the step are observed to be one-dimensional, we may use one-dimensional wave boundary conditions at the upstream and downstream boundaries. These use the fact that one-dimensional wave solutions of the governing equation (4.9) must be of the form

$$\phi = \phi \left(x \pm \sqrt{gh}\, t \right)$$

in each region of constant depth h. Since the waves must be radiating outwards from the step, we must have

$$\phi = \phi \left(x - \sqrt{gh_1}\, t \right) \qquad \text{in } x > 0 \,,$$

which implies the boundary condition

$$\phi_t + \sqrt{gh_1}\, \phi_x = 0$$

at the boundary in $x > 0$. Similarly we may use the boundary condition

$$\phi_t - \sqrt{gh_2}\, \phi_x = 0$$

at the boundary in $x < 0$. These expressions may be finite-differenced and solved simultaneously with the governing finite-difference equation to give the value of ϕ on the boundaries at the new time level.

With ϕ solved for at each time level, the vertical force Z and trim moment M are found in body-fixed coordinates using equations (4.55) and (4.56).

4.4 Results for a step depth change

We consider the same problem described in §3.3 and §4.2. The same symmetric cusped ship defined by equations (3.15) is used, in order to minimize spurious numerical production of radiated waves.

4.4.1 Numerical issues

The numerical problems encountered with the finite-difference method were similar to those found while solving the unsteady hydraulic theory. These were principally numerical wave radiation, numerical oscillation and drift.

In solving the constant-depth flow field for vessels with non-zero values of S' and S'' at the bow and stern, similar waves to those described in §3.4.1 were observed radiating from the bow and stern. With the cusped hull, however, these spurious waves were minimized.

Because of the need for numerical differentiation to determine Z and M, the results were significantly affected by random numerical oscillations. These manifested themselves principally in the time-derivative terms in equations (4.55) and (4.56). It is also in these terms that the error due to drift was most important.

Numerical drift in two dimensions was similar to the one-dimensional case. A similar analysis of the finite-difference method shows that in constant depth the error will grow linearly with time. It was noticed that this error increased as the time step was made smaller.

With a step present, the problem of drift proved difficult to correct in two dimensions. Attempts to do so using similar methods to that described in Chapter 3 produced questionable results. Therefore in order to prevent rather than cure the problem, the grid size and time step were prevented from being too small. However, a larger grid size and time step produced larger numerical oscillations, so a compromise had to be reached. In this way the grid size and time step were chosen so as to reach a balance between excessive numerical oscillation and excessive drift.

The wave boundary conditions were successful in allowing a smaller computational domain to be used in the $x-$direction, while avoiding any artificial reflection from the upstream and downstream computational boundaries.

4.4.2 Flow velocity

The fluid speed ϕ_x in the in $x-$direction is plotted in Figure 4.1 for a ship that has just passed a step depth change to shallower water. In this case the channel is quite narrow, with the relevant parameter $w/L = 0.2$. The fluid speed is plotted at three different points across the channel: in the centre ($y = 0$), halfway to the edge ($y = w/4$), and at the channel wall ($y = w/2$).

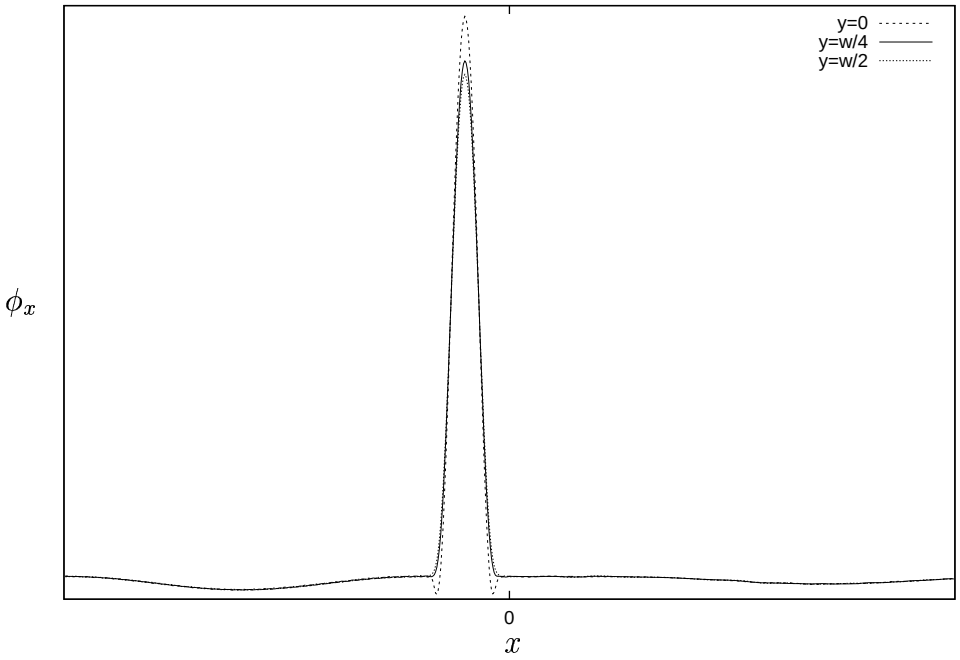

Figure 4.1: Streamwise fluid speed ϕ_x for a ship that has just passed a step depth change to shallower water, with $w/L = 0.2$

We can see that for this narrow channel the fluid speed past the hull is almost constant across the channel. In addition, it matches the linearized hydraulic flow found in Chapter 3 (see Figure 3.3). This confirms the result of Appendix B.4 that the two theories should agree in the narrow-channel limit.

Despite there being some variation across the channel in the flow speed past the hull, the travelling waves radiating away from the step are perfectly one-dimensional. For this narrow channel they are of a reasonable size, the same as that predicted using unsteady hydraulic theory.

Results were obtained for a wider channel with $w/L = 2.0$. In this case, as in steady slender-body shallow-water theory, the streamwise fluid speed ϕ_x was much faster near the ship's hull than near the channel walls. Waves were still radiated away from the step as the ship passed over, but for this wider channel they were almost negligible. Careful examination, however, showed them to be still perfectly one-dimensional.

At this increased channel width we see how the two-dimensional theory departs from the hydraulic theory: according to hydraulic theory, the flow is always uniform across the

channel and the amplitude of the radiated waves is proportional to the flow speed past the ship; in two-dimensional theory the flow tends towards the open-water flow as the channel width increases, with higher flow speed near the hull and insignificant radiated waves produced as the ship passes the step.

4.4.3 Vertical force and moment

For a narrow channel (e.g. $w/L = 0.2$) the transient force and moment were almost identical to that predicted using the unsteady hydraulic theory (see Figures 3.5 and 3.6). These showed a vertical force that was delayed in reaching the new steady state because of the radiating waves retarding the flow. Again, no overshoot or undershoot was witnessed. The trim moment was strongly bow-up while the ship was passing the step, and zero the rest of the time. As in hydraulic theory, for a narrow channel the ship did not "sense" the presence of the approaching step.

The results were quite different for a wider channel, with obvious departures from the hydraulic theory. Figure 4.2 shows the vertical force on the ship as a function of time as it passes the step. In this case the channel's width is double the shiplength. With two-dimensional theory the axes cannot be scaled in the same general way as for hydraulic theory. Instead we have used arbitrary values of the hull and channel parameters, with the relevant parameters affecting the form of the solution being $w/L = 2.0$, $F_1 = 0.143$ and $F_2 = 0.165$.

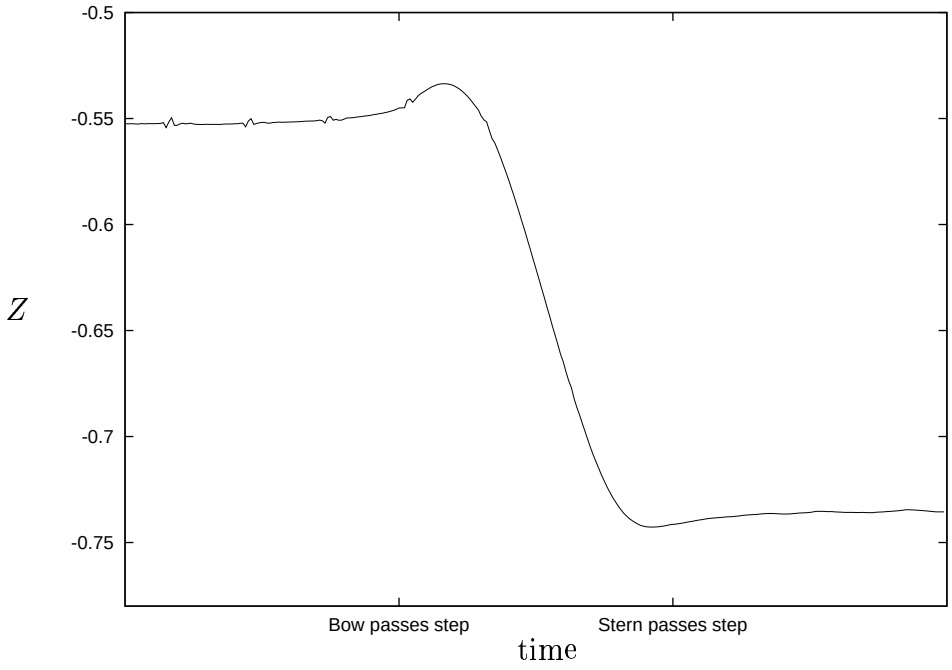

Figure 4.2: Vertical force for a ship passing a step depth change to shallower water, with $w/L = 2.0$

We see that in the wider channel the ship does sense the step before the bow reaches

it, as was predicted using the analytic image method of §4.2. Up until the bow reaches the step, the vertical force agrees with that predicted using the image method (equations 4.48,4.49).

For the wider channel, the flow is governed not by wave production (which is negligible here) but by the effect of having a constriction in the channel. This decreases the flow speed while the ship is moving toward or away from shallow water, and increases the flow speed when the ship is moving toward or away from deeper water. There is therefore a smaller downward force as the ship approaches the step and a larger downward force as the ship is moving away from the step.

The small spikes in the vertical force before the ship reaches the step are due to small irregularities in the initial conditions. Without any damping mechanism, these irregularities radiate out toward the channel walls at the natural wave speed $\sqrt{gh}$ and reflect back to periodically affect the flow at $y = 0$.

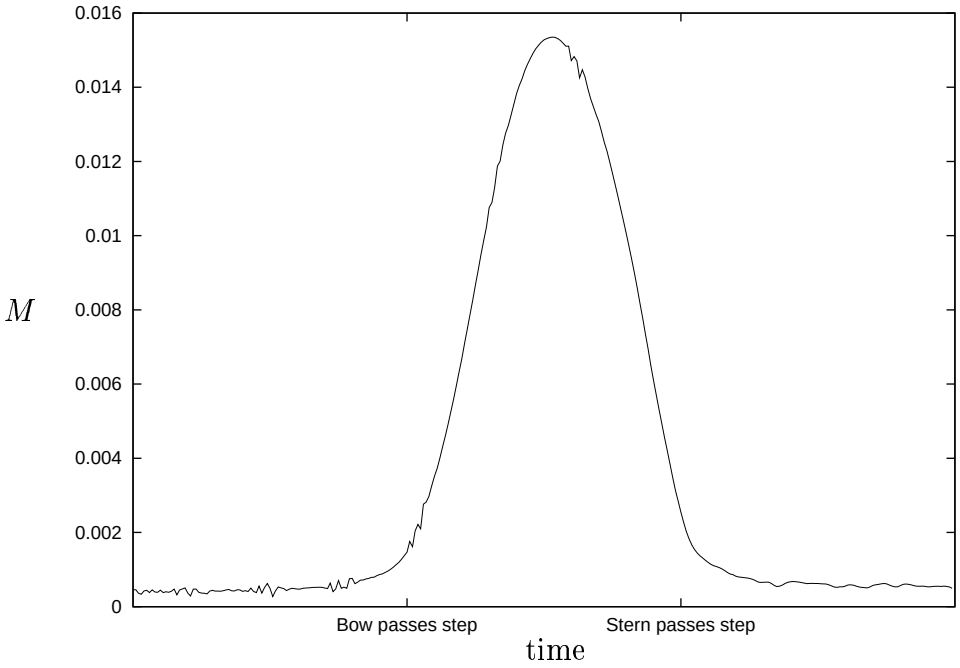

Figure 4.3: Bow-up trim moment for a ship passing a step depth change to shallower water, with $w/L = 2.0$

For the wider channel, the trim moment (Figure 4.3) is still bow-up while the ship is passing the step. Due to numerical error, the trim is apparently non-zero before and after the ship passes the step; this is spurious. However, we see that even for this fore-aft symmetric hull there is a small bow-up trim both before and after the ship passes the step.

4.4.4 Bow and stern sinkage

As discussed in §3.3.1, for a ship passing a sudden depth change we should use dynamic ship motion methods to determine the transient bow and stern sinkage of the ship. However we can gain some insight into the form of the bow and stern sinkage by considering the static equilibrium conditions (2.58) which are valid if changes in sinkage and trim occur sufficiently slowly.

Solving for the transient midship sinkage and trim using equations (2.58), the bow and stern sinkage are then given by $s \mp \ell\theta$ respectively. These are plotted in Figure 4.4 for the case with $w/L = 2.0$. For the narrow channel, the results were the same as in Figure 3.7.

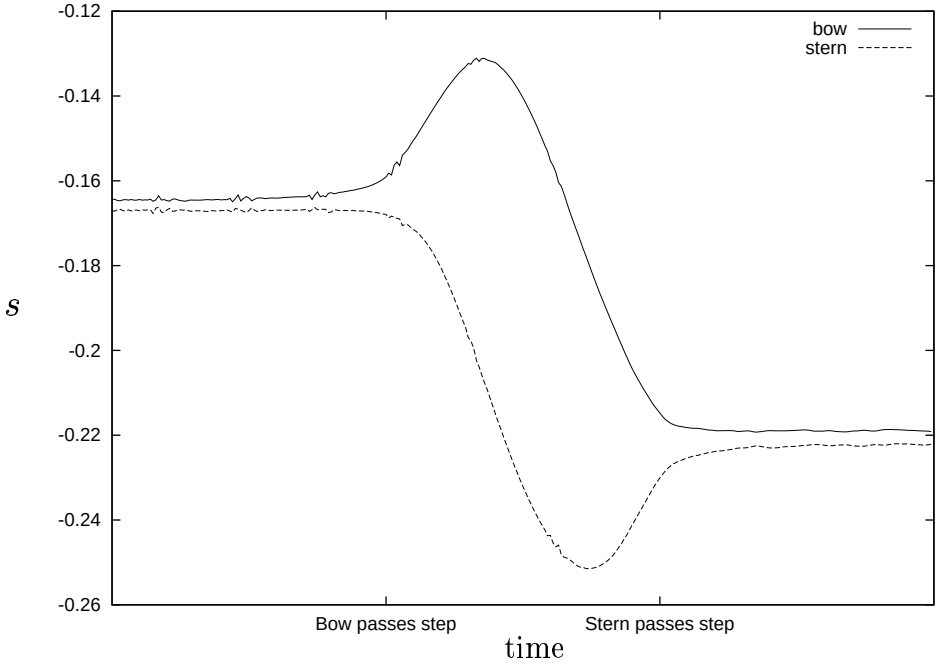

Figure 4.4: Bow and stern sinkage for a ship passing a step depth change to shallower water, with $w/L = 2.0$

We can ignore the spurious difference between the bow and stern sinkages before and after the ship passes the step, which is due to the small ongoing error in the trim moment. The effect of the strong bow-up trim is witnessed in the small bow sinkage and large stern sinkage while the ship is passing the step. Again, because the stern is not yet into the shallow water when it experiences the large sinkage, it is not in excessive danger of striking the sea floor. Once the stern reaches the step its sinkage is only slightly greater than in the shallow-water steady-state condition.

4.5 Conclusions

In this chapter we have extended slender-body shallow-water theory to describe unsteady flow past a ship in a channel of non-uniform depth. The resulting theory is valid for channels of any width, including open water. For narrow channels it reduces to the unsteady hydraulic theory developed in Chapter 3.

The two-dimensional nature of this theory means that it is necessarily more complex than the hydraulic theory, both mathematically and numerically. However, using the method of images it was possible to find analytic solutions in the case of a ship approaching a step depth change.

For a ship in a channel, stable finite-difference methods were developed which are valid for smooth or sudden depth changes. Using this method, we solved the problem of a ship passing a step depth change in a channel. The results agreed with the analytic results while the ship was approaching the step, and also agreed with the hydraulic theory in the case of a narrow channel.

Appendix A

Nomenclature

Coordinates

X Streamwise coordinate in body-fixed coordinates

x Streamwise coordinate in earth-fixed coordinates

y Transverse coordinate, ship centred on $y = 0$

z Vertical coordinate, undisturbed free surface at $z = 0$

Ship and channel dimensions

L Ship length, equal to 2ℓ.

B Ship's local waterline beam, function of X.

$B_{\max}$ Maximum beam

S Ship's local cross-sectional area, function of X.

$S_{\max}$ Maximum section area

Δ Ship's displacement (volume below the waterline when at rest)

A_{W} Waterplane area $\int_{-\ell}^{\ell} B(X)\,dX$

M_{W} $= \int_{-\ell}^{\ell} XB(X)\,dX$

I_{W} $= \int_{-\ell}^{\ell} X^2B(X)\,dX$

h Undisturbed water depth

w Channel width at the undisturbed waterline

S_0 Channel's undisturbed cross-sectional area

A Cross-sectional area taken up by water passing ship

Parameters

U Ship speed (earth-fixed coordinates) or
Free stream velocity (body-fixed coordinates)

g Acceleration due to gravity, $= 9.8$ m/s^2

F_h Depth-based Froude number $U/\sqrt{gh}$

β $= 1 - F_h^2$

γ Dispersion parameter $h^2/3$

Outputs

Φ Total velocity potential in body-fixed coordinates

$\mathbf{q}$ Fluid velocity in body-fixed coordinates, $= \nabla\Phi$

$\tilde{q}$ Scaled streamwise velocity Φ_X/U (for nonlinear flow)

u Streamwise velocity perturbation $\Phi_X - U$ (for linearized flow)

ϕ Total velocity potential in earth-fixed coordinates, or
Disturbance velocity potential in body-fixed coordinates

P Pressure excess above atmospheric

p Pressure excess above hydrostatic

Z Upward vertical force on ship

M Bow-up trim moment

ζ Free surface height above $z = 0$

$\tilde{\zeta}$ Scaled free surface height ζ/h

s Midship sinkage

$\tilde{s}$ Scaled midship sinkage s/h

σ Local sinkage, function of X

$\tilde{\sigma}$ Scaled local sinkage σ/h

θ Bow-up angle of trim

s_{bow} Bow sinkage

s_{stern} Stern sinkage

Fourier transforms

$\bar{B}(k) = \int_{-\infty}^{\infty} B(X) e^{ikX} dX$

$\bar{B}^*(k) = \int_{-\infty}^{\infty} B(X) e^{-ikX} dX$ (complex conjugate)

$B(X) = \frac{1}{2\pi} \int_{-\infty}^{\infty} \bar{B}(k) e^{-ikX} dk$ (inversion)

Appendix B

Some Mathematical Derivations

B.1 The basis of hydraulic theory

Hydraulic theory assumes that the only significant fluid velocity component is in the direction of the ship's motion, and that this velocity is almost uniform across the channel. If the fluid velocity in an earth-fixed frame of reference is $\nabla\phi = q_1\mathbf{i} + q_2\mathbf{j} + q_3\mathbf{k}$, this states that $q_2, q_3 \ll q_1$ and $q_1 \approx q_1(x,t)$ only. The requirements for this assumption to be valid can be found as follows.

The continuity equation written in the form

$$\frac{\partial q_1}{\partial x} + \frac{\partial q_2}{\partial y} + \frac{\partial q_3}{\partial z} = 0$$

tells us that

$$\begin{aligned} \frac{\delta q_2}{\delta q_1} &= O\left(\frac{\delta y}{\delta x}\right) \\ \frac{\delta q_3}{\delta q_1} &= O\left(\frac{\delta z}{\delta x}\right) , \end{aligned}$$

where δx represents a finite change in x, and similarly for the other quantities. So in order for q_2 and q_3 to be small compared to q_1 we require that the y and z length scales be small compared to the x scale. That is, the channel width and depth must be small compared to the ship length. In this case we have

$$\begin{aligned} \frac{q_2}{q_1} &= O\left(\frac{w}{L}\right) \\ \frac{q_3}{q_1} &= O\left(\frac{h}{L}\right) . \end{aligned}$$

If the surface of the ship's hull in $y > 0$ is defined by $y = Y(X,z)$, the kinematic condition on the ship's hull satisfies

$$q_2 = (U + q_1)Y_X + q_3 Y_z \qquad \text{on } y = Y(X,z) .$$

Looking at the magnitude of the terms tells us that for $q_2 \ll U$ we require $Y_X \ll 1$. Note that no such restriction is placed on Y_z. Therefore the ship can have any cross-sectional shape, provided that this shape varies slowly in the X-direction. A necessary criterion for this to be satisfied is that $S'(X)$ must be small, where $S(X)$ is the hull section area.

The kinematic condition on the sea floor

$$q_3 = -q_1 h_x - q_2 h_y \qquad \text{on } z = -h(x,y)$$

requires $h_x \ll 1$ for $q_3 \ll q_1$.

If, for simplicity, the channel walls are positioned at $y = \pm\frac{1}{2}w(x,z)$, the kinematic condition on the side walls states that

$$q_2 = \pm\frac{1}{2}\left(q_1 w_x + q_3 w_z\right) \qquad \text{on } y = \pm\tfrac{1}{2}w(x,z)\ .$$

For $q_2 \ll q_1$, therefore, we require that $w_x \ll 1$.

Again, no restrictions are placed on h_y or w_z. Therefore the channel can have any cross-sectional shape, so long as it varies slowly in the x-direction. For simplicity we will assume that the side walls are vertical at and near the free surface. This means that changes in the cross-sectional area taken up by the water are proportional to changes in the free surface height. This assumption may be dropped in the case of linearized flow where changes in the free surface height are small. However we will still require that the side walls are not excessively sloping at the free surface; otherwise, changes in free surface height would be accompanied by large variations in q_2.

We have shown that for $q_2, q_3 \ll q_1$ to hold we must have $w \ll L, h \ll L$ and the shape of the ship and channel must vary slowly in the x direction. We can now show that if these conditions are satisfied the flow will be almost uniform across the channel.

Using the irrotationality conditions

$$\begin{aligned} \frac{\partial q_1}{\partial y} &= \frac{\partial q_2}{\partial x} \\ \frac{\partial q_1}{\partial z} &= \frac{\partial q_3}{\partial x}\ , \end{aligned}$$

we can deduce that the fractional variation of q_1 in the y direction is

$$\frac{\delta q_1}{q_1} = O\left(\frac{\delta y}{\delta x}\frac{\delta q_2}{q_1}\right) = O\left(\left(\frac{w}{L}\right)^2\right)$$

and that the fractional variation of q_1 in the z direction is

$$\frac{\delta q_1}{q_1} = O\left(\frac{\delta z}{\delta x}\frac{\delta q_3}{q_1}\right) = O\left(\left(\frac{h}{L}\right)^2\right)$$

These quantities are both sufficiently small that q_1 may be considered constant across any cross-section x =constant.

With $q_1 = q_1(x,t)$ and q_2 and q_3 negligible, the velocity potential ϕ must be a function of x and t only. We can now use the Bernoulli equation to show that the free surface height ζ is also a function of x and t only. The Bernoulli equation as used here states that the quantity

$$\frac{P}{\rho} + gz + \frac{1}{2}|\nabla\phi|^2 + \phi_t$$

is constant throughout any simply-connected fluid domain if the flow is incompressible and irrotational. If we apply the Bernoulli equation on the free surface $z = \zeta$ and equate it to the value far ahead of the ship (where P, ζ, q_1 and ϕ_t are all zero) we obtain

$$g\zeta + \frac{1}{2}\,q_1^2 + \phi_t = 0\ .$$

Since ϕ and q_1 are functions of x and t only, ζ must also be a function of x and t only. Therefore the continuity and Bernoulli equations, which are sufficient to determine the flow, depend only on x and t.

In summary, we may make the approximation of one-dimensional flow provided that the channel dimensions satisfy

$$w \ll L$$

$$h \ll L$$

$$w_x \ll 1$$

$$h_x \ll 1$$

and the hull surface $y = Y(X,z)$ satisfies

$$Y_X \ll 1\ .$$

B.2 Finite-width and open-water TSWT agree in the infinite-width limit

We shall show here that the finite-width TSWT equations (2.73) for force and moment agree with the open-water TSWT equations (2.53) and (2.54) in the wide-channel limit. We shall do this by showing that

$$\lim_{w\to\infty}\int_{-\infty}^{\infty}\frac{k^2 f(k)}{\lambda}\coth\left\{\frac{\lambda w}{2}\right\}dk=\int_{-\infty}^{\infty}\frac{k^2 f(k)}{\lambda}dk \tag{B.1}$$

for any smooth bounded function $f(k)$ that tends to zero as $|k|\to\infty$. For the vertical force equation, $f(k)=\bar{S}(k)\bar{B}^*(k)$, while for the moment equation, $f(k)=\bar{S}(k)\overline{XB}^*(k)$.

In the open-water theory, λ must be defined by equation (2.43); for finite width it has the same definition except that its sign is irrelevant. Here, however, we shall use the same definition (2.43) for convenience, i.e.

$$\lambda=\begin{cases}\sqrt{\beta k^2-\gamma k^4} & \text{for} \quad \beta k^2-\gamma k^4>0\\ -i\sqrt{\gamma k^4-\beta k^2} & \text{for} \quad \beta k^2-\gamma k^4<0 \text{ and } k>0\\ +i\sqrt{\gamma k^4-\beta k^2} & \text{for} \quad \beta k^2-\gamma k^4<0 \text{ and } k<0\,.\end{cases} \tag{B.2}$$

We shall now study the finite-width integral and show that it limits to the open-water integral in each of the three ranges $[-\sqrt{\beta/\gamma},\sqrt{\beta/\gamma}]$, $[\sqrt{\beta/\gamma},\infty]$ and $[-\infty,-\sqrt{\beta/\gamma}]$ for subcritical flow. We shall then extend the proof to supercritical flow.

Subcritical case

When $|k|<\sqrt{\beta/\gamma}$, λ is real positive, so that as $w\to\infty$, $\coth(\lambda w/2)\to 1$. Therefore the limit (B.1) is true in this range.

When $k>\sqrt{\beta/\gamma}$, we put $\lambda=-i\alpha$, with

$$\alpha=\sqrt{\gamma k^4-\beta k^2} \tag{B.3}$$

being real positive. Therefore, using $\coth(-i\theta)=i\cot\theta$,

$$\int_{\sqrt{\beta/\gamma}}^{\infty}\frac{k^2 f(k)}{\lambda}\coth\left\{\frac{\lambda w}{2}\right\}dk=\int_{\sqrt{\beta/\gamma}}^{\infty}-\frac{k^2 f(k)}{\alpha}\cot\left\{\frac{\alpha w}{2}\right\}dk\,. \tag{B.4}$$

At this point we shall change variables and perform the integration in the $\alpha-$variable, which is a monotonically increasing function of k for $k>\sqrt{\beta/\gamma}$. Differentiating (B.3) gives

$$2\alpha\,d\alpha=\left(4\gamma k^3-2\beta k\right)dk\,, \tag{B.5}$$

so that the integral (B.4) can now be written

$$\int_0^\infty \frac{k\,f(k)}{-2\gamma k^2+\beta}\cot\left\{\frac{\alpha w}{2}\right\}\,d\alpha\ . \tag{B.6}$$

We recall that this integral is made up of the Cauchy principal value integral plus the sum of the arc integrals around each of the poles.

Cauchy principal value contribution

The poles in $\cot(\alpha w/2)$ are equally spaced at the points $\alpha_n = 2n\pi/w$ for integer values of n. Note that $-2\gamma k^3+\beta k$ is non-zero in the range of integration ($k > \sqrt{\beta/\gamma}$). We write the integral as a sum of integrals over ranges which have the poles as their midpoints:

$$\sum_{n=1}^{\infty}\int_{(2n-1)\frac{\pi}{w}}^{(2n+1)\frac{\pi}{w}} \frac{k\,f(k)}{-2\gamma k^2+\beta}\cot\left\{\frac{\alpha w}{2}\right\}\,d\alpha \tag{B.7}$$

with the error term

$$\int_0^{\frac{\pi}{w}} \frac{k\,f(k)}{-2\gamma k^2+\beta}\cot\left\{\frac{\alpha w}{2}\right\}\,d\alpha$$

becoming negligible as $\pi/w \to 0$.

As $w \to \infty$, each range of integration in (B.7) becomes a small region either side of $\alpha = \alpha_n$, so that we can expand in a Taylor series around α_n to give

$$\begin{aligned}\tan\left\{\frac{\alpha w}{2}\right\} &\sim \tan\left\{\frac{\alpha_n w}{2}\right\} + \frac{w}{2}\sec^2\left\{\frac{\alpha_n w}{2}\right\}(\alpha-\alpha_n)\\ &= \frac{w}{2}(\alpha-\alpha_n)\ .\end{aligned} \tag{B.8}$$

Therefore as each range of integration shrinks to zero size the sum (B.7) becomes

$$\sum_{n=1}^{\infty}\int_{(2n-1)\frac{\pi}{w}}^{(2n+1)\frac{\pi}{w}} \frac{k\,f(k)}{(-2\gamma k^2+\beta)}\,\frac{2}{w\,(\alpha-\alpha_n)}\,d\alpha\ . \tag{B.9}$$

We can now use the Taylor series result that

$$\lim_{\delta\to 0}\int_{c-\delta}^{c+\delta}\frac{g(\alpha)}{\alpha-c}\,d\alpha = 2\delta\,g'(c)$$

to evaluate each of the integrals in (B.9) as $\pi/w \to 0$, giving

$$\frac{2}{w}\sum_{n=1}^{\infty}\frac{2\pi}{w}\,\frac{d}{d\alpha}\left(\frac{k\,f(k)}{-2\gamma k^2+\beta}\right)\Bigg|_{\alpha=\alpha_n}\ . \tag{B.10}$$

This is a rectangle rule approximation to the integral

$$\frac{2}{w}\int_0^\infty \frac{d}{d\alpha}\left(\frac{k\,f(k)}{-2\gamma k^2+\beta}\right)\,d\alpha \tag{B.11}$$

which becomes exact in the limit as $\Delta\alpha = 2\pi/w \to 0$. This integral can be simply evaluated to give

$$\frac{2}{w}\left[\frac{k\,f(k)}{-2\gamma k^2+\beta}\right]_{\alpha=0}^{\alpha=\infty} = \frac{2}{w}\left[\frac{k\,f(k)}{-2\gamma k^2+\beta}\right]_{k=\sqrt{\beta/\gamma}}^{k=\infty} . \tag{B.12}$$

We know that $f(k) \to 0$ as $k \to \infty$, so the same must be true of $k\,f(k)/(-2\gamma k^2+\beta)$. The expression (B.12) then becomes

$$\frac{2}{w}\left[\frac{f\left(\sqrt{\frac{\beta}{\gamma}}\right)}{\sqrt{\beta\gamma}}\right] . \tag{B.13}$$

Since $f(k)$ is a smooth bounded function of k, this expression limits to zero as $w \to \infty$. Therefore the Cauchy principal value part of the integral (B.6) is zero in that limit.

Arc integral contribution

The arc integral contribution to the integral (B.6) is made up of the sum of the arc integrals around all of the poles α_n. Firstly we must decide which side of these poles the path of integration is to pass. In §2.3.5 we showed that the radiation condition dictates that the path of integration should pass *above* the poles in the complex $k-$plane. So which side of the poles should it pass in the complex $\alpha-$plane?

To determine this, we let

$$k = k_r + ik_i$$

$$\alpha = \alpha_r + i\alpha_i$$

near each pole, where $k_r > \sqrt{\beta/\gamma}\,, \alpha_r > 0$ and both k_i and α_i are small quantities as the pole is traversed. Since we are passing above the poles in the complex $k-$plane, $k_i > 0$. We must now find whether α_i is positive or negative.

The relation

$$\alpha^2 = \gamma k^4 - \beta k^2$$

becomes

$$\alpha_r^2 - \alpha_i^2 + 2\alpha_r\alpha_i i = -\beta\left(k_r^2 - k_i^2 + 2k_rk_ii\right) + \gamma\left(\left(k_r^2-k_i^2\right)^2 - 4k_r^2k_i^2 + 4k_rk_i\left(k_r^2-k_i^2\right)i\right) .$$

Equating imaginary parts gives

$$\alpha_r\alpha_i = k_rk_i\left(2\gamma\left(k_r^2-k_i^2\right)-\beta\right) . \tag{B.14}$$

Since $\gamma k_r^2 - \beta > 0$ and k_i is small, the term inside the square brackets is positive. Since k_r, α_r and k_i are all positive, α_i must also be positive. Therefore we must pass *above* the poles in the complex $\alpha-$plane.

The sum of the arc integral contributions to (B.6) is written

$$\sum_{n=1}^{\infty}\int_{C_n}\frac{k\,f(k)}{-2\gamma k^2+\beta}\cot\left\{\frac{\alpha w}{2}\right\}d\alpha\ , \tag{B.15}$$

where C_n is a small semicircular arc passing above the singular point α_n in the complex $\alpha-$plane. Using the residue theorem, these arc integrals can be evaluated to give

$$\sum_{n=1}^{\infty} -\pi i \operatorname{res}\left(\frac{k\,f(k)}{-2\gamma k^2+\beta}\cot\left\{\frac{\alpha w}{2}\right\}\;;\,\alpha_n\right)\;. \tag{B.16}$$

Using the expansion (B.8), this becomes

$$-i\sum_{n=1}^{\infty}\frac{2\pi}{w}\left(\frac{k\,f(k)}{-2\gamma k^2+\beta}\right)\Bigg|_{\alpha=\alpha_n}\;. \tag{B.17}$$

In the same way as we did for expression (B.10), we can write this as

$$-i\int_0^{\infty}\left(\frac{k\,f(k)}{-2\gamma k^2+\beta}\right)d\alpha \tag{B.18}$$

in the limit as $2\pi/w \to 0$. Returning to the $k-$variable using the differential form (B.5), we obtain

$$i\int_{\sqrt{\beta/\gamma}}^{\infty}\frac{k^2 f(k)}{\alpha}\,dk \tag{B.19}$$

or, replacing $\lambda = -i\alpha$,

$$\int_{\sqrt{\beta/\gamma}}^{\infty}\frac{k^2 f(k)}{\lambda}\,dk \tag{B.20}$$

in accordance with the open-water result.

When $k < -\sqrt{\beta/\gamma}$, λ is imaginary and given by equation (B.2) as $\lambda = i\alpha$. Here α has the same definition as before, i.e. $\alpha = \sqrt{\gamma k^4 - \beta k^2}$. Therefore the analysis is the same as for $k > \sqrt{\beta/\gamma}$ except that λ is now of opposite sign.

Firstly, in a similar manner to expression (B.4), we have

$$\int_{-\infty}^{-\sqrt{\beta/\gamma}}\frac{k^2 f(k)}{\lambda}\coth\left\{\frac{\lambda w}{2}\right\}dk = \int_{-\infty}^{-\sqrt{\beta/\gamma}} -\frac{k^2 f(k)}{\alpha}\cot\left\{\frac{\alpha w}{2}\right\}dk\;. \tag{B.21}$$

Since the same differential substitution (B.5) is used, the integral (B.21) becomes

$$\int_{\infty}^{0}\frac{k\,f(k)}{-2\gamma k^2+\beta}\cot\left\{\frac{\alpha w}{2}\right\}d\alpha\;. \tag{B.22}$$

Note that α is still monotonic in k, but k is negative here. Alternatively, this can be written

$$\int_0^{\infty}\frac{k\,f(k)}{2\gamma k^2-\beta}\cot\left\{\frac{\alpha w}{2}\right\}d\alpha\;. \tag{B.23}$$

The evaluation of the Cauchy principal value contribution is exactly the same as for $k > \sqrt{\beta/\gamma}$, except that the integrand is multiplied by -1. Therefore this contribution also vanishes in the $w \to \infty$ limit.

In evaluating the arc integrals, equation (B.14) still holds for determining the sign of α_i; in this case k_r is negative so α_i must also be negative. Therefore the path of integration must pass *below* the poles in the complex $\alpha-$plane. The sum of these arc integrals is now given by

$$\sum_{n=1}^{\infty} \pi i \,\mathrm{res}\left(\frac{k\,f(k)}{2\gamma k^2-\beta}\cot\left\{\frac{\alpha w}{2}\right\}\,;\,\alpha_n\right) \tag{B.24}$$

which is the same as equation (B.16) for $k > \sqrt{\beta/\gamma}$. The analysis continues unchanged to reach equation (B.18), whereupon substituting back in for k yields

$$i\int_{-\sqrt{\beta/\gamma}}^{-\infty} \frac{k^2 f(k)}{\alpha}\,dk \tag{B.25}$$

or

$$-i\int_{-\infty}^{-\sqrt{\beta/\gamma}} \frac{k^2 f(k)}{\alpha}\,dk\,. \tag{B.26}$$

Replacing $\lambda = i\alpha$, this becomes

$$\int_{-\infty}^{-\sqrt{\beta/\gamma}} \frac{k^2 f(k)}{\lambda}\,dk \tag{B.27}$$

in accordance with the open-water result.

Supercritical case

When $\beta < 0$, λ is imaginary for all k; it satisfies

$$\lambda = \begin{cases} -i\sqrt{\gamma k^4 - \beta k^2} & \text{for} \quad k > 0 \\ +i\sqrt{\gamma k^4 - \beta k^2} & \text{for} \quad k < 0\,. \end{cases} \tag{B.28}$$

As such, we put $\lambda = -i\alpha$ if $k > 0$ and $\lambda = i\alpha$ if $k < 0$. The analysis for $k > 0$ is the same as for $k > \sqrt{\beta/\gamma}$ in the subcritical case, with the same monotonic substitution for α being made. Here however the range of integration for k is $(0, \infty)$. One consequence of this is that the Cauchy principal value part of the integral now tends to zero even faster; the supercritical equivalent of equation (B.12) is

$$\frac{2}{w}\left[\frac{k\,f(k)}{-2\gamma k^2+\beta}\right]_{k=0}^{k=\infty} \tag{B.29}$$

which is zero.

In summing the arc integral contributions we note that α_0 in this case occurs at $k = 0$; the residue is zero at this point (from equation (B.16), so the summation is still valid. The rest of the analysis goes over unchanged, and we have

$$\lim_{w\to\infty}\int_0^{\infty} \frac{k^2 f(k)}{\lambda}\coth\left\{\frac{\lambda w}{2}\right\}\,dk = \int_0^{\infty}\frac{k^2 f(k)}{\lambda}\,dk$$
$$\lim_{w\to\infty}\int_{-\infty}^{0} \frac{k^2 f(k)}{\lambda}\coth\left\{\frac{\lambda w}{2}\right\}\,dk = \int_{-\infty}^{0}\frac{k^2 f(k)}{\lambda}\,dk\,,$$

so that the two theories agree in the $w \to \infty$ limit for supercritical flow also.

B.3 FDT and TSWT agree in the shallow-water limit

As we saw in the numerical results of §2.6, FDT and TSWT give very similar results for midship sinkage at small values of h/L. Here we show analytically that the theories become identical in the shallow-water limit when F_h is close to 1. We were not able to show this for general F_h because of the complicated manner of convergence of the $\Omega(k)$ integral; however, it seems likely that the theories are equivalent at all Froude numbers in the shallow-water limit.

The vertical force and trim moment expressions according to the two theories are

$$\begin{aligned} \text{FDT:} \quad Z &= -\frac{\rho U^2}{4\pi^2}\int_{-\infty}^{\infty} k^2\Omega(k)\bar{S}(k)\bar{B}^*(k)dk \\ M &= \frac{\rho U^2}{4\pi^2}\int_{-\infty}^{\infty} k^2\Omega(k)\bar{S}(k)\overline{XB}^*(k)dk \end{aligned} \tag{B.30}$$

where

$$\Omega(k) = -2\int_{|k|}^{\infty} \frac{dq}{\sqrt{q^2-k^2}}\left[1+\frac{q}{F_h^2k^2h - q\,\tanh(qh)}\right] . \tag{B.31}$$

$$\begin{aligned} \text{TSWT:} \quad Z &= -\frac{\rho U^2}{4\pi h}\int_{-\infty}^{\infty} \frac{k^2}{\lambda}\bar{S}(k)\bar{B}^*(k)dk \\ M &= \frac{\rho U^2}{4\pi h}\int_{-\infty}^{\infty} \frac{k^2}{\lambda}\bar{S}(k)\overline{XB}^*(k)dk \end{aligned} \tag{B.32}$$

where

$$\lambda^2 = \beta k^2 - \gamma k^4 . \tag{B.33}$$

The sign of λ is given for different values of k, β and γ by equation (2.43).

Writing $C(k) = \pi/(\lambda h)$, the theories will agree if and only if

$$\Omega(k) \to C(k) \;\text{ as }\; h \to 0 . \tag{B.34}$$

Note that we cannot directly use a small$-h$ expansion in the integral (B.31), as this would result in a divergent integral; it must be dealt with carefully in order to retain its convergence.

Since $\mathrm{Im}\{\Omega(k)\}$ and $\mathrm{Im}\{C(k)\}$ are both odd in k, and $\mathrm{Re}\{\Omega(k)\}$ and $\mathrm{Re}\{C(k)\}$ are both even in k, we need only consider $k > 0$ in the following proof.

Subcritical flow

When $\beta > 0$, $C(k)$ is given by

$$C(k) = \begin{cases} \frac{\pi}{h\sqrt{\beta k^2 - \gamma k^4}} & \text{when } k < \sqrt{\beta/\gamma} \\ \frac{-i\pi}{h\sqrt{\gamma k^4 - \beta k^2}} & \text{when } k > \sqrt{\beta/\gamma}\ . \end{cases} \tag{B.35}$$

Showing that $k_0 \to \sqrt{\beta/\gamma}$

We know that $\Omega(k)$ is pure-real for $k < k_0$, and $C(k)$ is pure-real for $k < \sqrt{\beta/\gamma}$. Both have imaginary parts for higher values of k. We must first prove that $k_0 \to \sqrt{\beta/\gamma}$ as $h \to 0$ and $\beta \to 0$.

k_0 is defined by

$$\frac{\tanh(k_0 h)}{k_0 h} = F_h^2\ . \tag{B.36}$$

Since F_h is close to 1, $k_0 h$ will be small. Using the expansion

$$\tanh(x) \to x - \frac{x^3}{3} \qquad \text{as } x \to 0\ , \tag{B.37}$$

(B.36) becomes

$$k_0 h \to \sqrt{3(1 - F_h^2)} \qquad \text{as } \beta \to 0 \tag{B.38}$$

so that $k_0 h = O(\beta^{1/2})$. As $\beta \to 0$, (B.38) gives for k_0

$$k_0 \to \sqrt{\frac{1 - F_h^2}{h^2/3}} = \sqrt{\frac{\beta}{\gamma}} \tag{B.39}$$

as required. Note that we were not required to take the limit as $h \to 0$; this result holds at all depths as $F_h \to 1$.

Showing that $\Omega(k) \to C(k)$ for $k < k_0$

To show that $\Omega(k) \to C(k)$ for $k < k_0$, we write $\Omega(k)$ as

$$\Omega(k) = -2(I_1 + I_2) \tag{B.40}$$

where

$$\begin{aligned} I_1 &= \int_k^\infty \frac{q\ dq}{\sqrt{q^2 - k^2}} \left[\frac{1 - \tanh(qh)}{F_h^2 k^2 h - q\ \tanh(qh)} \right] \\ I_2 &= \int_k^\infty \frac{dq}{\sqrt{q^2 - k^2}} \left[\frac{h F_h^2 k^2}{F_h^2 k^2 h - q\ \tanh(qh)} \right]\ . \end{aligned} \tag{B.41}$$

Both of the integrals in (B.41) exist separately for positive values of h. We see that as $h \to 0$, the numerator of I_1 is $O(1)$ while that of I_2 is of $O(h)$; therefore I_1 will formally dominate I_2 in this limit. Using the change of variables $\nu = \sqrt{q^2 - k^2}$, I_1 becomes

$$I_1 = \int_0^\infty \frac{1 - \tanh(qh)}{F_h^2 k^2 h - q \tanh(qh)} d\nu \ . \tag{B.42}$$

In the limit $h \to 0$, the numerator of the integrand in (B.42) tends to 1 except for very large q, in which case it tends to zero sufficiently fast for the integral to converge. We may therefore replace the numerator by 1 in the small-h limit, provided that the corresponding small-h expansion of the denominator still gives a convergent integral.

Using the expansion (B.37) for small (qh) then gives

$$I_1 \to \int_0^\infty \frac{d\nu}{F_h^2 k^2 h - qh^2 + \frac{1}{3} h^3 q^4} \ , \tag{B.43}$$

or, on substituting for ν,

$$I_1 \to \frac{1}{h} \int_0^\infty \frac{d\nu}{\gamma\nu^4 - (1 - 2\gamma k^2)\nu^2 - \beta k^2 + \gamma k^4} \ . \tag{B.44}$$

This integral can be solved exactly by closing the contour in the complex ν-plane. We write it in the form

$$I_1 = \frac{1}{2h\gamma} \int_{-\infty}^\infty \frac{d\nu}{(\nu^2 + (b - a))\,(\nu^2 - (b + a))} \tag{B.45}$$

where

$$\begin{aligned} a &= \frac{1}{2\gamma} - k^2 \\ b^2 &= \frac{1}{4\gamma^2} - \frac{F_h^2 k^2}{\gamma} \end{aligned} \tag{B.46}$$

and we choose b to be positive. Since in the small β, γ limit $k < k_0$ implies that $k^2 < \beta/\gamma$, we see that a is positive in this case. Also, since

$$b^2 - a^2 = \frac{1}{\gamma} \left(\beta k^2 - \gamma k^4 \right) \ , \tag{B.47}$$

$b - a$ is positive. Therefore the poles in (B.45) occur at $\nu = \pm\sqrt{b + a}$, $\pm i\sqrt{b - a}$. If we consider the integral as a Cauchy principal value integral, the residues on the real axis will cancel each other when we deform the contour beneath each of them.

Closing the contour in a large semicircular arc around the lower half of the complex ν-plane then tells us that

$$\begin{aligned} I_1 &= -2\pi i \, \frac{1}{2h\gamma} \, \mathrm{res} \left\{ \frac{1}{(\nu^2 + (b - a))\,(\nu^2 - (b + a))} \ ; \ -i\sqrt{b - a} \right\} \\ &= \frac{-\pi i}{h\gamma} \, \frac{-1}{4bi\sqrt{b - a}} \ . \end{aligned} \tag{B.48}$$

In the limit as $\gamma \to 0$ and $F_h \to 1$,

$$\begin{aligned} b &\to \frac{1}{2\gamma} \\ a &\to \frac{1}{2\gamma} \end{aligned} \tag{B.49}$$

so that

$$b - a = \frac{b^2 - a^2}{b + a} \to \beta k^2 - \gamma k^4 \tag{B.50}$$

and (B.48) becomes

$$I_1 \to \frac{-\pi}{2h\sqrt{\beta k^2 - \gamma k^4}} \, . \tag{B.51}$$

Hence, from (B.40),

$$\Omega(k) \to \frac{\pi}{h\sqrt{\beta k^2 - \gamma k^4}} \tag{B.52}$$

in agreement with $C(k)$.

Showing that Im$\{\Omega(k)\}$ →Im$\{C(k)\}$ for $k > k_0$

$C(k)$ is pure imaginary for $k > \sqrt{\beta/\gamma}$. To show that the imaginary parts of $\Omega(k)$ and $C(k)$ match for $k > k_0$ we use

$$\mathrm{Im}\{\Omega(k)\} = \frac{-2\pi q_0}{\sqrt{q_0^2 - k^2}\left(q_0 h \mathrm{sech}^2(q_0 h) + \tanh(q_0 h)\right)} \tag{B.53}$$

with q_0 defined by

$$q_0 h \tanh(q_0 h) = h^2 F_h^2 k^2 \, . \tag{B.54}$$

If we assume that F_h is close to one then we know from (B.38) that $k_0 h$ may be considered small. Similarly, since F_h is close to one, q_0 is close to k_0, so that $q_0 h$ may also be considered small. Therefore, using the expansion (B.37) in (B.54) gives

$$q_0^2 \to F_h^2 k^2 + \gamma F_h^4 k^4 \tag{B.55}$$

so that

$$q_0^2 - k^2 \to (F_h^2 - 1)k^2 + \gamma F_h^4 k^4 \, . \tag{B.56}$$

For F_h close to one, this limits to

$$q_0^2 - k^2 \to -\beta k^2 + \gamma k^4 \, . \tag{B.57}$$

Therefore in the limit as $h \to 0$, (B.53) becomes

$$\begin{aligned} \mathrm{Im}\{\Omega(k)\} &\to \frac{-2\pi q_0}{\sqrt{-\beta k^2 + \gamma k^4}\,(q_0 h + q_0 h)} \\ &= \frac{-\pi}{h\sqrt{-\beta k^2 + \gamma k^4}} \end{aligned} \tag{B.58}$$

in agreement with $C(k)$.

Showing that Im$\{\Omega(k)\}$ dominates Re$\{\Omega(k)\}$ for $k > k_0$

For $k > k_0$, Re$\{\Omega(k)\}$ can again be evaluated using (B.40) and (B.41). We note that $|I_1|$ for $k < k_0$ is of the same order in β and h as $|\mathrm{Im}\{\Omega(k)\}|$ is for $k > k_0$. Also, $|I_2|$ for $k < k_0$ is of smaller order than $|I_1|$; therefore $|\mathrm{Im}\{\Omega(k)\}|$ must dominate $|I_2|$ for $k > k_0$. We now show that the leading order term of I_1, which is the same order as $|\mathrm{Im}\{\Omega(k)\}|$, is identically zero for $k > k_0$, so that Re$\{\Omega(k)\}$ can be neglected for $k > k_0$.

For $k > k_0$, I_1 is again given by (B.45) and (B.46) in the small-h limit. In this case we have

$$\begin{aligned} a &> 0 \qquad \text{for} \qquad k^2 < \frac{1}{2\gamma} \\ b &> 0 \qquad \text{for} \qquad k^2 < \frac{1}{4\gamma F_h^2} \, . \end{aligned} \tag{B.59}$$

So provided that $k^2 < 1/(4\gamma F_h^2)$, both a and b are real and positive. As $\gamma \to 0$ this is true for all k. For $k > k_0$, $b^2 - a^2$ is negative from (B.47); therefore $b - a < 0$ and all four poles lie on the real axis. Taking the same contour integral dicussed previously for I_1, but in this case passing also beneath the other two poles on the real axis, we see that all residues cancel and this leading term of I_1 is zero.

Although I_1 is no longer zero for $k^2 > 1/(4\gamma F_h^2)$, the integrand in (B.30) dies away sufficiently quickly that the $k \to \infty$ behaviour of $\Omega(k)$ is irrelevant.

Supercritical flow

In this case $C(k)$ is given by

$$C(k) = \frac{-i\pi}{h\sqrt{\gamma k^4 - \beta k^2}} \tag{B.60}$$

for all $k > 0$. $\Omega(k)$ has real and imaginary parts for all $k > 0$. The proofs that Im$\{\Omega(k)\}$ $\to$Im$\{C(k)\}$, and that Im$\{\Omega(k)\}$ dominates Re$\{\Omega(k)\}$, are the same as for subcritical flow.

B.4 Unsteady slender-body shallow-water theory agrees with unsteady hydraulic theory in the narrow-channel limit

For simplicity we shall assume that the channel varies only in the $x-$direction, although the proof can easily be extended to channels of arbitrary depth if the slope h_y is independent of w.

We start with the equation of unsteady slender-body shallow-water theory, namely

$$\frac{\phi_{tt}}{g} = (h\phi_x)_x + (h\phi_y)_y \ , \tag{B.61}$$

subject to the boundary conditions

$$\phi_y = \frac{US'(x+Ut)}{2h} \qquad \text{on } y = 0$$

and

$$\phi_y = 0 \qquad \text{on } y = w/2 \ .$$

Introducing the scaled variable $Y = 2y/w$, equation (B.61) for $\phi(x, Y, t)$ now becomes

$$\frac{\phi_{tt}}{g} = (h\phi_x)_x + \frac{4h}{w^2}\phi_{YY} \tag{B.62}$$

with boundary conditions

$$\phi_Y(x, 0, t) = \frac{Uw}{4h}S'(x+Ut)$$

and

$$\phi_Y(x, 1, t) = 0 \ .$$

We now write ϕ_Y as a combination of a linear function of Y and a correction term ψ_Y:

$$\phi_Y(x, Y, t) = \frac{Uw}{4h}S'(x+Ut).(1-Y) + \psi_Y \ . \tag{B.63}$$

The boundary conditions require that ψ_Y be zero on $y = 0$ and $y = w/2$.

Integrating equation (B.63) gives

$$\phi(x, Y, t) = \frac{Uw}{4h}S'(x+Ut).\left(Y - \frac{Y^2}{2}\right) + \psi \ . \tag{B.64}$$

where the constant of integration is contained in ψ.

We shall now show that the function ψ is independent of Y in the small-w limit and dominates the first term in equation (B.64).

Substituting the expression (B.64) into the governing equation (B.62) gives

$$\frac{\psi_{tt}}{g} = (h\psi_x)_x + \frac{4h}{w^2}\psi_{YY} - \frac{US'}{w} + \frac{Uw}{4}\left\{S''' - \frac{h_x}{h}S'' + \left(\frac{h_x^2 - hh_x}{h^2}\right)S'\right\}\left(Y - \frac{Y^2}{2}\right) \tag{B.65}$$

where $S = S(x + Ut)$. In the limit as $w \to 0$ this becomes, to leading order $1/w^2$,

$$\psi_{YY} = 0 \ .$$

Since $\psi_Y = 0$ on both boundaries it must be zero everywhere, so that $\psi = \psi(X, t)$ only. Now to leading order $1/w$, equation (B.65) shows that ψ must be of order $1/w$ and satisfy

$$\frac{\psi_{tt}}{g} = (h\psi_x)_x - \frac{US'}{w} \ . \tag{B.66}$$

Therefore ψ formally dominates the first term in equation (B.64) as $w \to 0$, so that $\phi(x, Y, t) \to \psi(x, t)$ in this limit. But $\psi(x, t)$ satisfies equation (B.66), which is the unsteady hydraulic formula derived in Chapter 3. Therefore the unsteady slender-body shallow-water solution ϕ agrees with the unsteady hydraulic solution ψ in the narrow-channel limit.

Bibliography

Abramowitz, M. & Stegun, I.A. 1965 *Handbook of Mathematical Functions.* Dover Publications, New York.

Ang, W.T. 1993 Nonlinear sinkage and trim for a slender ship in shallow water of finite width. (Internal report, University of Adelaide).

Barrass, C.B. 1978 *Ship Squat.* Lorne and Maclean Publishers.

Broyden, C.G. 1965 A class of methods for solving nonlinear simultaneous equations. *Mathematics of Computation* **19**, 577–593.

Chen, X.-N. & Sharma, S.D. 1995 A slender ship moving at near-critical speed in a shallow channel. *J. Fluid Mech.* **291**, 263–285.

Constantine, T. 1961 On the movement of ships in restricted waterways. *J. Fluid Mech.* **9**, 247–256.

Dand, I.W. & Ferguson, A.M. 1973 The squat of full ships in shallow water. *Trans. RINA* **115**, 237–255.

Duffield, R.J. 1997 Investigation into steady and unsteady state squat. *B. Nav. Arch. thesis*, Australian Maritime College.

Ertekin, R.C., Webster, W.C. & Wehausen, J.V. 1985 Ship-generated solitons. *15th Symp. Naval Hydro.* ONR Washington DC, 347–361.

Du, Y-Z. & Millward, A. 1991 The effect of squat on the wave resistance of a fast round bilge hull in shallow water. *Int. Shipbuild. Progr.* **38**, no. 416, 341–360.

Edstrand, H. & Norrbin, N.H. 1978 Shallow water phenomena and scale model research. Some experience from the SSPA Marine Dynamics Laboratory. *Int. Ship build. Progr.* **287**, Vol. 25, 181–195.

Eryuzlu, N.E. & Hausser, R. 1978 Experimental investigation into some aspects of large vessel navigation in restricted waterways. *Proc. Symp. Aspects of Navigability of Constraint Waterways Including Harbour Entrances* Vol. 2, 1–15.

Eryuzlu, N.E., Cao, Y.L. & D'agnolo, F. 1994 Underkeel requirements for large vessels in shallow waterways. *Proc. 28th Int. Nav. Congr.* PIANC, Paper S II-2, 17–25.

FERGUSON, A.M., SEREN, D.B. & MCGREGOR, R.C. 1982 Experimental investigation of a grounding on a shoaling seabank. *Trans. RINA* **124**, 303–324.

GERTLER, M. 1954 A reanalysis of the original test data for the Taylor standard series. *David Taylor Model Basin Report* **806**, Department of the Navy, Washington D.C.

GOURLAY, T.P. & TUCK, E.O. 1998a Hydraulic and slender-body shallow-water theories for flow past a ship in a channel, and determination of squat. *Proc. 3rd Biennial Engineering Mathematics and Applications Conference*, Adelaide, July 1998, 233–236.

GOURLAY, T.P. & TUCK, E.O. 1998b One-dimensional theory for flow past a ship in a channel of variable depth. *ANZIAM Gazette* **25**, No. 4, 206–211.

GOURLAY, T.P. 1999 The effect of squat on steady nonlinear hydraulic flow past a ship in a channel. *Schiffstechnik* **46**, No. 4, 217–222.

GRAFF, W., KRACHT, A. & WEINBLUM, G. 1964 Some extensions of D.W. Taylor's standard series. *Trans. SNAME* **72**, 374–401.

HAVELOCK, T.H. 1939 Note on the sinkage of a ship at low speeds. *Z. Angew. Math. Mech.* **19**, 202–205.

HOOFT, J.P. 1974 The behaviour of a ship in head waves at restricted water depth. *Int. Shipbuild. Progr.* **244**, Vol. 21, 367–390.

HOUSTON, J.R. 1978 Interaction of tsunamis with the Hawaiian islands calculated by a finite-element numerical model. *J. Phys. Oceanog.* **8**, 93–102.

HUANG, D.B., SIBUL, O.J., WEBSTER, W.C., WEHAUSEN, J.V., WU, D.M. & WU, T.Y. 1982 Ships moving in the transcritical range. *Conference on behaviour of ships in restricted waters*, Varna, Proc. Vol. II, 26/1–10.

HUUSKA, O. 1976 On the evaluation of underkeel clearances in Finnish waterways. *Helsinki University of Technology Ship Hydrodynamics Laboratory, Otaniemi*, Report no. 9.

LAMB, H. 1932 *Hydrodynamics, 6th Ed.* Cambridge University Press.

LEE, S.J., YATES, G.T. & WU, T.Y. 1989 Experiments and analyses of upstream advancing solitary waves generated by moving disturbances. *J. Fluid Mech.* **199**, 569–593.

LEA, G.K. & FELDMAN, J.P. 1972 Transcritical flow past slender ships. *9th Symp. Naval Hydro.*, ONR Washington DC, 1527–1541.

MEI, C.C. 1976 Flow around a thin body moving in shallow water. *J. Fluid Mech.* **77**, 737–751.

MEI, C.C. 1983 *The Applied Dynamics of Ocean Surface Waves.* John Wiley and Sons.

MEI, C.C. & CHOI, H.S. 1987 Forces on a slender ship advancing near the critical speed in a wide canal. *J. Fluid Mech.* **179**, 59–76.

MICHELL, J.H. 1898 The wave resistance of a ship. *Phil Mag.* **45**, 106–123.

MILLWARD, A. 1992 A comparison of the theoretical and empirical prediction of squat in shallow water. *Int. Shipbuild. Progr.* **417**, Vol. 39, 69–78.

NAGHDI, P.M. 1978 Fluid jets and fluid sheets: a direct formulation. *12th Symp. Naval Hydro.*, ONR Washington D.C., 500–515.

NATIONAL TRANSPORTATION SAFETY BOARD 1993 Grounding of the United Kingdom passenger vessel RMS Queen Elizabeth 2 near Cuttyhunk Island, Vineyard Sound, Massachusetts on August 7, 1992, *Marine Accident Report* **PB93-916201**, March 1993.

NEWMAN, J.N. 1977 *Marine Hydrodynamics.* MIT Press, Cambridge, Mass.

RENILSON, M.R. & HATCH, T. 1998 A preliminary investigation into squat over an undulating bottom. *The Naval Architect*, February 1998.

ROSEMAN, D.P. (ed.) 1987 *The MarAd Systematic Series of full form ship models.* SNAME Publications.

SHASHKOV, M. 1996 *Conservative Finite-Difference Methods on General Grids.* CRC Press.

SHEARER, J.R. & CROSS, J.J. 1965 The experimental determination of the components of ship resistance for a mathematical model. *Trans. RINA* **107**, 459–473.

STOKER, J.J. 1957 *Water Waves.* New York: Interscience.

THEWS, J.G. & LANDWEBER, L. 1935 The influence of shallow water on the resistance of a cruiser model. U.S. Experimental Model Basin, Navy Yard, Washington D.C., Rep. No. 408.

TUCK, E.O. 1964 A systematic asymptotic expansion procedure for slender ships. *J. Ship Res.* **8**, 15–23.

TUCK, E.O. 1966 Shallow water flows past slender bodies. *J. Fluid Mech.* **26**, 81–95.

TUCK, E.O. 1967 Sinkage and trim in shallow water of finite width. *Schiffstechnik* **14**, 92–94.

TUCK, E.O. & TAYLOR, P.J. 1970 Shallow water problems in ship hydrodynamics. *8th Symp. Naval Hydro.* ONR Washington DC, 627–659.

TUCK, E.O. 1974 One-dimensional flows as slender-body problems, with applications to ships moving in channels. in Proc. *Workshop on Slender Body Theory*, Ann Arbor, Michigan. University of Michigan Report NAME **164**, 27–35.

TUCK, E.O. 1979 Models for predicting tsunami propagation. *N.S.F. Workshop on Tsunamis, California, May 1979.* Proceedings, Tetra Tech Inc., 43–109.

TUCK, E.O. 1997 Solution of free-surface problems by boundary and desingularised integral equation techniques. *Proc. Computational Techniques and Applications: CTAC97*, 11–26.

UNITED STATES COAST GUARD 1993 Grounding of the passenger liner Queen Elizabeth 2 near Cuttyhunk Island, Vineyard Sound, Massachusetts on August 7, 1992, *Marine Casualty Report.*

VANTORRE, M. 1996 A review of practical methods for prediction of squat. *Workshop on Ship Squat in Restricted Waters*, Soc. Nav. Archs. Mar. Engs., Panel H10, October 1995. Proceedings, ed, A. Lansburg, July 1996, 70–81.

WU, D.M. & WU, T.Y. 1982 Three-dimensional nonlinear long waves due to moving surface pressure. *14th Symp. Naval Hydro.*, ONR Washington DC, 103–125.

WU, T.Y. 1987 Generation of upstream advancing solitons by moving disturbances. *J. Fluid Mech.* **184**, 75–99.